JUSTUS-LIEBIG-
UNIVERSITÄT
GIESSEN

Analysis of diverse mobile genetic elements infecting *Shewanella oneidensis* MR-1

Dissertation

zur Erlangung des Doktorgrades der Naturwissenschaften (Dr. rer. nat.)

dem Fachbereich 8
-Biologie und Chemie-
der Justus-Liebig-Universität Gießen
vorgelegt von

Nicole Evelin Schmid

angefertigt am Institut für Mikrobiologie und Molekularbiologie

Gießen, März 2024

Erstgutachter:	Prof. Dr. Kai Thormann Institut für Mikrobiologie und Molekularbiologie, Justus-Liebig-Universität Gießen
Zweitgutachterin:	Prof. Dr. Julia Frunzke Institute of Bio- and Geoscience, Forschungszentrum Jülich

Die während der Promotion erzielten Ergebnisse sind zum Teil in folgender Preprint-Publikation veröffentlicht:

Schmid, Nicole E.; Brandt, David; Walasek, Claudia; Rolland, Clara; Wittmann, Johannes; Müsken, Mathias; Kalinowski, Jörn; Thormann, Kai M. (2023): A rolling circle-replicating plasmid as an Inovirus phage satellite. bioRxiv. DOI: https://doi.org/10.1101/2023.11.28.569023.

Ergebnisse aus einem Promotionsprojekt, welches in dieser Dissertation nicht erwähnt wurde, sind in der folgenden Originalpublikation veröffentlicht:

Kreienbaum, Maximilian; Dörrich, Anja K.; Brandt, David; **Schmid, Nicole E.**; Leonhard, Tabea; Hager, Fabian; Brenzinger, Susanne; Hahn, Julia; Glatter, Timo**;** Ruwe, Matthias**;** Briegel, Ariane; Kalinowski, Jörn; Thormann, Kai M. (2020): Isolation and Characterization of *Shewanella* Phage Thanatos Infecting and Lysing *Shewanella oneidensis* and Promoting Nascent Biofilm Formation. In: *Frontiers in Microbiology* 11, S. 573260. DOI: 10.3389/fmicb.2020.573260.

Eidesstattliche Erklärung

Hiermit versichere ich, die vorgelegte Thesis selbstständig und ohne unerlaubte fremde Hilfe und nur mit den Hilfen angefertigt zu haben, die ich in der Thesis angegeben habe. Alle Textstellen, die wörtlich oder sinngemäß aus veröffentlichten Schriften entnommen sind, und alle Angaben, die auf mündlichen Auskünften beruhen, sind als solche kenntlich gemacht. Bei den von mir durchgeführten und in der Thesis erwähnten Untersuchungen habe ich die Grundsätze guter wissenschaftlicher Praxis, wie sie in der „Satzung der Justus-Liebig-Universität zur Sicherung guter wissenschaftlicher Praxis" niedergelegt sind, eingehalten. Gemäß § 25 Abs. 6 der Allgemeinen Bestimmungen für modularisierte Studiengänge dulde ich eine Überprüfung der Thesis mittels Anti-Plagiatssoftware.

_____ _____

Datum Nicole E. Schmid

Abstract

Mobile genetic elements (MGEs) are autonomous genetic agents that utilise host cells for selfish reproduction. MGEs are considered to be drivers of microbial evolution, as they largely control horizontal gene transfer. Bacteriophages (Phages), the viruses that infect bacteria, are classified as MGEs. Phages are known to inject their genome into a host cell and then hijack the host cell, turning it into a virion-producing factory. Interestingly, not only host cells are exploited by MGEs, some MGEs also exploit other MGEs for their selfish horizontal spread. So-called phage satellites are specialised in the hijacking of phages. The majority of phage satellites are integrative elements present in bacterial chromosomes, which contain some, but not enough, structural genes to generate virions. They therefor are dependent on phage structural proteins for horizontal transfer via transduction. The resulting satellite-dependent exploitation of a phage often leads to a reduction in the virion output of the hijacked phage.

In this work, a new *Shewanella* phage, named Dolos, was characterised. Dolos belongs to the viral family *Inoviridae* and thus is a phage that carries out a chronic-productive infection. Consequently, Dolos-mediated virion release occurs independently of host cell lysis. Phage Dolos has been found to be exploited by a plasmid called pDolos. pDolos appears to be a cryptic, non-mobilizable plasmid that has been shown to be stable in cells during the absence of phage Dolos. In the presence of Dolos, pDolos can be transferred to other cells by transduction. Like other phage satellites, pDolos drastically reduces the virion output of the helper phage Dolos. Furthermore, a higher number of pDolos virions was detected in a supernatant containing both pDolos and Dolos virions. Interestingly, in contrast to all other phage satellites, pDolos has no recognisable phage genes. Thus, this study shows that phage satellites are much more diverse than previously assumed and that pDolos can be regarded as the first member of a new family of phage satellites, characterised by autonomously replicating plasmids without phage genes that hijack inoviruses. Considering the relatively simple requirements for a plasmid to hijack an inovirus, it is likely that such satellite systems are widespread. In addition, this study demonstrates a new transmission strategy for non-mobilizable plasmids by acting as phage satellites.

As an additional part of this study the mechanism of host acquisition by the virulent *Shewanella* phage Thanatos was investigated. Thanatos encodes two ADP-ribosyltransferases (ARTs), which are enzymes known to be host acquisition factors of *Escherichia* phage T4. These Thanatos ARTs are homologues of the phage T4 Alt protein and were consequently named Alt1 and Alt2. Phage particle proteomics demonstrated that both enzymes are highly abundant proteins of the Thanatos particle. In addition, both Thanatos ARTs are injected into the host cell during the phage DNA injection process and thus immediately ADP-ribosylate host proteins. Alt1 and Alt2 have been shown to be autocatalytic and have different ADP-ribosylation profiles. A protein interaction study revealed interactions with host proteins that are likely involved in anti-phage defence. Furthermore, it was shown that a functional loss of Alt2 drastically reduces the virion output of the phage Thanatos. This work therefor provides first insights into the function of ARTs for Thanatos-mediated host acquisition.

Zusammenfassung

Mobile genetische Elemente (MGEs) sind autonome genetische Einheiten, welche für die eigennützige Vermehrung auf Wirtszellen angewiesen sind. MGEs gelten als treibende Kraft der mikrobiellen Evolution, da sie den horizontalen Gentransfer weitgehend kontrollieren. Bakteriophagen (Phagen), Viren, die Bakterien infizieren, werden als MGEs klassifiziert. Phagen sind dafür bekannt, dass sie ihr Genom in eine Wirtszelle injizieren und diese dann in eine Virionen produzierende Fabrik umwandeln. Interessanterweise werden nicht nur Wirtszellen von MGEs ausgenutzt, einige MGEs beuten sogar andere MGEs aus, um ihren eigenen horizontalen Transfer zu erweitern. Sogenannte Satellitenphagen sind auf die Ausbeutung von Phagen spezialisiert. Die meisten Satellitenphagen sind integrative Elemente bakterieller Chromosomen, die einige, aber nicht genügend Strukturgene besitzen, um selbst Virionen zu produzieren. Diese MGEs sind daher für den horizontalen Transfer mittels Transduktion auf Phagenstrukturproteine angewiesen. Die daraus resultierende Satellitenphagen-abhängige Ausbeutung eines Phagen führt häufig zu einer verminderten Virionenproduktion des ausgebeuteten Phagen.

In dieser Arbeit wurde ein neuer *Shewanella* Phage namens Dolos charakterisiert. Dolos gehört zur Virusfamilie der *Inoviridae* und ist somit ein Phage, der eine chronisch-produktive Infektion durchführt. Die Dolos-vermittelte Freisetzung von Virionen erfolgt also unabhängig von einer Lyse der Wirtszellen. Es konnte in dieser Arbeit gezeigt werden, dass der Phage Dolos von einem Plasmid mit der Bezeichnung pDolos ausgenutzt wird. pDolos scheint ein kryptisches, nicht mobilisierbares Plasmid zu sein, welches auch in Abwesenheit des Phagen Dolos in Zellen stabil ist. In Gegenwart von Dolos kann pDolos sich mittels Transduktion verbreiten. Wie andere Satellitenphagen reduziert pDolos die Virionenproduktion des Helferphagen Dolos drastisch. Darüber hinaus konnte gezeigt werden, dass in einem Überstand, der sowohl pDolos- als auch Dolos-Virionen enthält, signifikant mehr pDolos-Virionen vorhanden sind. Interessanterweise besitzt pDolos im Gegensatz zu allen anderen Satellitenphagen keine erkennbaren Phagengene. Diese Studie zeigt also, dass Satellitenphagen viel vielfältiger sind als bisher angenommen und dass pDolos als erstes Mitglied einer neuen Familie von Satellitenphagen angesehen werden kann, welche sich durch autonom replizierende Plasmide ohne Phagengene auszeichnet, die Inoviren ausbeuten. Angesichts der relativ einfachen Bedingungen, die ein Plasmid erfüllen muss, um ein Inovirus auszubeuten, ist es wahrscheinlich, dass solche Satellitensysteme weit verbreitet sind. Darüber hinaus demonstriert diese Studie eine neue Übertragungsstrategie für nicht mobilisierbare Plasmide, indem diese als Satellitenphagen fungieren.

In einem weiteren Teil dieser Thesis wurde der Mechanismus des Wirtserwerbs durch den virulenten *Shewanella* Phagen Thanatos untersucht. Thanatos kodiert zwei ADP-Ribosyltransferasen (ARTs), Enzyme, die als Wirtserwerbsfaktoren des *Escherichia* Phagen T4 bekannt sind. Diese Thanatos-ARTs sind Homologe des Alt-Proteins des T4-Phagen und wurden daher Alt1 und Alt2 genannt. Eine Proteomanalyse der Phagenpartikel hat gezeigt, dass beide Enzyme in den Thanatos-Partikeln in sehr hoher Anzahl vorhanden sind. Außerdem werden beide Thanatos-ARTs während der Phagen-DNA-Injektion in die Wirtszelle

injiziert und ADP-ribosylieren daher sofort Wirtsproteinen. Alt1 und Alt2 sind nachweislich autokatalytisch und weisen unterschiedliche ADP-Ribosylierungsprofile auf. Eine Proteininteraktionsstudie weist auf Interaktionen mit Wirtsproteinen hin, die wahrscheinlich an der Abwehr von Phagen beteiligt sind. Darüber hinaus konnte gezeigt werden, dass ein Funktionsverlust von Alt2 die Virionenproduktion des Phagen Thanatos drastisch reduziert. Diese Arbeit liefert somit erste Einblicke in die Funktion von ARTs bei dem Thanatos-vermittelten Wirtserwerb.

Table of contents

1. Introduction

1.1 Mobile genetic elements

Mobile genetic elements (MGEs), are autonomous genetic agents that use host cells for their selfish propagation [1, 2]. The spread of MGEs occurs either vertically, together with the cell division of the host cell, or horizontally, by transmission from one cell to another [2, 3]. However, many MGEs use both distribution strategies. Horizontal transmission of MGEs occurs in microbes through conjugation, transduction, or transformation [4]. The transfer of genetic material through cell-cell contact is termed conjugation [5], whereas the transfer of genetic material through viral particles (virions) is termed transduction [6]. Both conjugation and transduction are types of horizontal transfer that can only be carried out by MGEs with specific capabilities. These horizontal transfer strategies are therefore active processes controlled by MGEs. Transformation, on the other hand, is a form of horizontal transfer of genetic information in which cells take up free DNA from the environment. This process is completely independent of any capabilities of a MGE [7]. In summary, the horizontal transfer of MGEs is considered to be the main driver of intercellular gene transfer leading to large pangenomes of microbial species [2].

MGEs are widespread in all three domains of life, and horizontal gene transfer mediated by MGEs has uniquely shaped life and biodiversity [1, 2, 8–10]. Coevolution of MGEs and cellular life is therefore regarded as a highly important factor for evolution [1, 2, 11–14]. In humans, it is currently estimated that one half to two thirds of the genome consists of MGEs [11, 15]. In bacteria, MGEs can make up to 40% of the genome, depending on the species [16]. In addition to their frequency within genomes, MGEs are also highly diverse. The group of MGEs includes, for example, integrative elements such as transposons, retrotransposons, group I and II introns, integrative conjugative elements (ICEs) as well as some viruses and satellite elements such as phage satellites. However, extrachromosomal MGEs such as plasmids or viruses, are also commonly found in all domains of life [1, 8, 9, 17, 18]. In Archaea, for example, plasmids can comprise more than 25% of the total genetic material of a cell [19, 20] and viruses that infect bacteria, known as bacteriophages, are the most abundant biological entities on earth with about 10^{31} virions [21, 22]. To illustrate this very large number, it is also estimated that there are one trillion bacteriophages for every grain of sand on earth [21].

Interestingly, the reproduction of MGEs is very successful, even though their replication within a cell is sometimes very costly for the host, as they utilise the host's resources for their selfish reproduction [2]. These elements could therefore also be described as genetic parasites that exploit their host cell for their own reproduction. However, it's often not that simple, many MGEs carry genetic cargo which benefits the host cell, like virulence factors or resistance mechanisms [23–25]. To a certain extent, these cargo can thus be seen as factors to out-compete the high cellular costs, resulting from these elements [13]. Remarkably, MGEs compete for resources not only with the host, but also with other MGEs within a cell. Some MGEs even utilise resources from other MGEs for selfish horizontal spread. Phage satellites, for example, are

parasitic genetic elements that exploit bacteriophages by hijacking their viral structural proteins to package the phage satellite's genome. Therefore, phage satellites can be thought of as the viruses of the viruses. The implicated interactions of MGEs with the host and MGEs with other MGEs led to the philosophical assumption, promoted by Eduardo Rocha's group, that cells are playgrounds for MGEs and that the genomes of cells are shaped by the associated coevolutionary conflicts [2].

In the following, bacterial plasmids as well as the transducible MGEs, bacteriophages and phage satellites will be described in more detail.

1.1.1 Plasmids

The term plasmid was coined by Joshua Lederberg in 1952 [6]. Today, plasmids are regarded as *mobile*, or at least self-transmissible, *extrachromosomal*, *circular* genetic elements that are transferred into other species as *naked* DNA [6, 26]. Plasmids are widespread in nature and are found in all domains of life [8, 18, 26, 27]. MGEs of this kind can be categorised according to their mobility or replication mechanism.

Depending on their mobility, plasmids can be divided into three different groups: mobile, mobilizable and non-mobilizable plasmids [26, 28]. Mobile plasmids, also called conjugative plasmids, are usually very large. The median genome size of proteobacterial mobile plasmids is about 181 kbp [28]. The smallest described conjugative proteobacterial plasmid has a size of about 20 kbp [28]. Mobile plasmids are transferred horizontally by conjugation [26, 29]. Therefore, these plasmids contain genes that are crucial for conjugation, including mobility (*mob*) genes and genes for mating pair formation. Mob proteins are relaxases, which play a crucial role in DNA processing during conjugative transfer [28, 30, 31]. In contrast, genes responsible for mating pair formation are typically part of a type IV secretion system that provides a mating channel for conjugative transfer [28, 32, 33]. So-called mobilizable plasmids only harbour *mob* genes and are therefore dependent on mobile plasmids for horizontal transfer, as they are not able to form a mating channel themselves [26, 28]. The median genome size of proteobacterial mobilizable plasmids is about 35 kbp [28]. Interestingly, about half of the described plasmids are categorised as non-mobilizable [26, 28]. Therefore, it is unclear how they are transferred horizontally, as transfer by conjugation requires at least a Mob relaxase for DNA processing. The plasmids of this group vary widely in genome size, with very small plasmids (about 1 kbp) and large plasmids (1.9 Mbp) classified as non-mobilizable [28]. Consequently, it is not known how the term "*mobile*" in the plasmid definition is sometimes fulfilled, as the exact mechanism of horizontal transmission for many non-mobilizable plasmids is unknown [26].

Plasmids can also be categorised according to their replication mechanism. Circular bacterial plasmids can replicate by theta replication, strand-displacement replication and rolling-circle replication [19]. Rolling-circle replication is quite common for plasmids of Gram-positive bacteria, whereas most plasmids of Gram-negative bacteria replicate by theta replication, which is also the main known replication mechanism for bacterial chromosomes [34–36]. The three replication mechanisms mentioned are described in more detail

in the following. In addition, a simplified representation of the three replication mechanisms is shown in **Figure 1**.

Theta replication is named after the Greek letter 'theta' (θ) because an intermediate theta structure, resembling the Greek letter, is formed during this replication [35, 36]. The theta replication process starts at the origin of replication (*ori*) where the two strands are unwound and two replication forks are formed. The theta replication mechanism requires two host-derived replisomes and is usually bidirectional, resulting in a continuous synthesis of the leading-strand and a discontinuous synthesis of the lagging-strand [36]. Hence, a coupled leading- and lagging-strand synthesis occurs during theta replication [36]. The synthesis terminates at the terminus region, which is located opposite the *ori* region on a plasmid [19]. Finally, the theta replication produces two dsDNA plasmids, each with a parental and a newly synthesized DNA strand [19].

The strand-displacement replication is also a bidirectional replication mechanism [36]. The special feature here is that plasmids that carry out this type of replication are quite independent, as no cellular replisome is required for the synthesis of the lagging-strand [19, 36]. Since this replication mechanism is quite independent, these plasmids carry a large gene set for their replication, including several *rep* (replication) genes. This required gene set of strand-displacement replicating plasmids as well as the rather independent replication mechanism lead to a size limitation, so that the currently described strand-displacement replicating plasmids are all between 5 - 15 kbp in size [36, 37]. To simplify, the replication initiation is mediated by the plasmid-encoded RepC protein, which melts the DNA duplex at the *ori* [35, 36]. Within this fused region, a secondary hairpin structure is formed in each single strand, with the base of the hairpin acting as the starting point of DNA synthesis, as the plasmid-encoded RepB primase primes strand-displacement replication at these secondary structures [12]. The subsequent DNA synthesis occurs on both strands independently of each other, and replication takes place continuously on both strands [36]. A specially plasmid-encoded helicase called RepA is important for the DNA synthesis. This helicase supports the DNA melting process and is crucial for the continuous synthesis of the lagging-strand [35]. Continuous DNA synthesis on a single strand produces a single daughter strand, which separates the two parental strands and displaces one of them, forming a D-loop [19, 36]. Thus, in contrast to theta replicating plasmids, the leading- and lagging-strand synthesis of strand-displacement replicating plasmids is decoupled [36].

Another plasmid replication mechanism is rolling-circle replication. As with strand-displacement replication, the synthesis of the DNA strands is an uncoupled process and the synthesis is continuous for both strands [36]. The special feature here is that replication is unidirectional and not bidirectional [36, 38, 39]. Consequently, one strand is amplified first and then the other. Simplified, replication begins at the *ori*, a structure within the double-stranded DNA (dsDNA) that forms a highly complex hairpin structure [38, 39]. Within this hairpin structure, a nicking of the leading-strand is initiated by a specific own encoded Rep protein [38, 39]. The leading strand of the double-stranded plasmid DNA is replaced by the Rep protein while simultaneously the host DNA polymerase synthesises a new leading-strand. This replacement of the parental leading-strand by a newly synthesised leading-strand leads to a rolling-circle phenomenon, which

gives this type of replication its name [19, 38]. A special feature of rolling-circle replication is that a circular single-stranded DNA (ssDNA) intermediate is produced [36, 38, 39]. For this purpose, the parental linearised leading-strand is sealed by the plasmid-encoded Rep protein, resulting in a circular intermediate [38]. This single-stranded intermediate acts as a template for the synthesis of the lagging-strand, which begins at the single-stranded *ori* (*sso*), located on the ssDNA intermediate. Characteristically, the *sso* forms hairpin structures that leads to priming by the host RNA polymerase followed by host-derived synthesis of the lagging-strand [38].

There are currently 17 known plasmid families that carry out rolling-circle replication [38, 40]. These families differ mainly in the Rep protein used and the sequence and position of the nick sequence [38]. The size of the currently described rolling-circle replication plasmids ranges from less than 1 kbp to 30 kbp [41]. The best described rolling-circle replicating plasmids are the plasmid pC194 with a genome size of 2.9 kbp, the plasmid pT181 with a size of 4.5 kbp and the plasmid pMV158 with a size of 5.5 kbp [38].

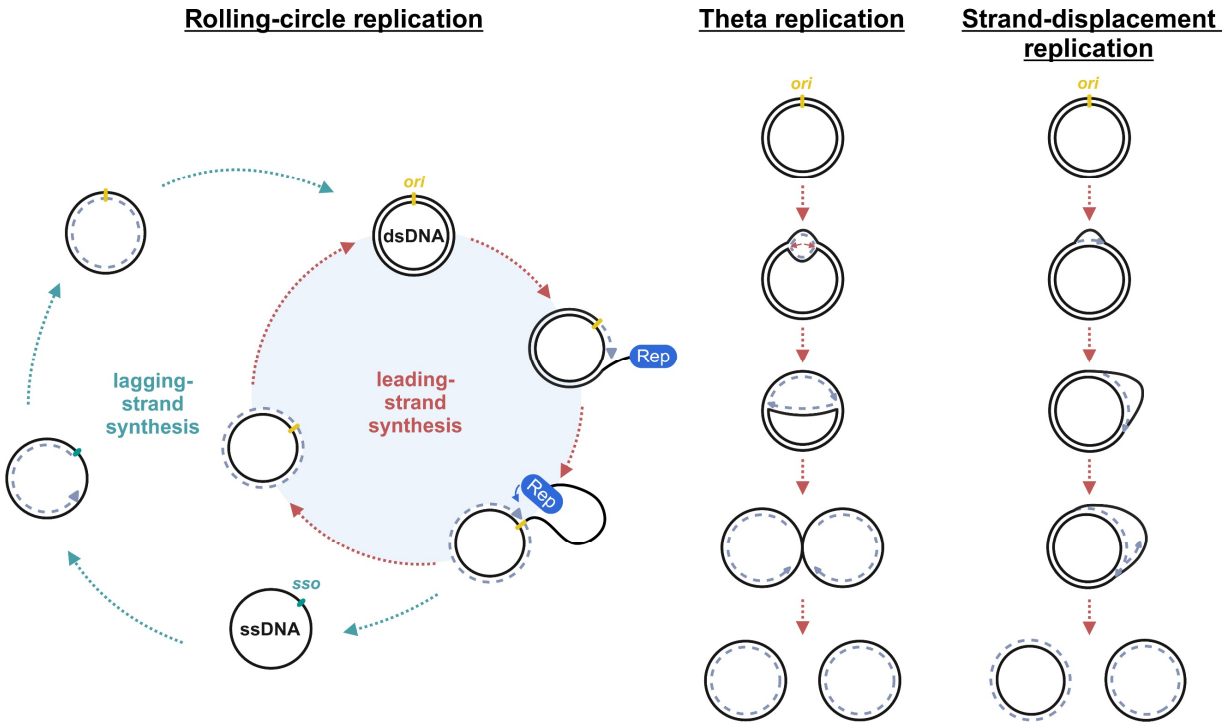

Figure 1: Plasmid replication mechanisms. Illustrated are in a simplified way the rolling-circle replication, the theta replication and the strand-displacement replication. *ori*: origin of replication, *sso*: single-stranded origin of replication, Rep: Rep protein.

1.1.2 Bacteriophages

Bacteriophages (phages) are viruses that infect bacteria. Such MGEs carry genes to package their own genetic information. Phages are therefore transmitted horizontally by transduction [1]. Bacteriophages are the most abundant biological entities on Earth with approximately 10^{31} particles [21, 22]. Moreover, phage particles are estimated to be 10 times more numerous than the most abundant organisms on Earth, bacteria [42]. Phages have been shown to influence bacterial communities in various ecosystems and thus drive bacterial evolution [43]. For example, phages are estimated to kill 15-40% of marine bacteria per day, resulting in a high turnover of biomass [25]. Since many phages lyse and thus kill their host at the end of their infection cycle, the phage-mediated selection pressure on bacteria is high, which leads to an arms race between bacteria and phages [42, 43]. This coevolutionary arms race is currently a focus of phage-host interaction research. Phages try to infect and control host cells in order to reproduce themselves. Bacteria, on the other hand, defend themselves with various anti-phage defence systems, which in turn are targeted by the viral invaders [44].

Phages are very diverse and can be categorised into several groups according to their virion morphology, their genome type and their main reproduction strategy [25, 45]. A grouping of phages according to their genome type or their virion morphology is illustrated in **Figure 2**.

Phages have diverse genome types, including dsDNA, ssDNA, dsRNA, and ssRNA. However, most of the phages currently described are dsDNA viruses with genome sizes ranging from 10 to 500 kbp [46, 47]. The morphology of phages can also differ drastically. More than 95% of the described phages have virions with a head-tail morphology (tailed phages) [48]. Tailed phages belong to the viral class *Caudoviricetes*, which can be divided into three morphological groups: the myoviruses, the siphoviruses and the podoviruses [49, 50]. Typically, myoviruses have long contractile tails, siphoviruses have long flexible non-contractile tails and podoviruses have short non-contractile tails [25]. However, other virion morphologies have also been described, such as the icosahedral enveloped particles of the *Cystoviridae*, or the rod-shaped particles of the *Plectroviridae*, or the long filamentous particles that characterise the viral family *Inoviridae* [45].

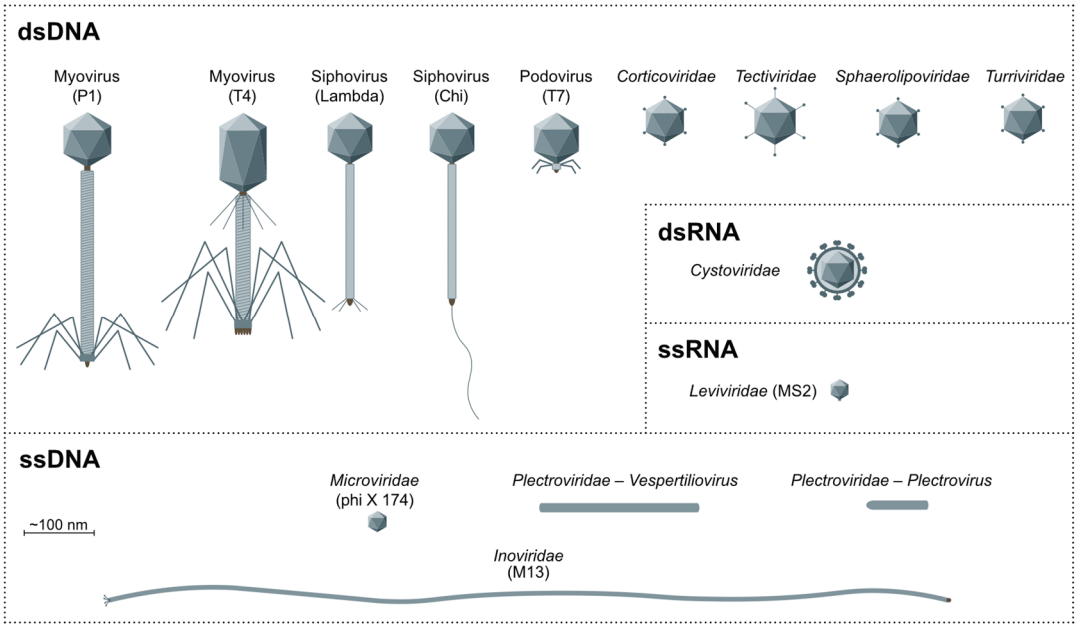

Figure 2: Phage grouping based on their genome type and virion morphology. Modified image from Hay and Lithgow, 2019 [45].

Phages can also be grouped according to their main reproduction strategy. Currently, five different phage propagation strategies on single-cell level have been described: the lytic life cycle, the lysogenic life cycle, the pseudolysogenic life cycle as well as a chronic-productive life cycle and a chronic life cycle which is non-productive [51]. The most frequently described and best-studied mechanisms of phage reproduction are the lytic and lysogenic life cycles [51].

For transduction and therefore horizontal transmission of the viral genome, the majority of the described phages lyse and thus kill a host cell at the end of their life cycle in order to release the produced virions. However, not all phages rely on host cell lysis to release virions for horizontal transfer; some phages carry out a so-called chronic infection [51]. Chronic infections can be non-productive, meaning that the potential virion release is not actively mediated by a phage (e.g. *Pseudomonas* phage phi6) [52], or productive, and thus depend on a phage-mediated virion release via a budding-like process (e.g. *Acholeplasma* phage L2) [53] or an extrusion process (e.g. *Escherichia* phage M13) [54]. The chronic life cycles performed at the single-cell level naturally lead to a stable infection at the population level. Interestingly, even phages that kill their host cell at the end of their infection cycle are often described to cause stable infections at the population level. This phenomenon at the population level is referred to as "carrier state life cycle" [51]. At the population level, a mixture of phage-sensitive and phage-resistant bacteria leads to an infection that results in a stable equilibrium. A special case, however, is the chronic but non-productive infection caused by the *Pseudomonas* phage phi6 [51]. It is known that phage phi6 is able to lyse and thus kill host cells, but also chronic phi6 infections are sometimes described at single-cell level [51]. The chronic life cycle of phi6 is thought to be a coevolutionary event, as some *Pseudomonas* strains are resistant to phi6-mediated cell lysis, resulting in carrier cells in which phi6 virions are produced but not released in a phage-dependent manner [52]. The release of

phi6 virions in a chronic but non-productive infection thus appears to be a rare and phage-independent event [51].
In the following the most prominent life cycles, the lytic and lysogenic life cycles as well as the rather rare chronic-productive life cycle performed by members of the viral family *Inoviridae*, will be described in more detail.

The lytic and lysogenic life cycles

Virulent phages carry out the lytic cycle in order to multiply [25]. This life cycle can be divided into five steps. First, a virion must adsorb to a host cell, whereupon the viral genome is injected into the host. This step is followed by host factor-dependent replication of the viral genome, as well as transcription and translation of the viral genes. The structural proteins of the phage are then assembled in the host cell, leading to the production of fully functional virions within the host. Finally, the infected host cell is lysed in a phage-dependent manner, which leads to the release of virions, after which the cycle can begin anew (**Figure 3**).
During the lytic life cycle, bacterial hosts are reprogrammed in a phage-dependent manner that transforms the cells into virion-producing factory [55, 56]. Many virulent phages are described to inject not only their DNA into the host, but also enzymes from the group of host acquisition factors (HAFs), which, among others, are able to modify host proteins and thus presumably change their function in such a way that they benefit the phage [55, 57]. In addition, some virulent phages use specific HAFs to completely degrade the host chromosome, leaving an enveloped space full of resources that benefit the viral invader [58, 59].

Temperate phages undergo the lysogenic life cycle in order to propagate [25]. After genome injection, the viral genome persists either episomally or integrates into the host chromosome (**Figure 3**). This state of persistence is referred to as prophage [25]. During the lysogenic life cycle, no virions are produced, so that no horizontal transmission takes place. Therefore, prophage transmission is performed vertically by cell division. Under certain stress conditions, such as DNA-damaging stress or a cold shock, prophage induction occurs and the temperate phage enters a pro-active life cycle, often the lytic life cycle.
Due to the persistence of temperate phages, one could assume that these viruses have a rather low impact on their host under stress-free conditions. However, this is not the case. Temperate phages often carry cargo, such as antibiotic resistance genes or virulence factors, which impact the bacterial lifestyle and the bacterial stress resistance [60, 61]. For example, only *Vibrio cholerae* strains carrying the prophage CTXφ are virulent and able to cause the diarrheal disease cholera [62]. In addition, stochastically induced spontaneous prophage induction has a major impact on the bacterial lifestyle. For example, it is known that spontaneous prophage induction has a positive effect on biofilm formation [61, 63–65]. This effect often is attributed to the fact that phage-dependent lysis of bacteria releases DNA, which increases the amount of extracellular DNA (eDNA), being an essential component of the biofilm matrix [63, 66–68].

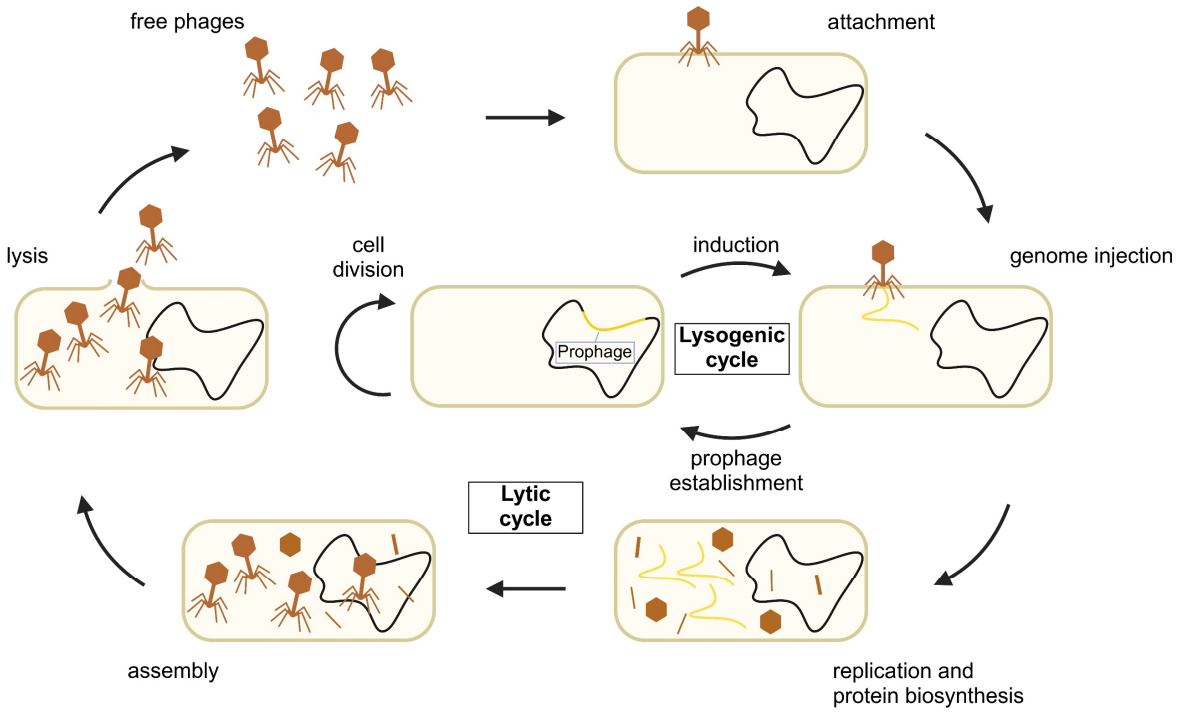

Figure 3: The lytic and lysogenic life cycles of phage propagation. Shown is the lytic propagation, which ultimately leads to cell lysis of the infected host cell, and the lysogenic propagation, which is characterised by a state of persistence in which the phages are transmitted vertically by cell division.

Inoviruses and their chronic-productive life cycle

Members of the viral family *Inoviridae* (inoviruses) are filamentous phages [45, 69]. Their long, filamentous particles measure 6 to 10 nm in width and 600 to 2500 nm in length [70]. Hence, these virions are comparatively thin and long. The most frequently found tailed phages are much shorter. For example, the *Escherichia coli* siphovirus Lambda has a virion length of approximately 200 nm [71] and the *Shewanella* myovirus Thanatos has a particle length of about 110 nm and a particle width of about 70 nm [72]. A characteristic feature of inovirus virions is that these particles all attach to pili to enter a host [70]. The genome of inoviruses typically consists of a circular (+)-sense ssDNA and is between 5.5 and 10.6 kbp in size, coding for 7 to 15 proteins [70]. Some inoviruses are able to integrate into the host chromosome and can therefore persist as prophages, such as the filamentous *Vibrio* phage CTXφ, which carries the well-known cholera toxin [62]. Other inoviruses do not integrate into the host chromosome. Instead, they remain extrachromosomally as a plasmid in a host cell [45]. Replication of the extrachromosomal circular inoviral genome typically occurs by the rolling-circle mechanism [45, 69]. Another characteristic of inoviruses is the absence of phage-dependent cell lysis, which is due to their unique chronic-productive life cycle [45]. Furthermore, inoviruses can produce a high yield of about 10^{13} virions per ml due to their chronic infections [45].

The best-studied members of the family *Inoviridae* are the Ff coliphages. Phages of this group infect *Escherichia coli* and attach to the F-pilus of the cells. The Ff coliphages include phage f1, phage fd and phage M13 [73]. These filamentous phages were discovered independently in the early 1960s, with f1 isolated at the Rockefeller University in 1960 [74] , M13 isolated in Munich in 1963 [75] and fd identified in Heidelberg in 1963 [76]. Genome analysis revealed that they are almost identical viruses with 98% nucleotide identity [73].

A schematic genome map of a Ff phage is illustrated in **Figure 4 A** and displays 11 open reading frames (ORFs), which are defined from gI to gXI [69]. The length of the ORFs, their location within the genome and the protein domains of the protein products encoded by them are crucial for the ORF assignment of inoviruses, as genes and proteins encoded by inoviruses are generally not conserved [69]. For instance, the major capsid protein of Ff coliphages and the major capsid protein of *Pseudomonas* phage Pf1 share only 13% amino acid identity [69].

The virion structure of a Ff coliphage is shown in **Figure 4 B**. This illustrated virion shows the inoviral structural proteins pIII, pVI, pVII, pVIII and pIX which are derived from the structural genes gIII, gVI, gVII, gVIII and gIX. A list of the functions of all Ff phage proteins is shown in **Table 1**.

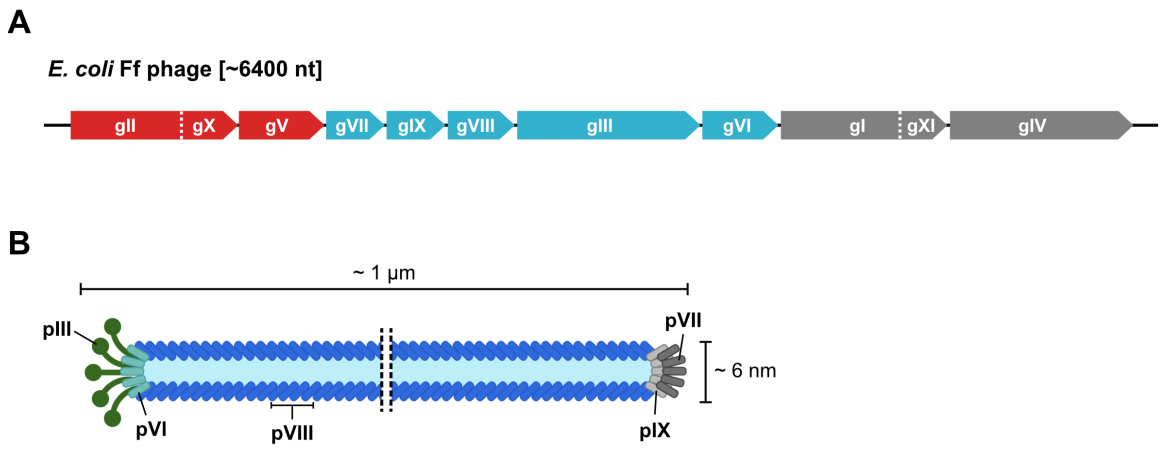

Figure 4: Filamentous Ff page. A. Genome chart of a filamentous Ff phage. Red: function in replication, blue: structural function, grey: secretional function. **B.** Schematic virion structure of a Ff phage.

Table 1: Filamentous Ff phage proteins and their function. aa: amino acids.

Protein name	Group	Function	Length [aa]
pII	Replication	Replication endonuclease	410
pX	Replication	Replication-associated protein	111
pV	Replication	ssDNA binding protein (protects ssDNA)	87
pVII	Structural	Minor coat protein	33
pIX	Structural	Minor coat protein	32
pVIII	Structural	Major coat protein	73
pIII	Structural	Attachment protein	424
pVI	Structural	Minor coat protein	112
pI	Assembly/Secretion	Virion assembly/secretory pore protein	348
pXI	Assembly/Secretion	Virion assembly/secretory pore protein	108
pIV	Assembly/Secretion	Virion assembly/secretory pore protein	426

Inoviruses carry out a chronic-productive infection and therefore do not lyse their host cell to release virions, as inovirus virions are released by extrusion [45, 69, 77] (**Figure 5**). A special feature is that the virions are not assembled in the cytoplasm and then released. Due to the large size of the viral particles, virion assembly and secretion occur simultaneously.

After the injection of the inoviral ssDNA genome into a host cell, the host RNA polymerase synthesises a short RNA primer [77], followed by host DNA polymerase III-dependent synthesis of the viral (-)-strand, which results in a dsDNA genome [77]. The viral dsDNA genome is the so-called replicative form (RF) of the genome [45]. On the one hand, the RF is used for the host-dependent gene expression of viral genes; on the other hand, the RF is important for viral replication, which is conducted by the rolling-circle mechanism [45, 70]. The viral endonuclease pII initiates rolling-circle replication by nicking the (+)-strand of the RF [77]. The circular ssDNA produced is usually an intermediate of replication for rolling-circle replicating plasmids (refer to section **1.1.1. Plasmids**), but in the replication of inoviruses the ssDNA serves as the infectious form (IF) of the viral DNA [45]. The IF is thus packaged into virions and secreted. For this purpose, the IF is first coated with pV and thus protected from nuclease digestion [69]. A small hairpin, the viral packaging signal, is not enveloped by pV and is therefore exposed [45, 77]. Viral assembly and secretion then take place at the membrane, as the viral structural proteins are all transmembrane proteins and therefore located within the inner membrane. The viral assembly and secretion proteins pI, pXI and pIV form a secretion channel across the outer membrane. Viral assembly and secretion is initiated by interaction of the minor capsid proteins pIX and pVII with the exposed packaging signal of the IF [45]. pIX and pVII form the cap of the virion, whereupon the pV proteins are removed in a continuous process and replaced by the major capsid protein pVIII [45]. Finally, the minor capsid proteins pIII and pVI cap the other end of the viral ssDNA genome and the assembled virion is completely released via the secretion channel.

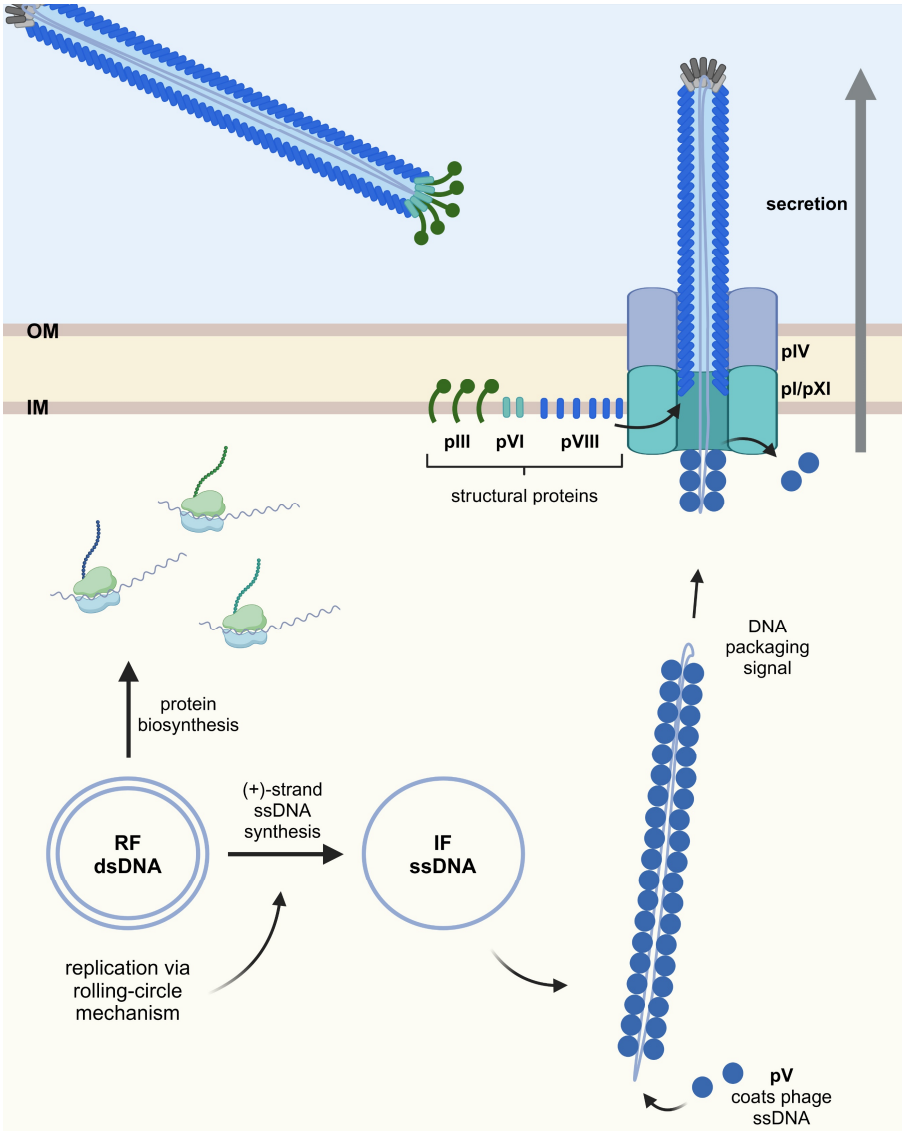

Figure 5: The chronic-productive life cycle of inoviruses. Intracellularly, the extrachromosomal genome of inoviruses is present as a replicative form (RF) or an infectious form (IF). The double-stranded RF is used for phage-mediated replication, which takes place via the rolling-circle mechanism. The replication mechanism used generates the (+)-stranded ssDNA, which represents the IF. Protein biosynthesis takes place using the RF as a template. The IF is enveloped by the ssDNA binding protein pV, but the packaging signal within the IF remains uncovered. Viral assembly and secretion take place simultaneously at the membrane. Initially, the viral proteins pIX and pVII interact with the packaging signal and form a cap, followed by the removal of the pV proteins, which are replaced by the major capsid protein pVIII. Finally, the minor capsid proteins pIII and pVI cap the other side of the virion and the virion is released through the secretory channel formed by pIV and pI/pXI.

Ff coliphages are the model system for inoviruses and have historically been a fundamental tool in biotechnology. In 1980, a vector derived from Ff phages was developed by Sanger *et al.* and used for rapid DNA sequencing [78]. In addition, a system for *in vitro* oligonucleotide-directed mutagenesis was developed on the basis of cloning vectors derived from Ff phages [79]. Moreover, the biotechnological method of phage display, which is still widely used, relies on filamentous phages [80, 81]. Phage display is a method for identifying protein-protein, protein-peptide or protein-DNA interactions. This biotechnological approach is of great importance as, for example, antibodies for therapy have been identified by phage

display [81, 82]. For phage display, huge recombinant phage libraries are created so that interaction partners can be determined using high-throughput screening. The special feature of these recombinant phages is that the bait protein fused to a viral coat protein are automatically linked to the genetic information it encode [81]. To produce these recombinant phages, a phagemid vector as well as a helper phage are required. Phagemid vectors typically comprise a recombinant viral coat gene and an inoviral intergenic region that includes the packaging signal and the viral origin of replication [80, 81]. The phagemid DNA is packaged by a helper phage, usually a derivative of an Ff coliphage, which provides the phagemid with the missing viral coat proteins. The helper phage itself, however, lacks the packaging signal and the natural origin of replication, so it is unable to package itself [80].
Inoviruses and their potential applications have therefore become an integral part of many biotechnological methods.

1.1.3 Phage satellites

Phage satellites are MGEs that actively utilise phages for their selfish replication [83]. Phage satellites are described as integrative MGEs and are frequently found in bacterial chromosomes [83]. Currently, 5 families of phage satellites have been described: the P4-like satellites, the phage-inducible chromosomal islands (PICIs), the capsid-forming PICIs, the phage-inducible chromosomal minimalist islands (PICMIs) and the phage-inducible chromosomal island-like elements (PLEs). The best-studied family is the P4-like satellite family. The research field of phage satellites is on the rise due to extended genome analysis and the development of new analytical tools [84] For example, two of the mentioned families were recently discovered and described: the familiy of capsid-forming PICIs in 2023 by Alqurainy *et al.* [85] and the family of PICMIs in 2024 by Barcia-Cruz *et al.* [86].

What all currently described satellite families have in common is that they are integrative elements that use phages for horizontal transfer. Phage satellites are characterised by the fact that they lack some structural proteins and that they are dependent on a helper phage for the production of satellite-containing virions [83]. They therefore hijack the phage packaging machinery. This hijacking often leads to a reduction in phage-containing virions [83]. Phage satellites therefore often have a negative effect on the viral fitness and can thus be regarded to a certain extent as viruses of viruses. Their size varies between about 6.7 kbp (PICMIs) and 18 kbp (PLEs) [2, 83, 86]. By default, the satellite genome is typically one third the size of the helper phage genome [83]. Each phage satellite family has specific characteristics, including the lifestyle of the helper phages used. For example, PICIs, capsid-forming PICIs and P4-like satellites typically utilise temperate phages, whereas PLEs and PICMIs typically exploit virulent phages [86].
Special features of the P4-like satellite family are that these satellites sometimes persist episomally in cells and that they have developed a distinctive mechanism for remodelling the capsids of their helper phages [87, 88]. Thus, when a cell carrying a P4-like satellite is infected with a potential helper phage, the phage capsid is remodelled in a specific way, resulting in smaller satellite-containing capsids [83, 88]. Capsid-

forming PICIs are unique among the phage satellite families in that they encode their own capsid and only require the tail proteins of a helper phage for complete virion formation [85]. PLEs are identified exclusively in *Vibrio cholerae* and are characterised by the fact that these satellites completely prevents the production of virulent helper phage progeny, while all other satellite families have only a limited influence on the proliferation of their helper phages [83]. PICMIs are characterised by their small size (average: 6.7 bp) and their low gene number [86]. In contrast to PLEs, PICMIs utilise virulent phages without strongly affecting the fitness of their helper phages [86]. PICIs, on the other hand, are the most widespread phage satellites and typically hijack temperate phages [83].

Recent research has shown that phage satellites are hotspots for anti-phage defence mechanisms [89, 90]. It has been demonstrated that both P4-like satellites [89] and PICIs [90] encode anti-phage systems. These systems provide satellite-dependent protection for the bacterial host and the hijacked temperate helper phage against invading virulent phages. Therefore, satellites are not only parasites of phages. Rather, it appears that under certain circumstances the parasitic relationship can change into a mutualistic relationship [89].

1.2 The model organism *Shewanella oneidensis* MR-1

Shewanella oneidensis MR-1 is a facultative anaerobic and motile gammaproteobacterium belonging to the genus *Shewanella*. Natural habitats of species of the genus *Shewanella* include the sea water, the deep sea, brackish water and freshwater sediments [91]. The genus *Shewanella* comprises more than 40 species, and the bacteria of this genus are known to utilise a wide range of organic and inorganic electron acceptors for respiration, such as radionuclides or chlorinated compounds [91]. Typical for the genus *Shewanella* is that it consists of a diverse group of facultatively anaerobic aquatic bacteria. Moreover, the genus *Shewanella* is widespread, partly due to the psychrotolerance of bacteria [92].

S. oneidensis MR-1 was originally isolated in 1988 from Lake Oneida in the state of New York (USA) [93]. *S. oneidensis* MR-1 cells have a single polar flagellum and are rod-shaped with a length of about 2-3 µm and a width of about 0.4-0.7 µm. *S. oneidensis* MR-1 is known for its ability to utilise insoluble manganese oxide as a terminal electron acceptor during anaerobic aspiration, which led to the name manganese-reducing (MR) [93]. The genome of *S. oneidensis* MR-1 consists of a circular chromosome of 4.9 Mbp with 4,318 protein-encoding genes and a megaplasmid of 161 kbp with 149 protein-encoding genes [94]. *S. oneidensis* MR-1 is able to form complex structured biofilms on a variety of surfaces, making it not only an interesting model for respiratory research, but also a lucrative model organism for biofilm research [95–97].

1.2.1 Biofilm formation of *S. oneidensis* MR-1

There are two main types of bacterial lifestyle: a planktonic and therefore a motile lifestyle, and a sessile lifestyle, usually referred to as a biofilm. Biofilms are defined as surface-associated bacterial communities embedded in a self-produced matrix [98]. For most bacteria, this type of sessile lifestyle is the predominant way of life. Biofilms are therefore widespread and occur in various environment [99]. Biofilms are characterised by the fact that the cells, which often originate from several species, share a unique social way of life [100]. Cells within a biofilm are protected against various stressors such as UV light, extreme pH levels, phages and antibiotics [101]. This lifestyle-related stress resistance of bacteria is therefore of great importance for mankind and especially for the healthcare system.

Biofilms are composed of cells embedded in a self-produced matrix. The self-produced biofilm matrix consists of 97% water. In addition to water, the matrix consists of extracellular polymeric substances (EPS) such as extracellular DNA (eDNA), extracellular polysaccharides and proteins. These EPS give the matrix unique properties that favour the stress resistance of bacteria [102]. The formation of a bacterial biofilm is divided into different stages (**Figure 6**). Firstly, individual planktonic cells attach to a surface [98]. Depending on the species, this step can take place via the cell pole, the flagellum or pili. For *S. oneidensis* MR-1, attachment to a surface is mediated by the mannose-sensitive haemagglutinin (MSHA) type IV pilus [96]. In general, type IV pili are complex protein machineries characterised by long extracellular filaments [103]. These filaments polymerise and depolymerise very rapidly, leading to extension and retraction of the extracellular filaments. The activity of the MSHA pilus, which is important for cellular attachment onto surfaces and therefore important for biofilm formation of *S. oneidensis* MR-1, is dependent on the second messenger cyclic di-guanylate (c-di-GMP) [104, 105]. This second messenger thus drastically influences the lifestyle of *S. oneidensis* MR-1. High c-di-GMP concentrations regulate the extension of the pilus and thus favour the attachment of individual cells to a surface. After the attachment of single cells to a surface, the biofilm matrix is formed, which leads to the development of microcolonies [98]. The subsequent growth of the biofilm leads to the development of a mature biofilm. A mature biofilm consists of complex three-dimensional architecture made up of cells embedded in their self-produced matrix. Finally, factors such as physical shear forces cause biofilm dispersal. In this process, cells are released from the biofilm and can switch to the planktonic lifestyle [98].

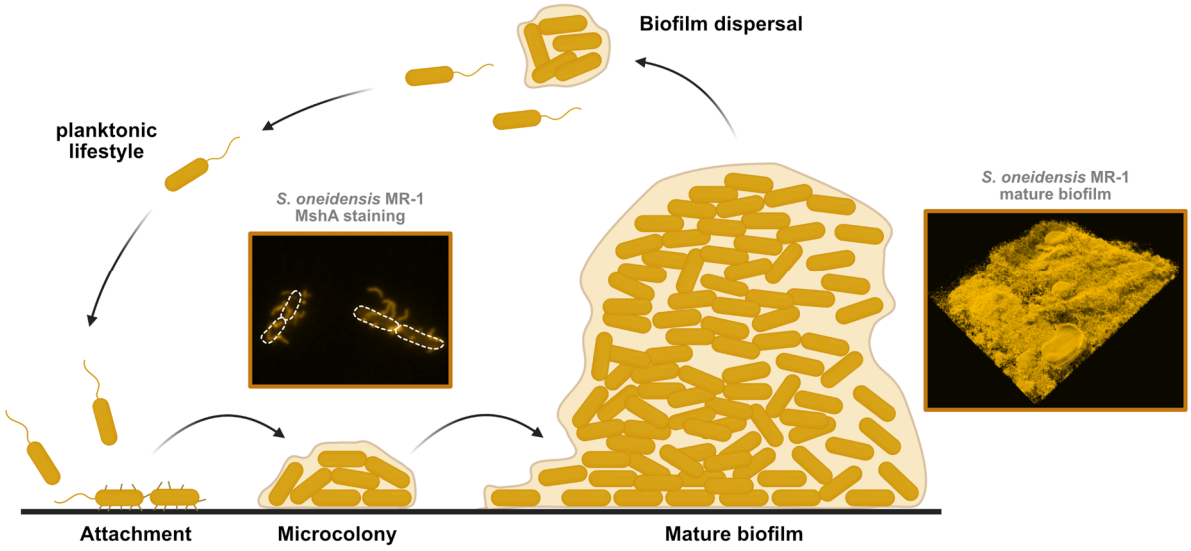

Figure 6: Development of a *S. oneidensis* MR-1 biofilm. The initial MSHA pilus-mediated cell attachment to a surface is shown. Subsequently, the formation of a microcolony can be seen. At this stage, the cells are already embedded in a self-produced matrix. Growth-mediated, a mature biofilm develops from this stage, which is characterised by a complex three-dimensional architecture. Factors such as physical shear forces cause biofilm dispersal. Detached cells are able to return to the planktonic lifestyle. A MshA stain is shown as a microscopic image visualising the MSHA pili, which are important for cell attachment to surfaces. A three-dimensional microscopic image of a mature *S. oneidensis* MR-1 biofilm is also shown, illustrating the complex biofilm architecture [106].

1.2.2 Phages of *S. oneidensis* MR-1

S. oneidensis MR-1 carries four prophages in its genome: LambdaSo, MuSo1, MuSo2 and CP4So. While LambdaSo, MuSoI and MuSoII were identified by the genome sequencing of *S. oneidensis* MR-1 in 2002 [107], CP4So was identified much later in 2016 [108]. LambdaSo and MuSo2 are known to be able to produce virions, whereas MuSo1 and CP4So are cryptic and therefore unable to form infectious particles [63, 108]. The prophages of *S. oneidensis* MR-1, in particular the active lambda-like phage LambdaSo, have been shown to strongly influence the biofilm formation of *S. oneidensis* MR-1, as spontaneous induction of the prophages increases the amount of eDNA within a biofilm, which stabilises the matrix and promotes biofilm formation [63]. It could therefore be shown that prophage-mediated lysis of a subpopulation can positively influence the growth of a bacterial community [63]. A positive effect caused by spontaneous prophage induction on biofilms has not only been demonstrated for *Shewanella*, but rather appears to be a quite common occurrence, which has also been described for *Staphylococcus aureus* [109] and *Streptococcus pneumoniae* [67].

The presence of four prophages as well as the presence of several anti-phage defence systems in the genome of *S. oneidensis* MR-1 suggests a high phage pressure. Consequently, it was investigated whether novel phages infecting *S. oneidensis* MR-1 could be isolated from freshwater sediment samples and whether *S. oneidensis* MR-1 could also serve as a model organism to analyse phage-host interactions. Therefore, an extensive sampling was carried out a few years ago in which new tailed phages infecting *S. oneidensis* MR-1 were identified in various aquatic and freshwater sediment samples. One of these newly described *Shewanella*

phages, named Thanatos, is a tailed phage that belongs to the morphological group of myoviruses [72]. The dsDNA genome of Thanatos has a size of 160 kbp and encodes 206 proteins [72]. The *Shewanella* phage Thanatos seems to be highly similar to the *E. coli* phage T4, as 66 Thanatos genes are homologous to genes of the phage T4. Most of these homologous genes code for structural proteins and proteins that are important for DNA replication and packaging. The large number of homologous genes suggests that the major viral functions of Thanatos and T4 are likely to be similar [72]. Thanatos performs the lytic life cycle, whereby the latency time of the phage Thanatos under the tested conditions was about 40 minutes and about 20 particles were produced per cell [72]. Furthermore, the addition of Thanatos during biofilm formation of *S. oneidensis* MR-1 was shown to enhance biofilm formation. This effect also appears to be due to a phage-mediated increase in the amount of eDNA within the biofilm. Interestingly, on the other hand, the addition of Thanatos to mature biofilms led to a drastic reduction in the biofilm biomass [72].

Recent work thus shows that *S. oneidensis* MR-1 could also serve as a lucrative model organism of biofilm-producing gammaproteobacteria to study phage-host interactions.

1.3 Project aim

The aim of this thesis was to identify and characterise new phages infecting *S. oneidensis* MR-1.

In addition, the mechanism of host acquisition of the virulent *Shewanella* phage Thanatos should be analysed in more detail to gain a deeper insight into how virulent phages hijack bacterial host cells and become phage-producing factories.

2. Results

2.1 Analysis of the *Shewanella* phage Dolos and the plasmid pDolos

One aim of this study was to characterise new bacteriophages infecting *Shewanella oneidensis* MR-1 in order to analyse phage-host interactions in more detail. In a previous study, freshwater sediment samples were collected from aquatic environments presumed to be habitats for *S. oneidensis* MR-1 [72]. One of these samples, was analysed in more detail in this thesis.

To obtain new phages infecting *S. oneidensis* MR-1, a freshwater sediment sample was incubated with *S. oneidensis* MR-1 ΔLambdaSo ΔMuSo2. This step was used to enrich potential phages contained in the sample. The mentioned bacterial strain used for this enrichment step lacks both active prophages (LambdaSo and MuSo2) and was taken as host organism for this study in order to exclude experimental side effects caused by the prophages of *S. oneidensis* MR-1. In the following, this strain is referred to as *S. oneidensis* ΔΔ. After incubation of the sample with *S. oneidensis* ΔΔ, the cell culture supernatant was collected and spotted onto a developing *S. oneidensis* ΔΔ cell lawn. Using this procedure, the successful enrichment of *Shewanella* phages was verified. The virion DNA was then isolated from the prepared virion-containing supernatant, and the collected DNA was analysed by gel electrophoresis to obtain a first indication of whether a single viral species or divers, possibly interdependent, infectious species were enriched. **Figure 7 A** displays the virion DNA of this sample, revealing several DNA bands of different sizes. Following, this mixture of purified virion DNA was sequenced by David Brandt and Jörn Kalinowski (CeBiTec, Bielefeld University) using the Oxford Nanopore method [110]. The resulting genomes were then annotated using the Prokka tool [111].

The sequencing yielded two different circular ssDNA sequences. Since ssDNA is able to form base pairs with itself, the large number of DNA bands of different sizes visible after gel electrophoresis could be due to self-interaction or different structures of the circular ssDNA (**Figure 7 A**). The two ssDNA genomes present in the virion-containing supernatant were 8,146 nt and 2,926 nt in size, of which the former was identified as a phage possessing 11 open reading frames (ORFs). One of these ORFs was predicted by BLASTp [112] to encode a protein possessing a Zot (zonular occludens toxin) domain, which is a highly conserved domain of ssDNA viruses of the family *Inoviridae* [113, 114]. The protein containing the Zot domain has been annotated as pI (protein I) virion assembly and export protein and is listed in the schematic genome chart as gI (gene I) (**Figure 7 C**). The newly isolated inovirus was named "Dolos", after the spirit of trickery from ancient Greek mythology [115], as these phages cause a chronic infection of the host, which is often overlooked due to the lack of viral lysis [116, 117]. The further classification of the viral proteins was carried out as usual for inoviruses, mainly by analysing the protein domains via InterPro [118], the protein length and the order of the ORFs in the genome (**Supplementary Table 1**). The inovirus structural proteins pVIII, pIII and pVI as well as the pII and pV proteins important for replication were predicted. 4 proteins of Dolos remained with unknown function.

The other isolated circular ssDNA genome with a size of 2,926 nt was identified as a plasmid and was named pDolos because of its associated isolation with phage Dolos. pDolos comprises 5 ORFs, 4 of which have an unknown function and one of which was predicted by BLASTp [112] to encode a Rep protein (**Figure 7 B**). Rep proteins are essential for plasmid replication and are therefore involved in theta, rolling-circle and strand-displacement replication [39]. None of the pDolos ORFs were predicted to code for packaging proteins. However, pDolos must also be packaged in some way, since the plasmid DNA was isolated from virions.

Further sequencing of chromosomal DNA from infected *S. oneidensis* MR-1 cells indicated that neither the phage Dolos nor the plasmid pDolos are integrated into the host chromosome, suggesting that phage Dolos cannot persist as a prophage in *S. oneidensis* MR-1, as for example the inovirus CTXφ does in *Vibrio cholerae* [119].

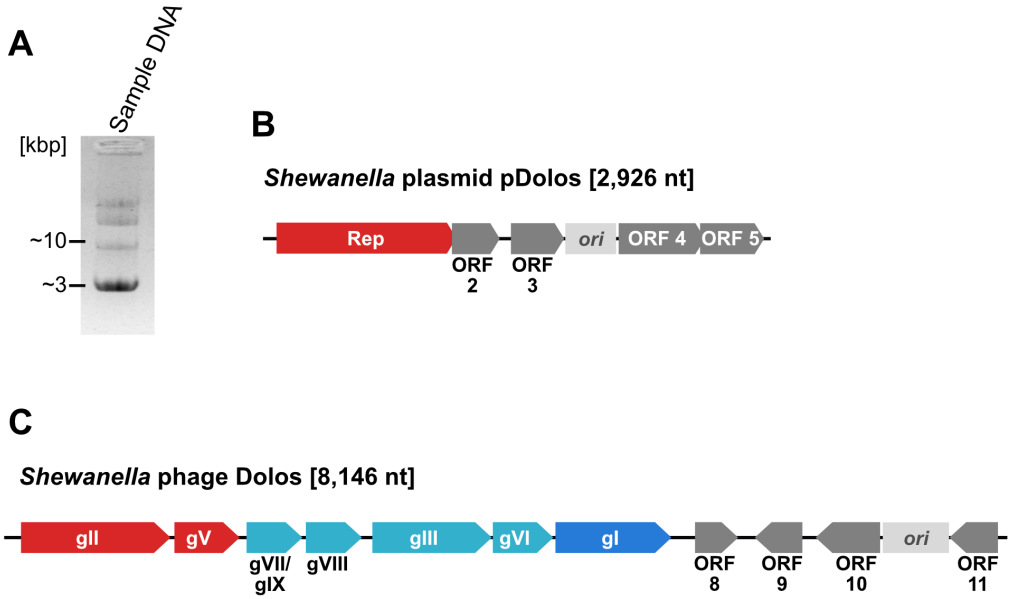

Figure 7: Isolation of virion DNA from a new sample revealed two different circular ssDNA genomes packaged in particles. A. The purified DNA of a new virion-containing sample was separated by gel electrophoresis, revealing DNA bands of different sizes. **B.** and **C.** Schematic representations of the two genomes isolated from this virion-containing sample. **B.** 2,926 nt long ssDNA plasmid (*Shewanella* plasmid pDolos) harbouring 5 ORFs. **C.** 8,146 nt long ssDNA genome of a phage (*Shewanella* phage Dolos) harbouring 11 ORFs. Red: genes important for replication, light blue: structural genes, blue: secretional genes, grey: genes of unknown function, light grey: putative single-stranded origin of replication (*ori*).

2.1.1 Characterization of the *Shewanella* phage Dolos

In order to analyse the relationship of plasmid pDolos and phage Dolos to each other and to the host, both mobile genetic elements need to be individually characterised. For this purpose, the phage was separated from the mixed virion-containing supernatant by single plaque isolation and enrichment steps. During this

isolation process, it was found that all individual plaques tested by PCR contained the purified phage, indicating that pDolos cannot produce visible plaques (**Supplementary Figure 1**). It was therefore initially only possible to separate and characterise the phage Dolos and not the plasmid pDolos.

Basic viral characteristics

After isolation of phage Dolos, the basic viral characteristics were analysed. First, a plaque assay was performed to analyse the plaque morphology of Dolos. For this purpose, Dolos-containing supernatant and the viral host organism *S. oneidensis* ΔΔ were added to soft agar and the mixture was plated on a common agar plate (agar overlay method). During incubation, plaques formed within the cell lawn, which originally resulted from the infection of a single cell with a single virion. The assay displays a cloudy plaque morphology of the phage Dolos, which is typical for inoviruses, as plaques are not caused by cell lysis but by a slight growth delay of the infected cells [54] (**Figure 8 A**).

Subsequently, Clara Rolland, Mathias Müsken and Johannes Wittmann (Leibniz Institute DSMZ, Braunschweig) took electron micrographs of Dolos to determine the size and shape of the virus. For this, Dolos virions were purified via a caesium gradient, negatively stained and analysed using transmission electron microscopy (TEM). **Figure 8 B** shows a representative TEM image of a filamentous Dolos particle with a virion length of about 1 µm and a width of about 7.5 nm. The attachment site, which is characterised by the pIII protein tuft, is clearly visible.

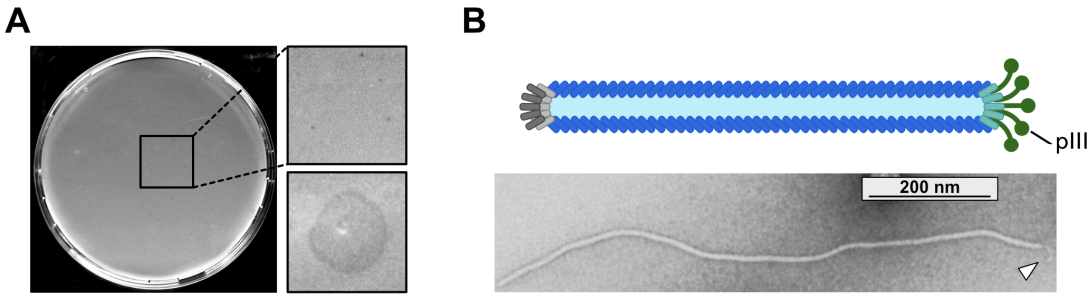

Figure 8: Plaque morphology and virion morphology of phage Dolos. A. Plaque assay displaying small and turbid Dolos plaques. Plaque assay plates were analysed after 48 h of incubation of phage Dolos with the host *S. oneidensis* ΔΔ. **B.** TEM picture of phage Dolos. The phage-containing supernatant was purified by caesium density gradient centrifugation and negatively stained for microscopic imaging. Arrow indicates the phage attachment site. The attachment site, marked by the pIII proteins, is also shown in green in the schematic representation of an inovirus virion above the TEM image.

Next, the host spectrum of phage Dolos was tested by spotting a Dolos-containing supernatant onto agar overlay plates with different bacterial species. 9 *S. oneidensis* strains, 5 *S. baltica* strains, 12 other *Shewanella* strains as well as *Escherichia coli* MG1655, *Pseudomonas putida* KT2440 and *Vibrio cholerae* El Tor N16961 were tested. Only *S. oneidensis* MR-1 and two *S. baltica* isolates were infected by phage Dolos (**Supplementary**

Table 2). In addition, a viral proteomic tree was created using the VipTree software tool [120] to better classify *Shewanella* phage Dolos within the viral family *Inoviridae*. The phylogenetic tree shows that Dolos is most closely related to known *Vibrio* phages of the family *Inoviridae* (**Figure 9**).

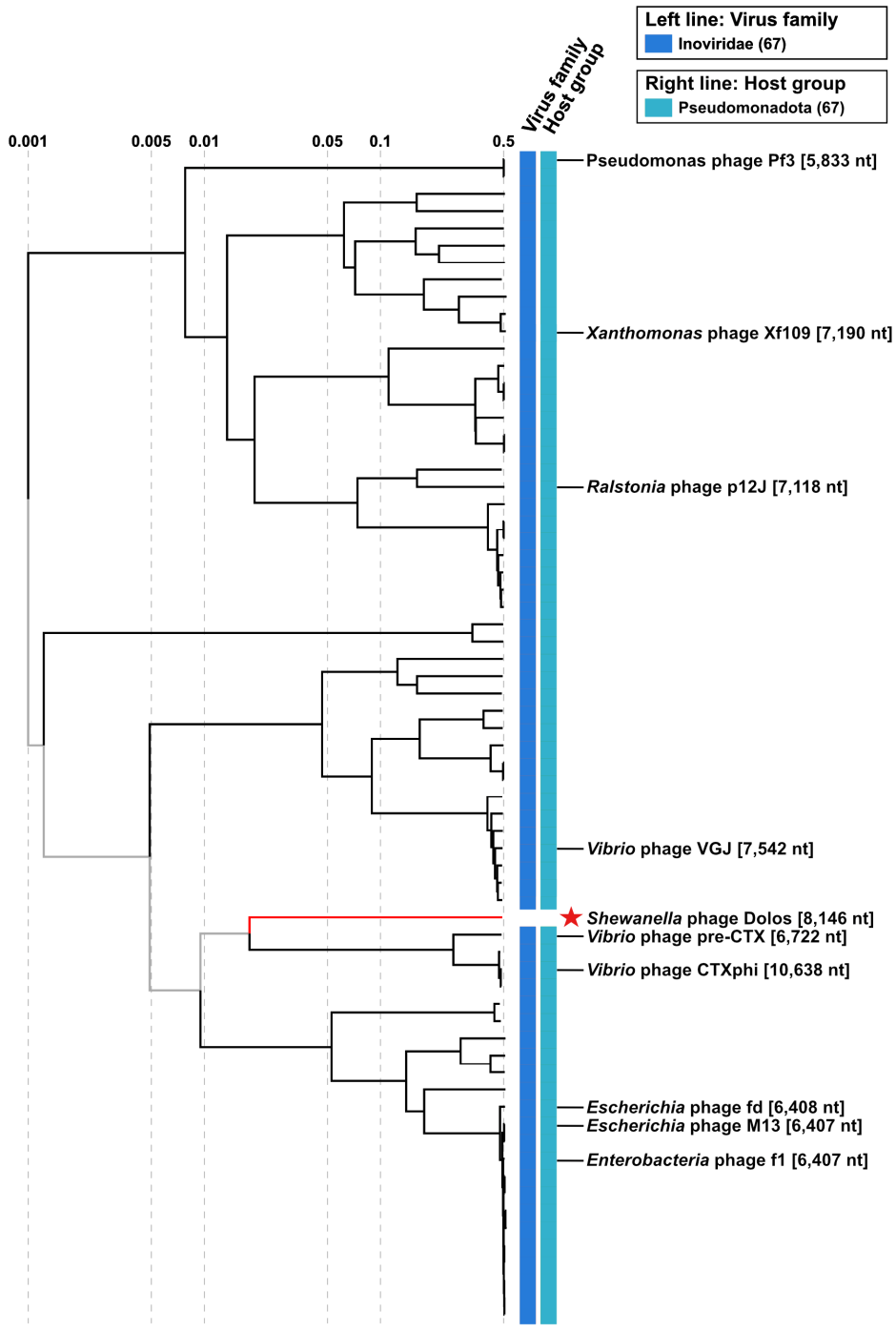

Figure 9: Viral proteomic tree of *Shewanella* phage Dolos. Phylogenetic tree was made with the software tool VipTree [120]. *Shewanella* phage Dolos and all prokaryotic ssDNA viruses of the virus host DB (RefSeq Release 220) were included in this analysis. The colouring of the left and right line indicates the virus family and host group, respectively. *Shewanella* phage Dolos is highlighted with a red star.

The heat and pH stress stability of the Dolos virions was then tested by exposing the virions to the respective stressors for 24 hours. The serially diluted virions were subsequently spotted onto agar overlay plates containing *S. oneidensis* ΔΔ. Stress experiments show a distinct pH stability from pH 4 to pH 12 and a heat stability up to 40°C (**Figure 10**).

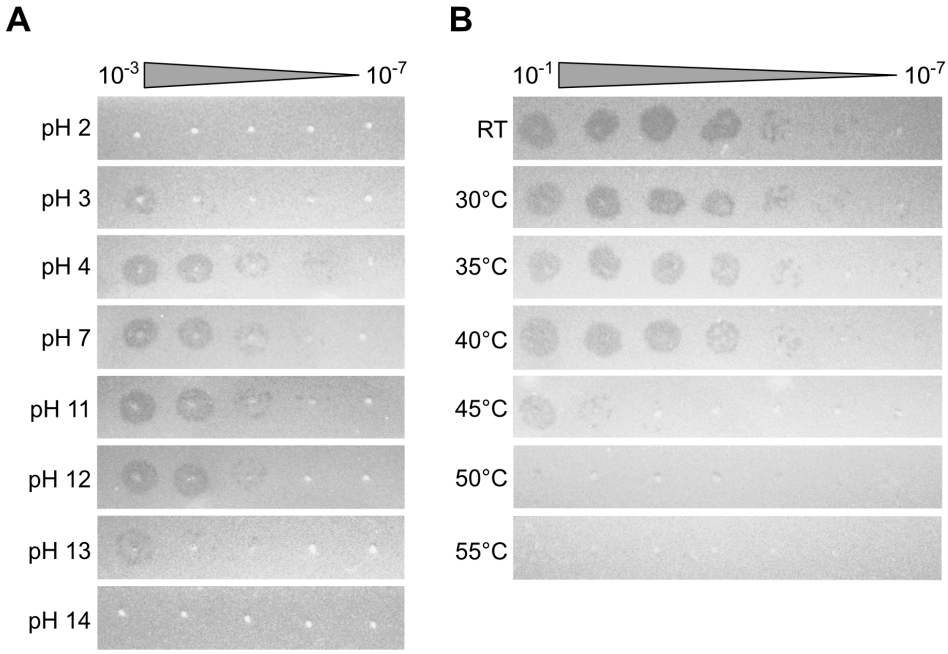

Figure 10: pH and temperature sensitivity of Dolos particles. 24 hours pH (A.) or temperature (B.) exposed phage-containing supernatants were serially diluted and subsequently spotted onto agar overlay plates containing *S. oneidensis* ΔΔ. Spot documentation was conducted after 48 h of bacterial growth.

Phage Dolos attaches to the MSHA pilus of S. oneidensis MR-1

After analysing basic viral characteristics such as plaque morphology and virion stability, the adsorption receptor which Dolos uses should be determined. Therefore, several strains individually lacking common surface proteins known to be used by phages were tested via spotting Dolos onto them. The result shows that the major pilin subunit MshA of the MSHA pilus proves to be a potential adsorption receptor, as no phage spots are formed on an *mshA* deletion strain (**Figure 11 A**).

Since MshA is part of a large multi-protein complex, being the MSHA pilus [103, 121, 122], it was tested whether the major pilin subunit MshA is indeed the protein that Dolos utilises for adsorption. This was investigated as the absence of the MshA protein could lead to a loss of surface-exposed pilus components, meaning that the minor pilins of the MSHA pilus could also be inaccessible at the surface in the absence of MshA [103]. To investigate the role of the MshA protein, a protein interaction assay was performed. For this purpose, a bacterial adenylate cyclase two-hybrid assay (BACTH) was conducted and the phage attachment protein pIII and the MshA protein of *S. oneidensis* MR-1 were fused to subunits of an adenylate

cyclase. The BACTH assay shows enzymatic activity, indicated by the blue colour, and thus an interaction between pIII and MshA (**Figure 11 C**). This result proves that the phage adsorbs directly to the major pilin subunit MshA.

A subsequent phage adsorption test displays that Dolos requires time for to attach to MshA. For this assay, *S. oneidensis* ΔΔ cells were infected with the phage Dolos during mid-exponential growth at a multiplicity of infection (MOI) of 0.1. Samples were taken at different time points after infection and the PFU per ml was determined by plaque assay. The percentage of extracellular phages within these samples was calculated by normalising to the initial phage concentration. The result shows that it takes approximately 1 hour for more than 50% of the initially added phages to be adsorbed to the host (**Figure 11 B**).

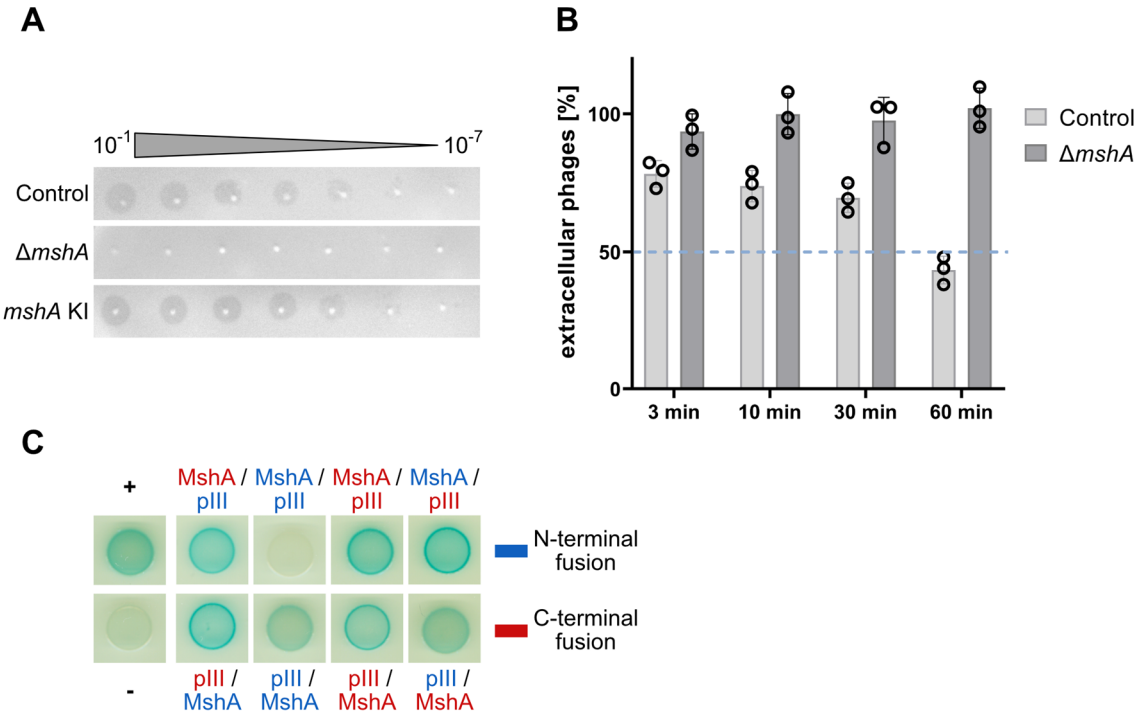

Figure 11: The used adsorption receptor of Dolos is the major pilin subunit MshA of the MSHA pilus. A. Spot assay displaying the importance of the gene *mshA* for phage infection. Serial diluted Dolos-containing supernatant was spotted on top of agar overlay plates containing different *S. oneidensis* strains. KI: knock-in (re-integration of *mshA*). **B.** Phage adsorption assay showing the percentage of extracellular phages during a time-serial infection. Mid-exponential *S. oneidensis* ΔΔ cells were infected with Dolos at a MOI of 0.1. Phage samples were taken at different time-points post-infection. PFU per ml was determined via plaque assay and the percentage of extracellular phages was calculated by normalisation to the initial concentration of phages. Grey line indicates 50% extracellular phages. **C.** BACTH assay showing interaction of Dolos attachment protein (pIII) with MshA. For each interaction, proteins named first are fused to the T25 subunit, while proteins named last are fused to the T18 subunit of an adenylate cyclase. Blue coloration of the spots indicates catalytic activity of the adenylate cyclase and thus also protein interaction. +: positive control, -: negative control. All experiments were conducted in independent biological triplicates.

The effect of altered pilus activity on viral infectivity

Compared to other common adsorption receptors, such as components of the lipopolysaccharide (LPS) structure, MshA is rarely found on the cell surface. In addition, it is not a direct component of the cell surface, meaning that pilus retraction is required for Dolos to reach the outer membrane. Hence, it was investigated whether a change in pilus activity could have an effect on the adsorption rate and infectivity of Dolos. For this purpose, mutants were generated that are known to alter the activity of the MSHA pilus and thus potentially alter the efficiency of Dolos binding to MshA and the entry of Dolos into the periplasmic space to reach the secondary receptor. Therefore, some amino acids of the extension ATPase MshE were substituted (MshE$^{L9A/L53A/L57A}$), which are known to lead to a constitutively active state of the MSHA pilus in *Vibrio cholerae* by preventing c-di-GMP binding [104, 123, 124]. Furthermore, an amino acid of the retraction ATPase PilT was substituted to attenuate ATPase function (PilT^{K136A}), which is known to lead to a phenotype with more accessible pili in *Vibrio cholerae* [104, 123].

To analyse the influence of these substitutions in the pilus extension and retraction ATPase on MSHA pilus activity, MshA was stained with a maleimide protein stain. This was made possible by the selectivity of maleimides for thiol groups, which are part of cysteine residues [125]. The strain MshA^{S69C} was therefore used for the staining. Fluorescence micrographs of maleimide stained mid-exponential cells were taken and the pilus length as well as the amount of MSHA pili per cell were examined from these images. The analysis shows a reduced length of the MshA filaments of MshE$^{L9A/L53A/L57A}$ cells and an increased amount of elongated MshA filaments of the PilT^{K136A} cells compared to the control cells (**Figure 12 A**). The data also shows that most MshE$^{L9A/L53A/L57A}$ cells do not have a single exposed MSHA pilus. In contrast, the number of pili per cell of the PilT^{K136A} strain is increased (**Figure 12 B**).

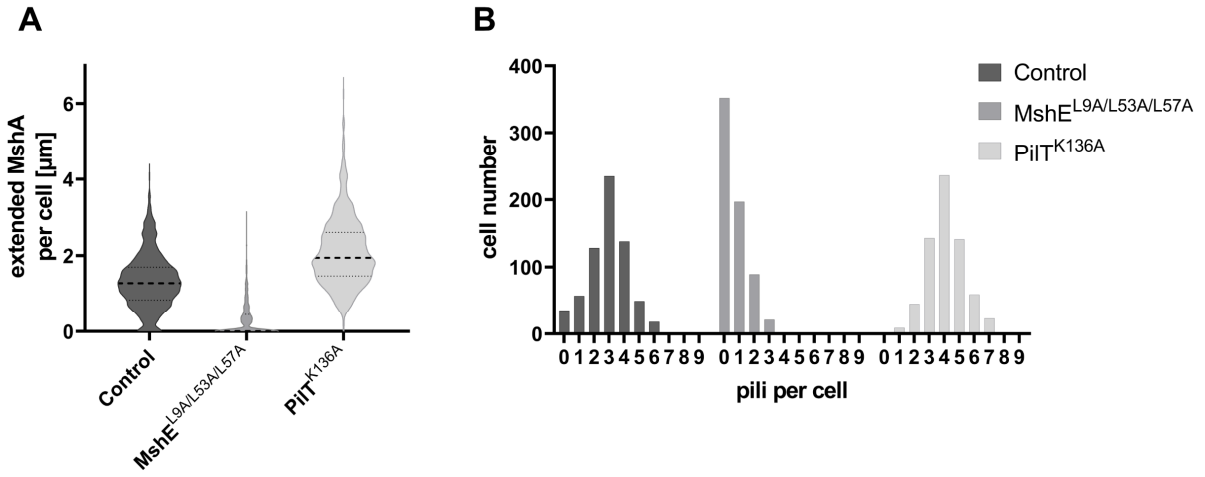

Figure 12: Different MSHA pilus activity due to activity-influencing mutations of the pilus extension ATPase (MshE) and the pilus retraction ATPase (PilT). The length of extended MshA per cell (**A.**) and the count of pili per cell (**B.**) of mid-exponential *S. oneidensis* ΔΔ cells harbouring a point mutation in *mshA* (MshA^{S69C}) and further mutations in pilus ATPases are shown. MshA filaments of the different strains were visualized via fluorescence microscopy by using a maleimide protein stain to stain MshA proteins. Experiment was conducted in independent biological triplicates. N = 660 cells.

After determining the pilus activity of these mutants, changes in the adsorption efficiency and the infectivity of Dolos were investigated.

For this purpose, the Dolos adsorption efficiency was analysed in the strains with altered pilus activity. Phage-containing supernatants were isolated after one hour of infection (MOI 0.1). The test shows that the measured amount of extracellular phages is significantly increased compared to the control when phages are added to strain MshE$^{L9A/L53A/L57A}$. This indicates reduced adsorption to the MshE$^{L9A/L53A/L57A}$ strain (**Figure 13 A**). When incubated with PilT^{K136A} only a slight increase in extracellular phages is shown.

Viral infectivity was also analysed using serial spot test. For this, mid-exponential *S. oneidensis* strains with altered MSHA pilus activity were infected with Dolos at a MOI of 0.1. 24 h after infection, Dolos-containing supernatants were prepared and spotted onto agar overlay plates. The result displays that the total virion production of the MshE$^{L9A/L53A/L57A}$ strain is similar to that of the control. However, the PilT^{K136A} strain produces a slightly lower level of Dolos virions (**Figure 13 B**).

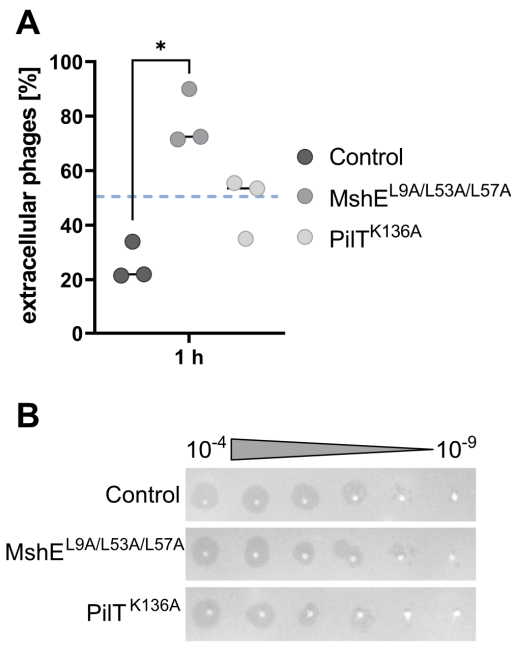

Figure 13: Alteration in Dolos infection dynamics when cells with altered MSHA pilus activity are infected. A. Phage adsorption assay displaying the count of extracellular phages during an infection. Mid-exponential *S. oneidensis* ΔΔ strains with altered MSHA pilus activity were infected with Dolos at a MOI of 0.1. Phage samples were taken 1 h after infection via centrifugation and sterile filtration of the cell culture supernatants. PFU per ml was determined via plaque assay and the percentage of extracellular phages was calculated by normalisation of the calculated PFU per ml to the initial concentration of phages. Grey line indicates 50 %. Black lines indicating the mean values. *: $p<0.05$ (t-test). **B.** Serial spot assay to visualize changes in phage concentration and plaque morphology. Several *S. oneidensis* ΔΔ strains with altered MSHA pilus activity were infected during mid-exponential growth with Dolos at a MOI of 0.1. Phage samples for spot assay performance were taken 24 h after infection. The experiments were performed in biological triplicates.

2.1.2 Interplay of inovirus Dolos and plasmid pDolos with themselves and with the host

Since the originally isolated virion-containing supernatant comprises not only the phage Dolos but also a plasmid termed pDolos, it was investigated whether this plasmid interacts with the phage Dolos. In addition, the influence of these two newly discovered MGEs on the host *S. oneidensis* MR-1 was investigated in more detail.

pDolos acts as phage satellite of inovirus Dolos

In order to determine a possible influence of the plasmid pDolos on the phage Dolos, a reproduction assay was performed in which the reproduction of Dolos was measured at different time points after infection. For this purpose, mid-exponential *S. oneidensis* ΔΔ cells were infected with a Dolos-containing supernatant or a Dolos- and pDolos-containing supernatant at a MOI of 0.1. Since plaques are only formed by infection with the phage, the MOI could only be defined for the phage, but not for the plasmid. The phage concentration of the samples collected over time was calculated and normalised to the original phage concentration at the time of infection, indicating the reproduction rate of Dolos. The result shows a reduced reproduction of phage Dolos in the presence of pDolos compared to infection with Dolos alone (**Figure 14 A**). In addition, the Dolos concentration measured after 24 hours of infection, showing an approximately 10-fold decrease in the amount of Dolos virions when the cells were infected with the mixed virion-containing supernatant (**Figure 14 B**).

To obtain a ratio of Dolos virions to pDolos virions within such mixed virion-containing supernatants, the virion genomes were quantified by qPCR. For this purpose, virion DNA was purified from mixed supernatants containing Dolos and pDolos and the amount of Dolos and pDolos genomes was subsequently analysed. The qPCR analysis displays a mean Ct value of 19.9 for the Dolos genome and a mean Ct value of 12 for the pDolos genome (**Figure 14 C**). A ΔCt value of 7.9 was quantified and a normalisation was conducted according to the formula $2^{-\Delta Ct}$ [126]. This calculation clearly showed that pDolos virions are 250 times more abundant in a mixed virion-containing supernatant than Dolos virions.

Furthermore, infection series were conducted by infecting *S. oneidensis* ΔΔ cells at mid-exponential phase with a Dolos-containing supernatant or a Dolos- and pDolos-containing supernatant at a MOI of 0.1. Samples were taken at different time points after infection and the DNA of the infected cells was isolated. Again, qPCR was performed and the genome quantity of *S. oneidensis*, the phage Dolos and the plasmid pDolos was calculated. Following, the time-serial reproduction rate of Dolos and pDolos was determined. The result shows a reduced phage replication when cells are infected with the mixed virion-containing supernatant compared to cells infected with the pure Dolos-containing supernatant (**Figure 14 D**). Hence, the reproduction rate determined by qPCR and the reproduction rate determined by plaque measurement

(see **Figure 14 A**) show the same trend: the reproduction of Dolos is reduced in the presence of the plasmid pDolos.

When analysing the qPCR-derived Dolos reproduction rates shown in **Figure 14 D** in detail, it is noticeable that, the reproduction of Dolos is increasing from 2 to 4 hours after infection (Dolos-containing supernatant: 16.8-fold increase, Dolos + pDolos-containing supernatant: 10-fold increase) and from 4 to 6 hours after infection (Dolos-containing supernatant: 26.3-fold increase, Dolos + pDolos-containing supernatant: 12.8-fold increase). Thereafter, the reproduction rate of Dolos slows down when the cells reach the transitional growth phase. The time-serial reproduction rate of plasmid pDolos compared to phage Dolos shows a shift in the Gaussian distribution of the reproduction rate (**Figure 14 E**). The highest reproduction rate of pDolos is measured from 6 to 8 hours after infection (9.5-fold increase), indicating that the phage replicates first and then the plasmid.

The results show that pDolos behaves in a certain way like a phage satellite and exploits the phage Dolos. Satellite-dependent hijacking of a phage is often characterised by a reduction of the virion quantity of the so-called helper phage. Phage satellites have insufficient structural proteins themselves and therefore utilise the structural proteins of a phage to package the satellite genome instead of the phage genome being packaged [2, 83]. This observed exploitative behaviour of the plasmid pDolos has contributed to the name "satellite plasmid pDolos".

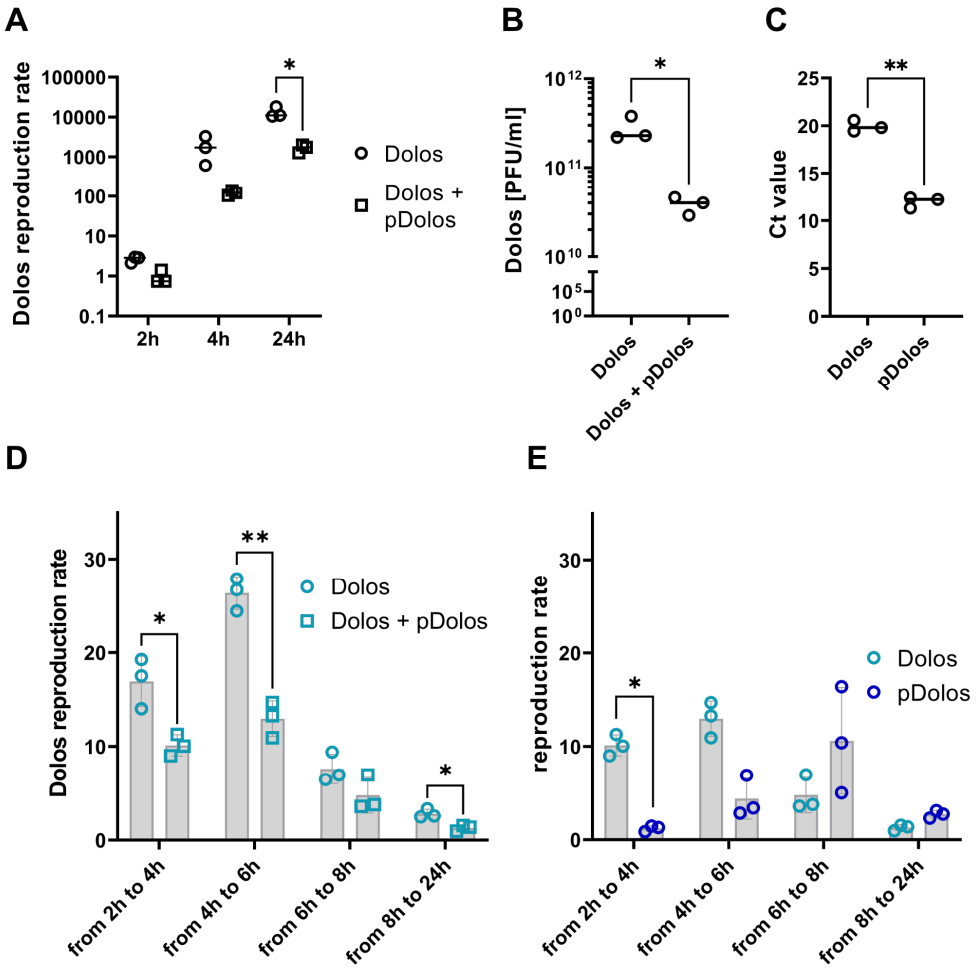

Figure 14: pDolos acts like a phage satellite of inovirus Dolos. A. Dolos reproduction assay displaying decreased phage reproduction when pDolos is also present. During mid-exponential growth, *S. oneidensis* ΔΔ cells were infected with a supernatant containing Dolos or Dolos + pDolos at a MOI of 0.1. Phage samples for plaque assay were taken at different times after infection. Reproduction rate was estimated by normalisation of the phage concentration to the initial amount of phages. **B.** Phage concentration of phage-containing supernatants. Mid-exponential *S. oneidensis* ΔΔ cells were infected with Dolos or Dolos + pDolos at a MOI of 0.1. Samples for plaque assay were taken 24h after infection. **C.** Ct values of Dolos and pDolos DNA of a mixed virion-containing supernatant, measured by qPCR. The Ct value difference complies with a plasmid to phage ratio of about 250 to 1. **D** and **E.** Reproduction rate of Dolos and pDolos estimated by qPCR. A time-serial infection of mid-exponential cells infected with Dolos or Dolos + pDolos at a MOI of 0.1 was conducted. Samples for analysis were taken 2h, 4h, 6h, 8h and 24h after infection **D.** Time-serial reproduction rate of Dolos when cells were infected with a pure phage-containing supernatant or a mixed virion-containing supernatant (Dolos + pDolos). **E.** The reproduction rate of Dolos related to the reproduction rate of plasmid pDolos. All experiments were conducted in biological triplicates. Error bars indicating the standard deviation of the mean values. * = $p < 0.05$, ** = $p < 0.01$ (t-test).

Interaction of phage Dolos and satellite plasmid pDolos with planktonic cells

To analyse the interaction of phage Dolos and the satellite plasmid pDolos with the host, the growth of *S. oneidensis* ΔΔ cells was examined. For this purpose, the time-serial optical density (OD) was measured after mid-exponential cells had been infected with Dolos or the mixed virion-containing supernatant holding Dolos and pDolos virions (MOI 0.1). The experiment shows that cells infected with the inovirus Dolos exhibit a slight growth delay compared to uninfected control cells (**Figure 15 A**). Notably, the growth delay

of cells infected with the mixed virion-containing supernatant is slightly more pronounced than in cells infected with phage Dolos alone, possibly indicating a greater consumption of host resources when cells are infected with inovirus Dolos and satellite plasmid pDolos. When analysing the growth of pre-infected cells, being cells infected one day before the start of the growth experiment, an equal growth retardation of cells infected with Dolos or Dolos and pDolos is observed (**Figure 15 B**). Examination of these growth curves also shows that long-term infected cells do not have a more pronounced lag phase, meaning that the growth retardation appears to be the same during all growth phases.

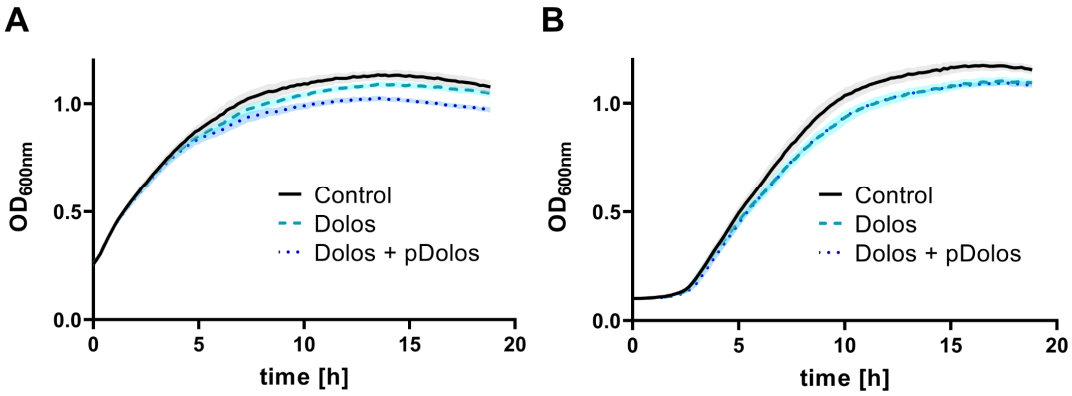

Figure 15: Minor growth delay of cells infected with inovirus Dolos or infected with the inovirus Dolos as well as the satellite plasmid pDolos. A. Serial measured growth of mid-exponential *S. oneidensis* ΔΔ cells infected with Dolos or Dolos + pDolos at a MOI of 0.1. **B.** Growth curve of pre-infected cells. Mid-exponential *S. oneidensis* ΔLambdaSo ΔMuSo2 cells were infected with Dolos or Dolos + pDolos at a MOI of 0.1. 18 h after infection cells were diluted and time-serial growth was measured. All experiments were conducted in biological triplicates. The shaded bands represent the standard deviation of the mean values.

Infected *S. oneidensis* ΔΔ cells were also analysed morphologically by TEM. For this purpose, cells were infected with a supernatant containing Dolos or Dolos and pDolos at a MOI of 5 for 2.5 hours. The morphological examination started after fixation and negative staining of the cells. Microscopic images indicate a thicker capsular structure of cells infected with Dolos or Dolos and pDolos compared to the uninfected control (**Figure 16**).

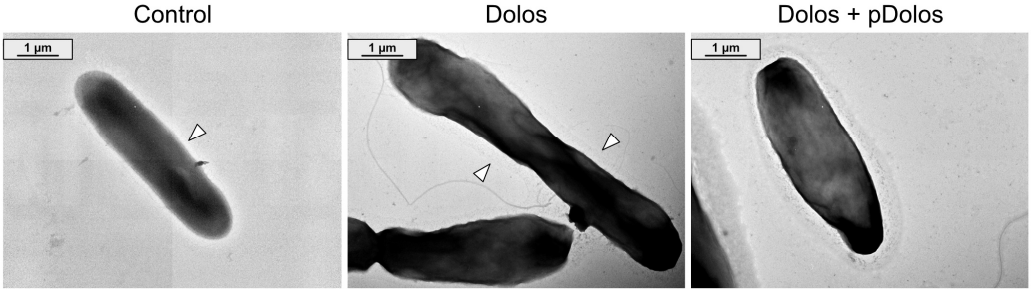

Figure 16: Cells infected with phage Dolos or phage Dolos and pDolos show increased capsule formation in the late-exponential growth phase. *S. oneidensis* ΔΔ cells were infected with Dolos or Dolos + pDolos at a MOI of 5 during mid-exponential growth. 2.5 hours after infection, cells were fixed and negatively stained for TEM. White arrows indicate capsules difficult to recognise.

Interaction of phage Dolos and satellite plasmid pDolos with biofilms

As the adsorption receptor of phage Dolos is part of the MSHA pilus, which is important for cell attachment to surfaces and thus essential for the first step of biofilm formation, the influence of phage Dolos and the satellite plasmid pDolos on biofilm formation and mature biofilms was investigated. For this purpose, biofilm tests were performed with the strain *S. oneidensis* MR-1, which carries both prophages, as the prophages have been shown to be very significant for biofilm formation of *S. oneidensis* [63].

To analyse static biofilm formation, cells of an OD_{600nm} of 0.15 were statically incubated and infected with a Dolos-containing supernatant or a Dolos- and pDolos-containing supernatant (10^8 PFU per ml) at different time points after the start of the static incubation. The amount of biomass was quantified after 24 hours of static incubation through a crystal violet staining. The test shows that only the mixed virion-containing supernatant has a positive effect on biofilm formation, while Dolos alone has no significant effect on biofilm formation (**Figure 17 A and C).** Especially in the early stages of biofilm formation (0 and 3 hours after the start of static incubation), the mixed virion-containing supernatant has a positive effect on biofilm formation. A biofilm biomass of up to 150% is achieved here (**Figure 17 C**).

To investigate the effect of Dolos and pDolos on statically grown mature biofilms, cells of an OD_{600nm} of 0.15 were statically incubated for 24 hours and then infected with Dolos or Dolos and pDolos (~ 10^8 PFU per ml). At different time points after infection, the biomass of the biofilm was measured by crystal violet staining. The assay displays no effect of phage Dolos or of phage Dolos together with the satellite plasmid pDolos on mature biofilms (**Figure 17 B and D**).

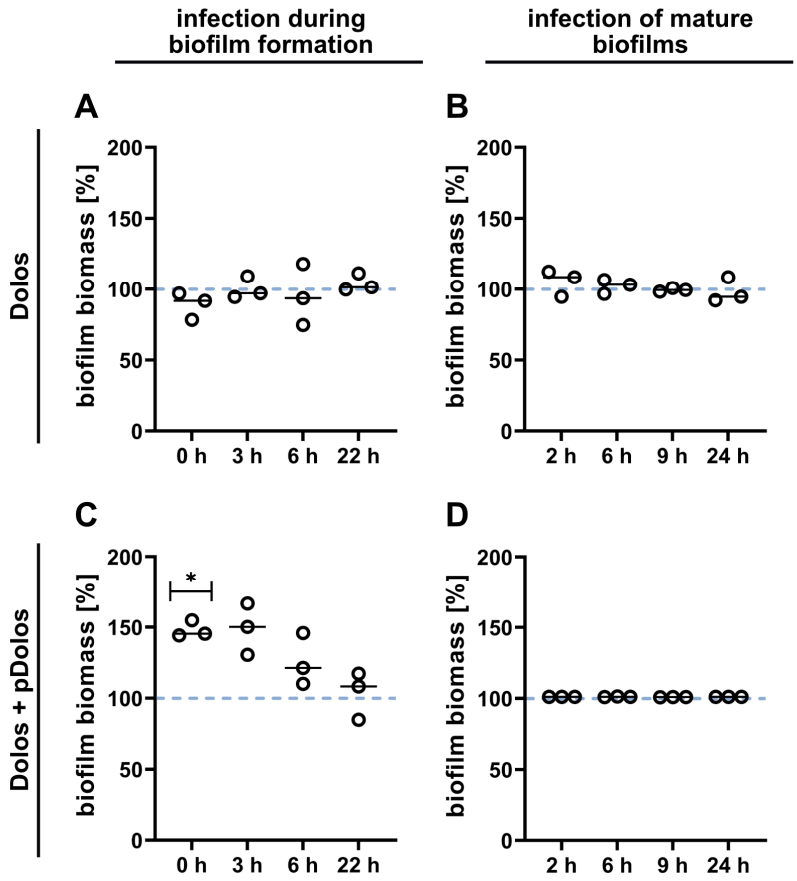

Figure 17: Increased amount of biofilm biomass when phage Dolos together with satellite plasmid pDolos are infecting *S. oneidensis* MR-1 during an early stage of biofilm formation. Displayed are static biofilm assays. *S. oneidensis* MR-1 cells were infected with virion-containing supernatants (10^8 PFU/ml) at different times of static incubation. The amount of biofilm biomass was measured by crystal violet staining. The static incubation of non-infected cells was always considered as 100% biofilm biomass. To analyse the influence of Dolos and Dolos + pDolos during biofilm formation (**A** and **C**), diluted cells (OD_{600nm} 0.15) were statically incubated and infected at different time points after the start of static incubation. Biofilm biomass was quantified after 24 h of incubation. To analyse the influence of Dolos and Dolos + pDolos on mature biofilms, 24 h statically grown cells were infected with virion-containing supernatants and the biofilm biomass was quantified at different time points after infection of these mature biofilms (**B** and **D**). **A** and **B**: infected with Dolos, **C** and **D**: infected with Dolos + pDolos. * = $p<0.05$ (t-test). Black strokes represent the mean values of biological triplicates.

In addition, the influence of long-term infected cells on static biofilm formation was tested. For this purpose, *S. oneidensis* MR-1 cells were infected with either a pure Dolos-containing supernatant or a Dolos- and pDolos-containing supernatant one day before the start of the static biofilm assay. Cells with an OD_{600nm} of 0.15 were statically incubated, and 24 hours after the start of static incubation, the biofilm biomass was quantified by a crystal violet staining or a Live/Dead staining was performed to determine the amount of living and dead cells within the biofilm. The results show a reduced biofilm biomass of 86% in the mean of cells pre-infected with Dolos after 24 hours of static growth compared to the uninfected control (**Figure 18 A**). The opposite was observed when the cells were pre-infected with the mixed Dolos- and pDolos-containing supernatant. Here, biofilm formation is increased with an average of 113% biofilm biomass after 24 hours of static growth compared to the uninfected control. The Live/Dead staining

indicates a high quantity of dead cells and thus eDNA as part of the biofilm when the cells were pre-infected with the mixed virion-containing supernatant instead of the pure Dolos-containing supernatant prior to static growth (**Figure 18 B**). Several studies have already shown a correlation between cell death and biofilm growth due to an increased amount of eDNA as a stabilising factor of the biofilm matrix [63, 127, 128].

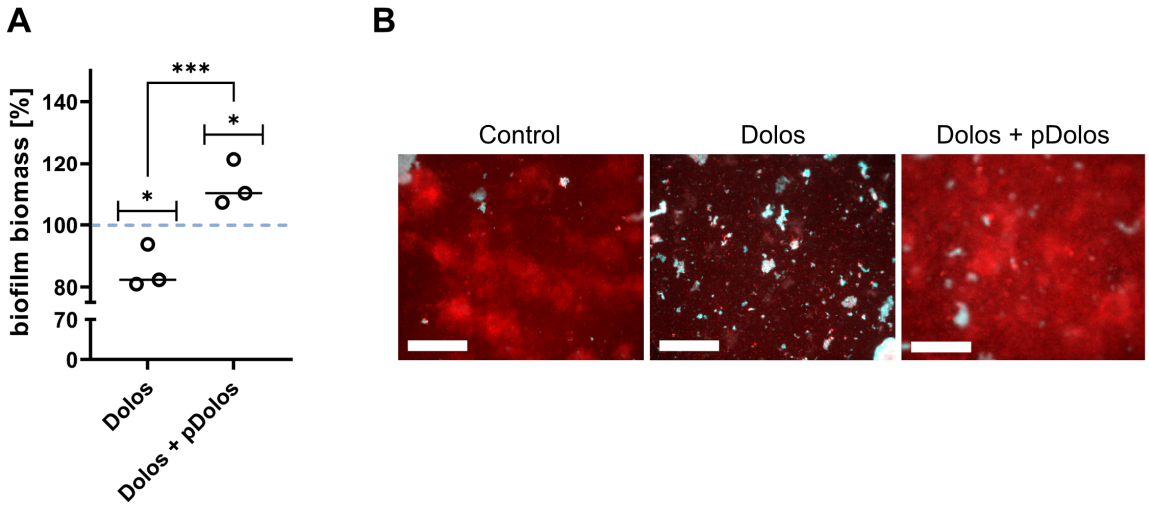

Figure 18: In cells that were already pre-infected before static incubation, phage Dolos reduced the biofilm biomass, while infection with Dolos and satellite plasmid pDolos increased biofilm formation. Shown are static biofilm assays of *S. oneidensis* MR-1 cells. Cells were pre-infected with virion-containing supernatants at a MOI of 0.1 one day before the start of the assay. Pre-infected cells were diluted (OD_{600} 0.15) and statically incubated for 24 h. **A.** Amount of biofilm biomass was measured by crystal violet staining. The static incubation of non-infected cells was always considered as 100% biofilm biomass. * = $p<0.05$, *** = $p<0.001$ (t-test). Black lines represent the mean values of biological triplicates. **B.** Representative images of a Live/Dead staining of biofilms using a SYTO9 (blue) / propidium iodide (red) mixture. Scale bar = 20 µm.

After the effect of Dolos alone and the phage Dolos together with the plasmid pDolos on statically grown biofilms had been investigated, the effect on biofilms that had grown under a constant liquid flow was analysed. For this purpose, pre-infected *S. oneidensis* MR-1 cells, which constitutively produce GFP (*S. oneidensis* MR-1 *Tn7:::egfp* (Cm^r)), were analysed microscopically after 24 hours of biofilm growth in a flow chamber system. Representative 3D micrographs of these grown biofilms are shown in **Figure 19 A**.

The microscopic images were analysed using the software tools BiofilmQ [129] and ImageJ Fiji [130]. Biofilm surface properties such as roughness and global height were determined. The biofilm surface property results show a tendency towards rougher and higher biofilms when the cells were pre-infected with Dolos and pDolos, and a decreasing tendency in the roughness and height of the biofilm when the cells were pre-infected with Dolos only (**Figure 19 B and D**). In addition, the local density of the biofilms was measured, showing a tendency towards denser biofilms when the cells were pre-infected with phage Dolos exclusively (**Figure 19 C**). Furthermore, general biofilm properties such as the cell amount of the biofilms, the volume and the relative biofilm biomass were analysed, whereby no tendencies in the cell amount and the biofilm volume were shown (**Figure 19 E and F**). The relative biofilm biomass was

measured by determining the relative fluorescence of the microscopic images, as the cells constitutively produce GFP. The result shows a tendency towards a reduced biofilm biomass when the cells were pre-infected with Dolos alone and a tendency towards an increased biofilm biomass when the cells were pre-infected with Dolos and pDolos (**Figure 19 G**). This trend in relative biofilm biomass grown in a flow chamber system matches the results obtained from static biofilm tests (see **Figure 18 A**).

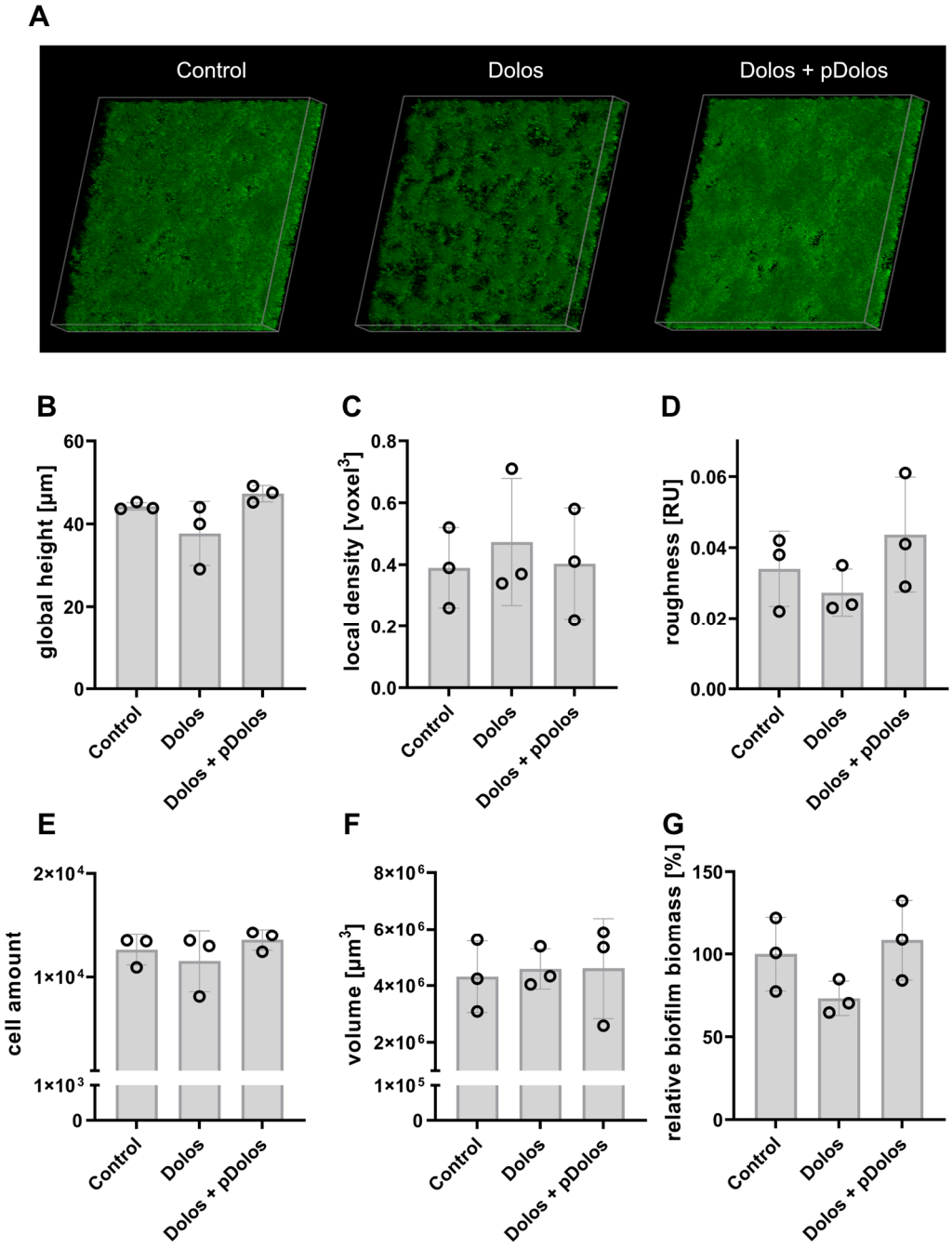

Figure 19: In a flow chamber system grown biofilms from cells pre-infected with the inovirus Dolos and the satellite plasmid pDolos tend to have an increased relative biofilm biomass and higher as well as rougher biofilms compared to cells pre-infected with the phage Dolos alone. *S. oneidensis* MR-1 cells, which continuously produce GFP (*S. oneidensis* MR-1 *Tn7::egfp*), were pre-infected with virion-containing supernatants at an MOI of 0.1 18 hours before the start of the flow chamber experiments. 24 h after injection of cells (OD_{600nm} 0.05) into the chambers, images were taken using a confocal microscope **A.** Displayed are representative confocal 3D micrographs of 24 h old biofilms grown in a flow chamber system. The horizontal edge of each image represents 580 µm. **B** – **G**. Analysis of in flow chamber system grown biofilm properties using BioflimQ [129] and ImageJ Fiji [130]: global height (**B.**), local density (**C.**), roughness (**D.**), cell amount of biofilms (**E.**), biofilm volume (**F.**) and relative biofilm biomass (relative fluorescence intensity) (**G.**). Experiment was conducted in biological triplicates. Error bars indicating the standard deviation of the mean values. RU: roughness unit.

2.1.3 Characteristics of satellite plasmid pDolos

After studying the interaction of phage Dolos and the satellite plasmid pDolos with each other and with the host, the satellite plasmid pDolos was to be characterised in more detail.

pDolos is mainly packaged as a single copy in virions that are smaller than the phage virions

Firstly, the packaging of pDolos was investigated. Since inovirus virion assembly and secretion is a simultaneous process, it was hypothesised that the virion length might change due to the smaller genome size of pDolos compared to the genome size of phage Dolos. To test this hypothesis a native agarose gel assay was performed. Therefore, virion-containing supernatants were loaded onto an agarose gel and the virions were separated according to their size. The different virion fractions were visualised by staining the virion DNA after disruption of the particles with NaOH. As a control, heat-inactivated virion-containing supernatants were also loaded to show the running behaviour of the ssDNA genomes through the agarose gel. When analysing the running behaviour of the free ssDNA genomes of Dolos and pDolos, it is noticeable that double bands are visible, which are probably caused by secondary structures of the ssDNA genomes (**Figure 20**). When analysing the intact virions, it is striking that DNA bands only appear after disruption of the particles with NaOH. In addition, the mixed supernatant containing Dolos and pDolos virions shows bands corresponding to virions of different sizes (**Figure 20**). The most prominent DNA band of the mixed virion-containing supernatant corresponds to much smaller virions than Dolos virions. In addition, two other but very weak DNA bands were detected, corresponding to virions of other size. The gel was subsequently used to isolate these three virion fractions from the mixed virion-containing supernatant. The virion DNA of these three fractions was then tested and it was found that all fractions contained exclusively the pDolos genome (**Supplementary Figure 2**). The results indicate that in most cases a single pDolos genome is packaged in particles, and in rare cases more than one pDolos genome is packaged in a single particle. The simultaneous presence of both Dolos and pDolos genomes in a single particle was not detected. The most abundant virion band detected in the Dolos- and pDolos-containing supernatant represents individual satellite pDolos virions. This result supports the previous qPCR result showing that the ratio of Dolos to pDolos in the mixed virion-containing supernatant is approximately 1 to 250 (see **Figure 14 C**).

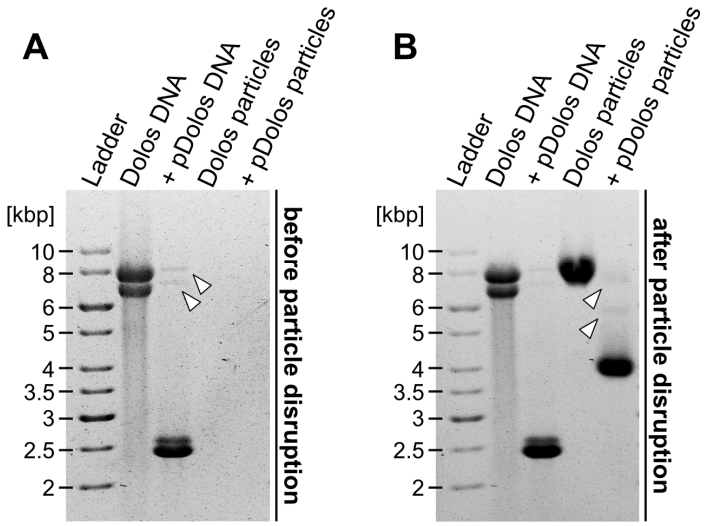

Figure 20: *Shewanella* phage Dolos and satellite plasmid pDolos are packaged separately in particles of different sizes. Native agarose gel displaying virions of different sizes. A virion-containing supernatant of Dolos and a virion-containing supernatant of Dolos and pDolos (+pDolos) were heat inactivated, which destroyed the particles so that only the virion DNA was separated by gel electrophoresis. Native virion-containing supernatants (particles) were also separated by gel electrophoresis. **A.** Agarose gel stained with ethidium bromide before particles were disrupted with NaOH. **B.** Agarose gel from A., which was stained again with ethidium bromide after the particles were disrupted with NaOH. White arrows indicate weak DNA bands. DNA of inactivated particles often appeared as a double band on the gel. The experiment was performed in biological triplicates. The images are representative.

pDolos is stable as a plasmid in cells without the presence of phage Dolos

Since it was not possible to isolate pure pDolos-containing virions by isolating single plaques, analysis of pDolos without Dolos was not possible so far. To analyse the plasmid without the presence of the phage Dolos, a pDolos plasmid containing a kanamycin resistance cassette directly downstream of ORF 5 was cloned (see **Figure 7 B**). The newly cloned plasmid was named pDolos_K. Using kanamycin, the plasmid stability of pDolos could be investigated. For this purpose, cells harbouring the plasmid pDolos_K were cultivated over three consecutive growth and re-growth cycles without kanamycin pressure. Finally, mid-exponential cells were diluted and plated on LB agar plates with and without kanamycin to calculate the percentage of cells still containing pDolos_K. The assay displays a high pDolos stability of 92% on average (**Figure 21 A**). This result demonstrates that pDolos remains stable as a plasmid in the cells through autonomous replication and vertical transmission.

In addition, a growth curve was generated with cells containing the plasmid pDolos_K. The assay shows a slight growth delay of cells having the plasmid, which could be caused by the plasmid itself or by the inserted kanamycin resistance cassette using host resources (**Figure 21 B**).

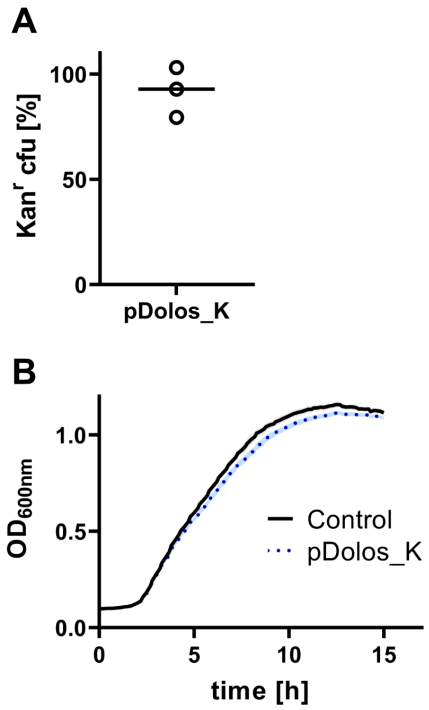

Figure 21: Satellite pDolos is stable in *S. oneidensis* cells as plasmid pDolos_K without the presence of phage Dolos. A. Percentage of kanamycin-resistant cells harbouring plasmid pDolos containing a kanamycin resistance cassette (pDolos_K). *S. oneidensis* ΔΔ cells harbouring pDolos_K were cultivated without kanamycin pressure over three days to estimate plasmid stability. **B.** Growth curve of *S. oneidensis* ΔΔ cells harbouring pDolos_K. Cells were cultivated without kanamycin pressure. All experiments were conducted in biological triplicates. The shaded bands represent the standard deviation of the mean values.

The size of pDolos virions varies depending on the genome size of the pDolos constructs

Next, it was asked whether variations in the genome size of pDolos would change the size of the pDolos virions. For this purpose, a pDolos variant with a kanamycin resistance cassette (pDolos_K: 4,015 nt), a pDolos variant with a kanamycin resistance cassette and the fluorophore *venus* (pDolos_KV: 5,533 nt) and a pDolos variant that also contains an *E. coli lacZ'* gene (pDolos_KVL: 9,850 nt) were used to test possible variations in virion size. To generate virions containing these plasmid variants, mid-exponential *S. oneidensis* ΔΔ cells harbouring these plasmids were infected with phage Dolos at a MOI of 0.1. 24 hours post-infection, the virion-containing supernatants were purified. The virion sizes of these supernatants were analysed by a native agarose gel assay. The assay displays that the size of the virions increases depending on the size of the genome packaged within the particles (**Figure 22**). A distinct band of pDolos_KVL virions is not visible. It is therefore unclear whether virions can be assembled if the genome to be packaged is larger than the genome of the helper phage (pDolos_KVL: 9,850 nt; Dolos: 8,146 nt). Furthermore, it is noticeable that the amount of virions of the pDolos variants is very low compared to the amount of native pDolos virions. Under these experimental conditions, the previously described effect of virus establishment prior to increased pDolos propagation could presumably cause this difference in the amount of pDolos (see **Figure 14 E**).

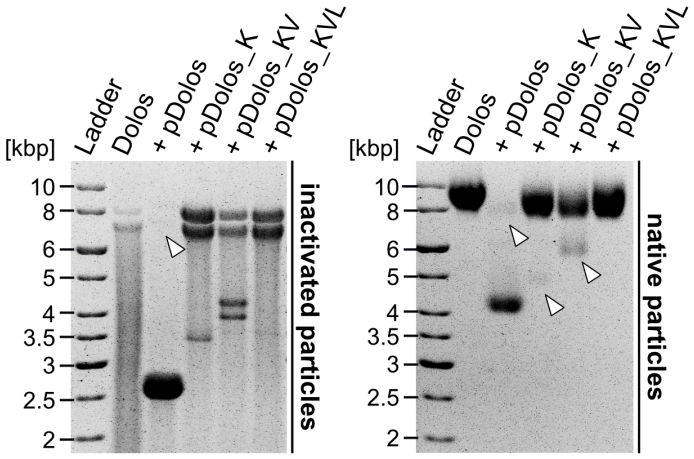

Figure 22: Extension of the pDolos genome leads to lager virions. Agarose gel displaying DNA of virions after separation of the heat-inactivated particles (left panel) and native particles (right panel) by gel electrophoresis. To picture DNA of native particles, staining was achieved after disruption of particles by NaOH. The samples contained exclusively phage Dolos or, in addition, pDolos constructs of increasing sizes (pDolos_K, pDolos_KV and pDolos_KVL). DNA of inactivated particles often appeared as a double band on the gel. White arrows indicate DNA bands difficult to recognize. The experiment was performed in biological duplicates. The images are representative.

Transfer of diverse genes by transduction of pDolos variants

Subsequently, the transduction of the pDolos virions had to be demonstrated. For this purpose, cells containing pDolos_K were infected with phage Dolos, while a control group remained uninfected. 24 hours after infection, the cells were diluted and co-incubated with *S. oneidensis* MR-1 cells containing a chromosomal encoded chloramphenicol resistance cassette (*S. oneidensis* MR-1 *Tn7:::egfp* (Cm^r); MR-1 Cm^r). After 24 hours of co-incubation, the cells were spotted on agar plates containing kanamycin, chloramphenicol or both antibiotics. The experiment shows that infection with the phage Dolos is essential for the efficient horizontal transfer of pDolos_K into chloramphenicol resistant cells (**Figure 23**). Therefore, the horizontal transfer of pDolos occurs mainly by transduction and not by transformation or conjugation. Additionally, this experiment demonstrates that the plasmid pDolos relies on a helper phage for effective horizontal transfer. This finding further supports the notion that pDolos functions as a satellite system. The described experiment was carried out with the kind support of my colleague Dorian Fischer.

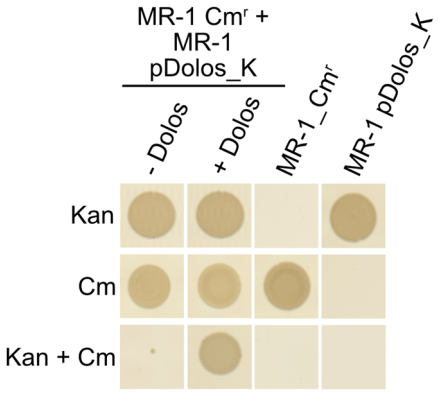

Figure 23: Dolos-mediated transduction of the satellite plasmid pDolos into other cells. *S. oneidensis* MR-1 cells possessing a resistance cassette to chloramphenicol (MR-1 Cm^r) were co-incubated with *S. oneidensis* MR-1 cells carrying the plasmid pDolos_K (MR-1 pDolos_K). After 24 hours of co-incubation, the cells were plated on agar plates containing kanamycin (Kan), chloramphenicol (Cm), or both antibiotics. Colony growth was imaged after 48 hours of incubation. + Dolos: MR-1 pDolos_K cells were pre-infected with Dolos; - Dolos: MR-1 pDolos_K cells were not pre-infected with Dolos. The experiment was performed in biological and technical duplicates.

It was then tested whether pDolos_KVL virions were produced and whether they could be transmitted by transduction, as pDolos_KVL virions could not be clearly detected in a native agarose gel assay (see **Figure 22**). For this purpose, mid-exponential *S. oneidensis* ΔΔ cells harbouring the plasmids pDolos_K, pDolos_KV or pDolos_KVL were infected with phage Dolos at a MOI of 0.1. 24 hours post-infection the virion-containing supernatants were purified. Following, mid-exponential *S. oneidensis* ΔΔ cells were infected with these mixed virion-containing supernatants at a MOI of 2. 24 hours after infection, the re-grown cells were further analysed to determine whether they had received the variants by horizontal transfer. The test shows that the cells infected with supernatants containing pDolos_K, pDolos_KV or pDolos_KVL virions grow on kanamycin plates, which indicates a successful transduction of all pDolos variants (**Figure 24 A**). Hence, also virions containing genomes larger than the Dolos genome are assembled (pDolos_KVL: 9,850 nt; Dolos: 8,146 nt). Furthermore, the cells were analysed microscopically to determine whether the Venus expression system of the variants pDolos_KV and pDolos_KVL are functional. The result shows a successful Venus fluorescence of cells infected with virion-containing supernatants harbouring pDolos_KV and pDolos_KVL (**Figure 24 B**).

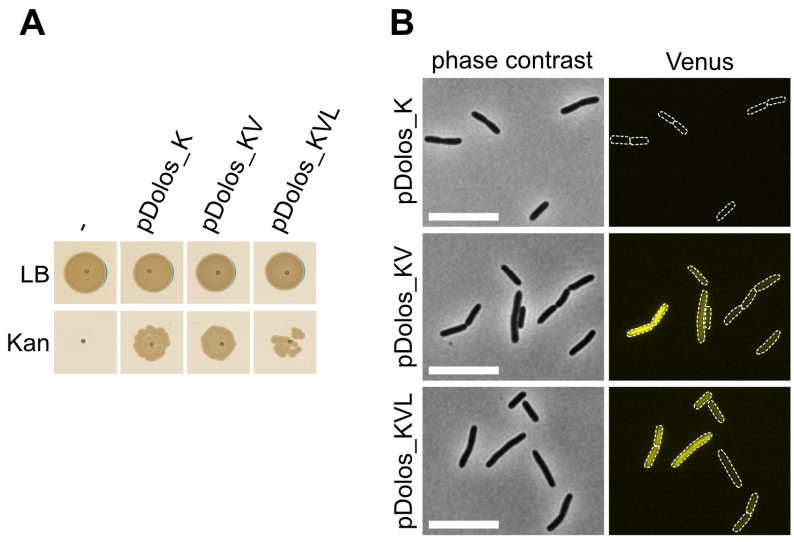

Figure 24: Horizontal gene transfer mediated by pDolos variants of different sizes. *S. oneidensis* ΔΔ cells were infected with virion-containing supernatants prepared from Dolos infected cells harbouring plasmid pDolos_K, pDolos_KV or pDolos_KVL. **A.** Successful horizontal transfer of all pDolos variants into *S. oneidensis* ΔΔ. 24 h after infection with the prepared infectious supernatants, cells of an OD_{600} 1 were spotted on LB or LB + Kanamycin (Kan) plates. Colony growth was imaged after incubation for 24 h. **B.** Horizontal transmission of *venus* by pDolos constructs. 24 h after infection with virion-containing supernatants, the Venus fluorescence of infected cells (OD_{600} 0.4) was analysed by fluorescence microscopy. Scale bar = 5 µm. The experiments were performed in biological triplicates.

Next, transduction to other species was tested. For this purpose, the virion-containing supernatant holding pDolos_K was used to infect the other identified hosts of the phage Dolos, *S. baltica* isolate S4 and S44 (see **Supplementary Table 2**). Following a 24-hour infection, the cells were spotted on agar plates with

kanamycin to test for possible pDolos-dependent resistance to the antibiotic. The test shows a successful horizontal transfer of pDolos_K into *S. baltica* isolate S4 and S44 (**Figure 25**).

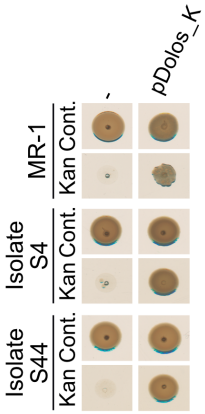

Figure 25: Successful horizontal transfer of pDolos into other *Shewanella* species. Mid-exponential cells were infected with a MOI of 2 with a supernatant prepared from Dolos-infected cells containing the plasmid pDolos_K. 24 h after transduction with the prepared infectious supernatant, cells of an OD_{600} 1 were spotted on 4M (Cont.) and 4M Kanamycin (Kan) agar plates. Colony growth was pictured after 48 h of incubation. The experiments were performed in biological triplicates. S4: *S. baltica* isolate S4, S44: *S. baltica* isolate S44, MR-1: *S. oneidensis* ΔΔ.

In summary, the results of all these transduction experiments demonstrate that pDolos can transfer additional genes into different host cells susceptible to Dolos infection.

Potential functions of pDolos proteins

To further characterise the satellite plasmid pDolos, the ORFs of the plasmid were analysed in more detail to determine their function. For this purpose, the PDB structures of the 5 proteins were predicted by using AlphaFold [131]. Subsequently, a Foldseek [132] analysis was performed to identify structurally similar proteins. In addition, a protein BLAST [112] and an InterPro [118] analysis were conducted. The analysis is shown in **Table 2**. ORF 1 of pDolos was predicted to encode a Rep protein. The Rep protein family is known to be essential for plasmid replication [19]. The protein product of ORF 2 remained of unknown function, while ORF 3 was predicted by Foldseek analysis to encode a potential transcriptional repressor. The overlapping ORFs 4 and 5 were predicted by operon-mapper [133] to be part of an operon system. Whereby ORF 4 was predicted by Foldseek to encode a potential MazE-like antitoxin. ORF 5, on the other hand, was predicted to encode a potential ssDNA-binding protein. Looking at these two ORFs, it is striking that toxin-antitoxin (TA) systems of the MazF-MazE family, which belong to the type II TA systems, have similarly structured ORFs that are operons [134]. The promoter of these systems is followed by a palindromic regulatory sequence, which is then followed by the antitoxin gene, which usually overlaps with the toxin gene. The toxins of this TA system family are mRNA-binding proteins. Under normal growth conditions, the toxin and the antitoxin form a stable protein complex that blocks the enzymatic activity of the toxin [135]. Stress conditions mediate proteolytic cleavage of the antitoxin, resulting in free toxins, which lead to cell growth arrest through sequence-specific cleavage of mRNAs [135–138]. Since some ssDNA-binding proteins, such as gp32 of the phage T4, are known to bind mRNAs, it was hypothesised that ORF 4 and 5 could encode for a potential type II TA system of the MazF-MazE family [139]. In

addition, a prediction by AlphaFold [131] revealed that a protein complex formation of pDolos protein 4 and 5 is quite possible **(Supplementary Figure 3)**.

Table 2: Protein analysis of the predicted pDolos ORFs using AlphaFold [131] (Benchling version (2023.4.MB.1)), Foldseek (web search version) [132], Protein BLAST (standard web version) [112] and InterPro (version: 96.0) [118]. The primary UniProt [140] access number of the Foldseek hits is shown in brackets. TM: template modelling, aa: amino acids.

pDolos						
						
ORF No.	**Protein structure (AlphaFold *)**	**aa**	**Foldseek analysis**	**Protein BLAST**	**InterPro**	**Assignment**
1	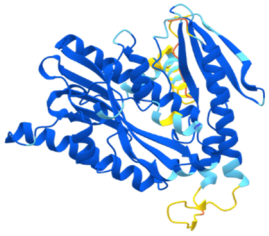	359	RepA protein [P36229] TM score: 0.65	Rep protein	Rep domain	Rep protein
2		47	Protein of unknown function	-	-	-
3	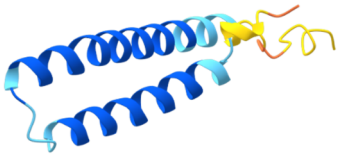	81	Potential transcriptional repressor [A0PLB8] TM score: 0.78	-	-	-
4	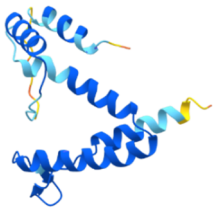	130	Potential antitoxin (MazE family) [P9WJ84] TM score: 0.48	-	-	-
5	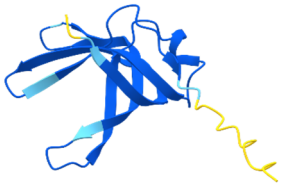	109	Potential ssDNA binding protein [Q9PKZ4] TM score: 0.40	-	-	-

*** model confidence:** dark blue: very high (pLDDT > 90), blue: confident (< 90 pLDDT > 70), yellow: low (< 70 pLDDT > 50), orange: very low (pLDDT < 50)

Satellite plasmid pDolos does not interfere with other Shewanella phages

As pDolos may contain a TA system, it was investigated whether ORF 4 and ORF 5 affect other *Shewanella* phages. This investigation was driven by the fact that many studies suggest that TA systems play an important role in anti-phage defence through inducing abortive infection, in which infected cells die in order to protect the entire population from the invader [141–143]. In particular, it was shown that phage P1 proliferates less in an *E. coli* strain possessing the MazF-MazE TA system than in an *E. coli* strain lacking the TA system, indicating protection by the MazF-MazE-TA system against phages [142]. In addition, some phage satellites have been shown not only to exploit their helper phages, but also to protect their helper phages by using anti-phage defence systems, including TA modules [89, 144].

To test a possible pDolos-mediated anti-phage defence, the effect of pDolos on the *S. oneidensis* MR-1 prophages as well as its effect on two lytic *Shewanella* phages was investigated. The strains *S. oneidensis* ΔLambdaSo and *S. oneidensis* ΔMuSo2 harbouring or not harbouring the plasmid pDolos_K were used to test the influence of pDolos on the prophages. These strains each contain a single prophage, the prophage LambdaSo or the prophage MuSo2. Prophages were induced either spontaneously by cultivating the strains for 48 hours or by using the DNA-damaging agent mitomycin C (MMC). The generated phage lysates were serially diluted and spotted on agar overlay plates containing *S. oneidensis* ΔΔ to determine any effects of pDolos on prophage proliferation. The spot test shows no effect of pDolos on the proliferation of LambdaSo or MuSo2 (**Figure 26 A**).

To test the effect of pDolos on the lytic phages Thanatos and Phonos, mid-exponential *S. oneidensis* ΔΔ cells harbouring or not harbouring the plasmid pDolos_K were infected with the lytic myoviruses Thanatos or Phonos at a MOI of 0.1. 24 hours after infection, phage lysates were prepared, serially diluted and spotted onto agar overlay plates containing *S. oneidensis* ΔΔ. This test also displays no effect of pDolos on the viral propagation of Thanatos or Phonos (**Figure 26 B**). Consequently, no influence of pDolos on the proliferation of the tested phages, which do not function as helper phages, could be demonstrated.

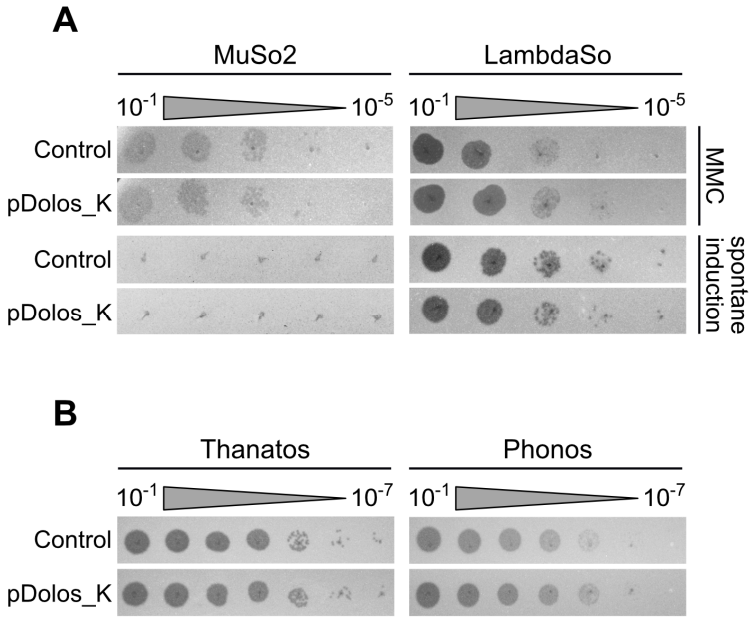

Figure 26: pDolos has no effect on prophage reproduction and virulence of lytic *Shewanella* phages. Shown are spot assays of serial diluted lysates **A.** Spot assay of lysates generated in *S. oneidensis* ΔLambdaSo or *S. oneidensis* ΔMuSo2, which were cultivated for 48 h (spontaneous prophage induction) or were treated during mid-exponential growth with 100 µg/ml MMC for 2 h (MMC). **B.** Spot assay of lysates generated in *S. oneidensis* ΔΔ cells infected with lytic phage Thanatos or Phonos at a MOI of 0.1 during mid-exponential growth. Lysate preparation was conducted 24 h after infection. pDolos_K: strain for lysate generation contained pDolos_K. The experiment was conducted in biological triplicates. The images are representative.

pDolos protein 4 and 5 are important for plasmid stability

Since pDolos does not appear to affect the proliferation of other phages, it was investigated whether ORF 4 and 5, which could encode a potential type II TA system, have an effect on plasmid stability, as many studies suggest that TA systems affect plasmid stability within a host [145–147]. To test this hypothesis, *S. oneidensis* ΔΔ cells containing pDolos lacking ORF 4 and ORF 5 (pDolos_ΔORF4-5) were cultured for three consecutive growth and re-growth cycles without kanamycin pressure. Finally, mid-exponential cells were diluted and plated on LB agar plates with and without kanamycin to determine the percentage of cells still containing pDolos. The experiment displays a mean stability of pDolos_ΔORF4-5 of 39% (**Figure 27 A**). Compared to the stability of pDolos_K (mean: 92%) which harbours ORF 4 and ORF 5, a reduction in plasmid stability is recognisable (see **Figure 21 A**).

In addition, the growth of cells expressing pDolos protein 5 was analysed. If the predicted ssDNA-binding protein is indeed a toxin, the growth of cells that exclusively express pDolos protein 5 should be arrested. For this purpose, the pBAD33 vector was used and expression of pDolos protein 5 was induced by arabinose during mid-exponential growth of *S. oneidensis* ΔΔ cells. The OD_{600} of the cells was measured serially for more than 15 hours, which showed no effect of pDolos protein 5 on the growth of *S. oneidensis* ΔΔ (**Figure 27 B**). The successful detection of pDolos protein 5 expression by Western Blot analysis is

shown in the appendix (**Supplementary Figure 4**). This result suggests that despite the influence of protein 4 and 5 on plasmid stability, protein 5 does not function as a classical toxin of a TA system in *S. oneidensis* MR-1.

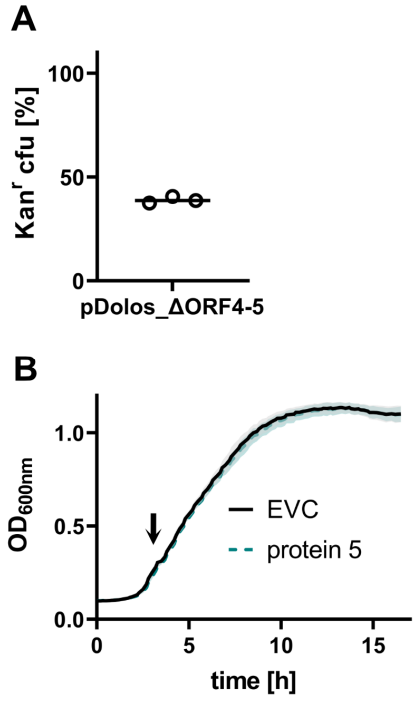

Figure 27: ORF 4 and ORF 5 of pDolos are important for long-term plasmid stability, but do not appear to function as a TA system. A. Percentage of kanamycin-resistant *S. oneidensis* ΔΔ cells containing pDolos_ΔORF4-5 after three days of cultivation without kanamycin pressure. **B.** Growth curve of cells containing pBAD expression vectors. Arrow indicates time-point of gene induction via 0.2 % arabinose. Experiment was conducted in biological triplicates. The shaded bands representing the standard deviation of the mean values. EVC: empty vector control.

2.2 Analysis of *Shewanella* phage Thanatos ADP-ribosyltransferases Alt1 and Alt2

Another aim of this study was to analyse the takeover of host cells by the lytic *Shewanella* phage Thanatos. In the centre of this study were the two host acquisition factors TH1_028 and TH1_029. Both Thanatos proteins, TH1_028 (Alt1) and TH1_029 (Alt2), are ADP-ribosyltransferases (ARTs) and are homologous to the *Escherichia* phage T4 protein Alt. In phage T4 three different ARTs are known: Alt, ModA and ModB. All these enzymes ADP-ribosylate host proteins and thereby likely regulate the viral reproductive cycle by reprogramming the host [148]. The phage T4 Alt is part of the phage particle and is injected directly into the host to ADP-ribosylate host proteins such as the RNA polymerase, which then most likely preferentially transcribes early T4 genes [149]. ModA and ModB are part of these early phage genes and in turn modify various host proteins [150, 151]. Since only 2 ARTs are present in phage Thanatos and both appear to be Alt homologues, their function during infection of *S. oneidensis* MR-1 with phage Thanatos was investigated in more detail.

2.2.1 The Thanatos virion proteins Alt1 and Alt2 are injected into cells as active proteins

At first, it was investigated whether Thanatos Alt1 and Alt2 are part of the Thanatos phage particles, as in the case of the T4 phage Alt protein. For this purpose, a Thanatos phage lysate was purified using a sucrose gradient. This method was carried out in collaboration with the Höfer group of the MPI Marburg (Nadiia Pozhydaieva and Dr. Katharina Höfer). Following, a Liquid Chromatography (LC)- Mass Spectrometry (MS) analysis was performed on the purified phage particles to identify the Thanatos virion proteins. This LC-MS analysis was gratefully conducted in collaboration with the Glatter group of the MPI Marburg. The result of the LC-MS analysis shows that 72 proteins are part of a Thanatos particle including both Thanatos ARTs Alt1 and Alt2 (**Table 3** and **Supplementary Table 3** (lists all 72 protein hits)). Here the protein TH1_029 (Alt2) stood out by being the second most abundant protein of Thanatos particles, with only the major capsid protein (TH1_010) being more abundant.

Table 3: Thanatos phage particle proteomics. Listed are the 15 most abundant phage protein hits of a LC-MS proteomics analysis of sucrose gradient purified Thanatos phage particles. TH1_028 (Alt1) and TH1_029 (Alt2) are highlighted in bold. LFQ: label free quantification.

Number	Protein ID	Protein name	LFQ
1	TH1_010	Major capsid protein	1561
2	**TH1_029 (Alt2)**	RNA polymerase-ADP-ribosyltransferase	413
3	TH1_003	Tail sheath protein	318
4	TH1_011	Capsid vertex protein	258
5	TH1_058	Lipoprotein	167
6	TH1_204	Straight tail fiber protein	128
7	TH1_032	Tail fiber protein	121
8	TH1_005	Portal protein	107
9	**TH1_028 (Alt1)**	RNA polymerase-ADP-ribosyltransferase	103
10	TH1_205	Neck whiskers protein	95
11	TH1_004	Tail tube protein	90
12	TH1_170	Tail fibers protein	74
13	TH1_198	Baseplate wedge initiator	57
14	TH1_202	Baseplate wedge protein gp10	54
15	TH1_201	Baseplate wedge tail fiber connector	49

Next, it was investigated if the ARTs Alt1 and Alt2 are injected into the host and whether they ADP-ribosylate host proteins. For this purpose, cells were harvested at various time points after infection with Thanatos. The collected samples were analysed by Western Blot using an anti-pan-ADP-ribose reagent to detect ADP-ribosylation of proteins. The analysis shows detection of ADP-ribosylated proteins as early as 5 minutes after infection. The amount of ADP-ribosylated proteins increases during the infection progresses (**Figure 28**). This result indicates that these proteins must be injected parallel or even prior to the injection of the phage DNA in order to directly manipulate the host proteins, as Thanatos requires about 2 minutes to adsorb to the host [72].

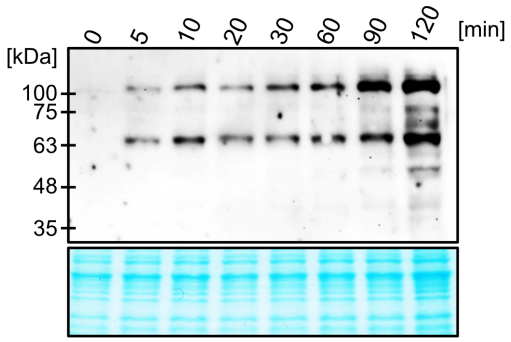

Figure 28: Thanatos-mediated ADP-ribosylation of host proteins starts immediately upon phage infection. Shown is a Western Blot analysis using an anti-pan-ADP-ribose binding reagent to analyse phage-mediated ADP-ribosylation of proteins. Mid-exponential *S. oneidensis* ΔΔ cells were infected with phage Thanatos at a MOI of 0.1. Cell samples for Western Blot analysis were taken at different time-points after phage infection. Upper panel: detection of ADP-ribosylated proteins, lower panel: Coomassie stain of total proteins. The experiment was conducted in biological triplicates. The image is representative.

2.2.2 Different Alt1 and Alt2 host protein interaction profiles

The Alt1- and Alt2-dependent protein modification profiles were then analysed. For this purpose, the pBAD33 expression vector system was used to analyse the Alt1- and Alt2-dependent modification of host proteins without phage infection. Gene expression of the pBAD33 vectors was induced by adding arabinose to mid-exponential *S. oneidensis* ΔΔ cells containing different expression plasmids. 1.5 hours after induction, cells were harvested and analysed by Western Blot using the anti-pan-ADP-ribose reagent to detect ADP-ribosylation of proteins. The Western Blot analysis indicates that Alt2 has a more diverse and stronger ADP-ribosylation profile of the host proteins compared to Alt1 (**Figure 29 A**). In addition, this Western Blot analysis displays that specific amino acid substitutions in Alt1 ($Alt1^{E521A}$) and Alt2 ($Alt2^{E541A}$) disrupt the enzymatic activity of the ARTs.

Following, His-tagged Alt1 and Alt2 proteins were purified by affinity chromatography and following size exclusion chromatography to analyse a possible autocatalytic activity of Alt1 and Alt2, which has been described for the T4 phage ART ModB [152]. Protein purification record charts are shown in the **Supplementary Figure 5** and **6**. Western Blot analysis of the purified proteins using an anti-His antibody shows His-tagged proteins at about 63 kDa in the case of Alt1 (Alt1: 68 kDa) and His-tagged proteins at about 75 kDa in the case of Alt2 (Alt2: 73 kDa), indicating successful purification of Alt1 and Alt2. The use of the anti-pan-ADP-ribose reagent to detect ADP-ribosylation shows that the signals correspond to the protein sizes of Alt1 and Alt2, suggesting autocatalytic activity of both proteins (**Figure 29 B**).

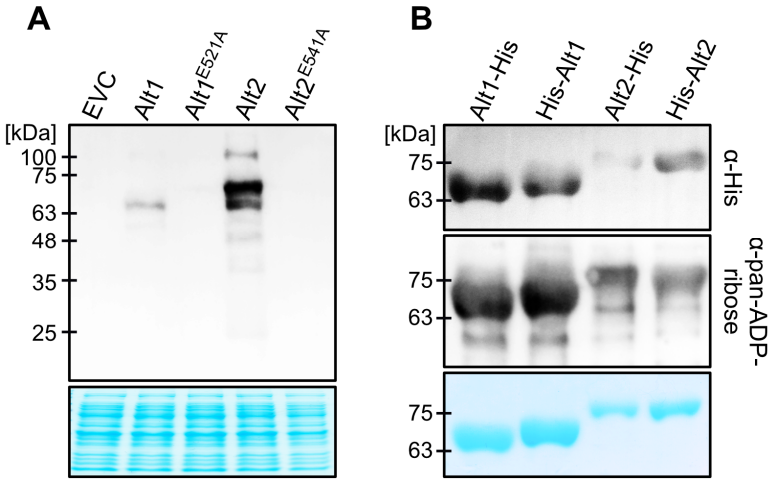

Figure 29: Autocatalytic activity and differential ADP-ribosylation profiles of Thanatos ADP-ribosyltransferases Alt1 and Alt2. Shown are Western Blot analysis using the anti-pan-ribose binding reagent to examine ADP-ribosylation of proteins. **A.** ADP-ribosylation profile analysis of *S. oneidensis* ΔΔ cells harbouring different pBAD33 overexpression plasmids. 1.5 h after arabinose induction of genes, samples for Western Blot analysis were taken. EVC: Empty Vector Control. **B.** Autocatalytic-activity Western Blot analysis of purified His-tagged Alt1 and Alt2 proteins using a chromatography system for protein purification. Upper panel: detection of His-tagged proteins using an anti-His antibody, middle panel: detection of ADP-ribosylated proteins, lower panel: Coomassie stain of total proteins. The experiments were conducted in biological triplicates.

After clarifying that the Thanatos ARTs Alt1 and Alt2 exhibit autocatalytic activities and have a distinct host interaction profile, the host proteins with which they interact were investigated. For this purpose, N-terminal V5-labelled Alt1 or Alt2 proteins were expressed in *S. oneidensis* MR-1 and the cells were subsequently disrupted to isolate the cytoplasmic proteins (**Supplementary Figure 7**). Co-immunoprecipitation (IP) was then performed with these samples and the precipitated proteins were subsequently analysed by LC-MS. The mentioned co-IP was performed in collaboration with Prof. Dr. Lienhard Schmitz (JLU Giessen) and the subsequent LC-MS analysis was kindly performed by Aleksandra Bogucka (Lochnit group, JLU Giessen).

The MS analysis reveals significant interactions of six *S. oneidensis* MR-1 proteins with Alt1 and eight *S. oneidensis* MR-1 proteins with Alt2 (**Table 4**). In both cases, a toxin of a TA system potentially interacts with a Thanatos ART. In addition to toxins, which in some cases have a function in anti-phage defence [89], other proteins known to play a role in anti-phage defence, such as a dGTPase (deoxyguanosinetriphosphate triphosphohydrolase) [153], have also been identified as potentially interacting proteins. Interestingly, the ART Alt2 also appears to interact with several metabolic proteins such as CfaS (cyclopropane-fatty acyl-phospholipid synthase CfaS).

Table 4: *Shewanella oneidensis* MR-1 proteins that interact with phage Thanatos ARTs Alt1 or Alt2. Listed are *Shewanella oneidensis* MR-1 protein hits resulting from an LC-MS analysis of a co-IP. The bait proteins used in the co-IP were the Thanatos proteins Alt1 and Alt2. Experiment was conducted in biological triplicates. Interacting proteins are sorted in descending order of results p-value significance (limma t-test).

	Protein ID	Protein name	p-value
Alt1			
	SO_4641	Toxin-antitoxin system toxin RelE family	0.002
	SO_3081	UPF0115 protein YfcN	0.009
	SO_2485	Deoxyguanosinetriphosphate triphosphohydrolase-like protein	0.012
	SO_0427	Bifunctional diguanylate cyclase / phosphodiesterase with PAS sensory domain	0.035
	SO_3676	DUF2956 domain-containern protein	0.035
	SO_0768	NAD dependent epimerase/dehydratase family protein	0.043
Alt2			
	SO_0138	MoeA (Molybdopterin molybdenumtransferase)	0.004
	SO_2180	Periplasmic metalloprotease M23B family	0.006
	SO_3519	GlnB (Regulatory protein for nitrogen assimilation by glutamine synthetase GlnB)	0.009
	SO_3379	CfaS (Cyclopropane-fatty-acyl-phospholipid synthase CfaS)	0.015
	SO_0301	RsmI (Ribosomal RNA small subunit methyltransferase I)	0.023
	SO_2722	4-hydroxybenzoyl-CoA thioesterase family protein	0.033
	SO_0063	Toxin-antitoxin system toxin HipA family	0.036
	SO_3024	TrpA (Tryptophan synthase alpha chain)	0.040

2.2.3 Activity of Alt2 positively influences Thanatos propagation

To further analyse the Thanatos ARTs Alt1 and Alt2, Thanatos mutants showing loss of activity were generated. Since modification of lytic phages is very difficult due to the lack of selection markers [154], a method described by Shitrit *et al.* 2022 [155] was used where the activity-disrupting substitutions were provided along with a small Tag (~70 bp) for homologous recombination. For the subsequent screening for phage mutants, phage enrichment steps were first carried out, followed by a large-scale PCR screening using the inserted Tag as a primer binding site. Finally, the Thanatos mutants Alt1^{E521A}, Alt2^{E541A} and a double mutant with amino acid changes in both ARTs (Alt1^{E521A}, Alt2^{E541A}), were generated.

These three mutants were used to perform an infection assay in which mid-exponential *S. oneidensis* ΔΔ cells were infected with a Thanatos variant at a MOI of 0.1. Protein samples were taken 30 minutes after infection

and analysed by Western Blot using the anti-pan-ADP-ribose reagent. The analysis again shows a stronger ADP-ribosylation profile of Alt2 compared to Alt1, as functional loss of Alt2 prevents Thanatos Alt2-dependent ADP-ribosylation (**Figure 30 A**, see **Figure 29 A**). In addition, a complete loss of ADP-ribosylation is seen when both enzymes are inactivated.

To analyse potential phenotypes caused by Alt1 and Alt2, a growth curve of infected cells and a Thanatos reproduction assay were performed. For both assays, mid-exponential *S. oneidensis* ΔΔ cells were infected with different Thanatos variants at a MOI of 0.1.

The OD_{600} and thus the bacterial growth was serially monitored for about 20 hours after infection. The generated growth curves showed that cellular growth stagnated around 2 hours after Thanatos infection, after which the optical density decreased continuously due to cell lysis (**Figure 30 B**). Looking at the first killing curve, the lysis behaviour of the Thanatos mutants compared to the Thanatos wt does not differ. However, it should be noted that a second Thanatos-dependent lysis of Thanatos wt phages is observed approximately 15 hours after infection, suggesting that Alt1 and Alt2 may be important for the evolutionary adaptation of Thanatos to the host or the prevention of the evolutionary adaptation of the host to Thanatos.

In addition, a phage reproduction assay was performed in which the supernatants were collected 2, 4 and 24 hours after infection. The phage concentration of these samples was then determined. The result shows a significant decrease in the Thanatos Alt2^{E541A} and Thanatos double mutant phage concentration after 4 hours of infection compared to the Thanatos wt phage concentration (**Figure 30 C**). Furthermore, this difference compared to Thanatos wt is still present after 24 hours of infection. Interestingly, the extracellular concentration of the Thanatos Alt2^{E541A} and the Thanatos double mutant phage particles is approximately 10 times lower after 4 hours of infection compared to 2 hours of infection. This observation led to the hypothesis of particle degradation, as the growth curve (see **Figure 30 B**) indicates that there is no difference in host cell number during infection with the different Thanatos variants and thus no variation in the amount of potential adsorption surfaces.

Furthermore, a plaque assay was performed with the different Thanatos mutants to analyse the morphology of the plaques. The test shows larger plaques of the Thanatos Alt2^{E541A} mutant and the Thanatos double mutant compared to the Thanatos wt (**Figure 30 D**). This phenomenon is directly related to Alt2^{E541A}, as the double mutant was generated based on Thanatos Alt1^{E521A}, meaning that Alt2^{E541A} was newly inserted.

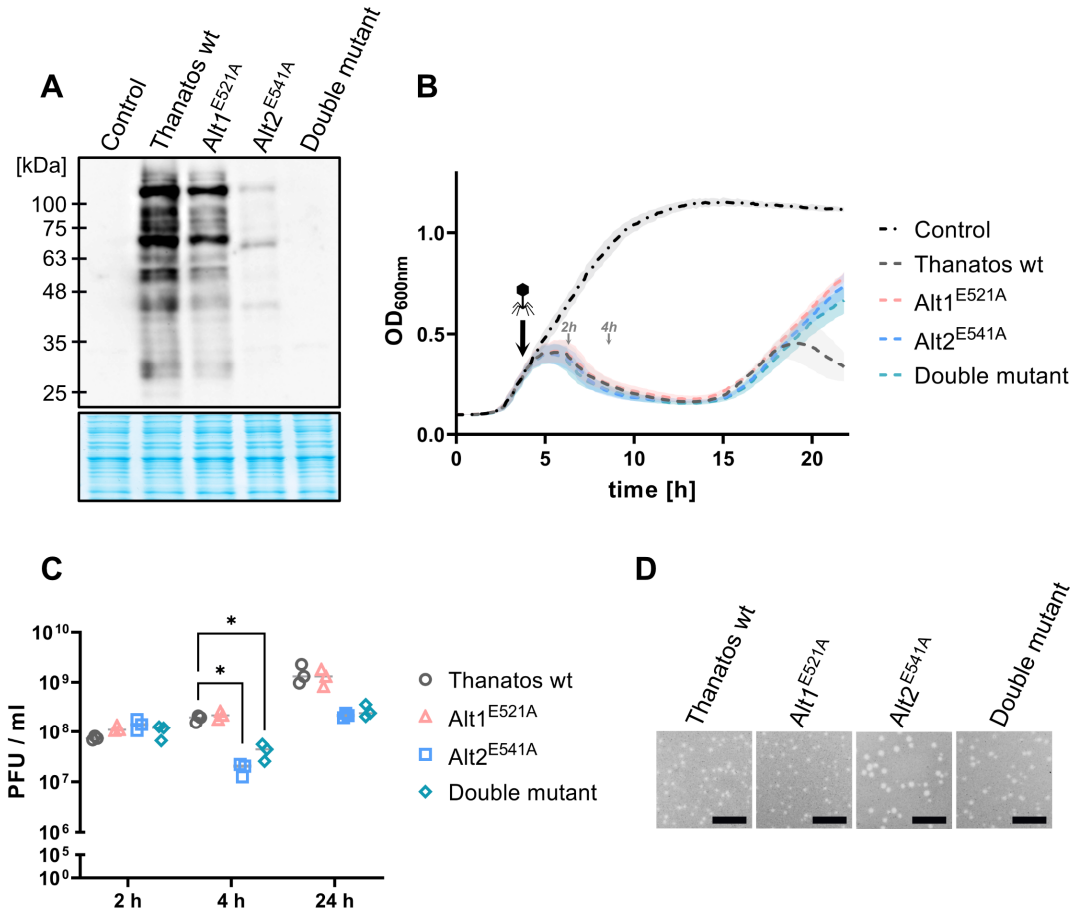

Figure 30: Alt-dependent ADP-ribosylation of host proteins is important for total phage reproduction and a stable long-time infection. A. Western Blot analysis of ADP-ribosylation profiles of Thanatos mutants. Mid-exponential *S. oneidensis* ΔΔ cells were infected with Thanatos phages at a MOI of 0.1. **A.** Samples for Western Blot analysis were collected 30 min after infection. Upper panel: detection of ADP-ribosylated proteins, lower panel: Coomassie stain of total proteins. **B.** Growth of *S. oneidensis* ΔΔ cells infected during mid-exponential growth-phase with different Thanatos phage variants (MOI 0.1). OD_{600} of cell cultures was measured subsequently for 22 h. Infection time-point is indicated by a phage symbol. Shown in light grey letters are the time-point of growth stagnation (~2 h after infection) and the time-point of phage-dependent extensive lysis (~4 h after infection). Experiment was conducted in biological triplicates. The shaded bands representing the standard deviation of the mean values. **C.** Phage reproduction assay showing the amount of phage particles in the cell culture medium during different time points of an infection cycle. Mid-exponential *S. oneidensis* ΔΔ cells were infected with Thanatos phage variants at an MOI of 0.1. Samples were taken 2 h, 4 h and 24 h after infection and the PFU per ml was determined by plaque assay. * : $p < 0.05$ (t-test) **D.** Plaque assay showing plaque morphology of Thanatos variants. Scale bar = 5 mm. Control: no infection, Double mutant: $Alt1^{E521A}$ $Alt2^{E541A}$. All experiments were conducted in biological triplicates.

3. Discussion

3.1 Analysis of the *Shewanella* phage Dolos and the plasmid pDolos

3.1.1 Characterization of *Shewanella* phage Dolos

Inoviruses are filamentous phages that cause chronic infections and maintain a stable state within the host while continuously producing and releasing virions [51]. The infection of cells with inoviruses is difficult to detect using conventional plating methods due to the lack of lysis [116, 117]. Viral plaques are caused only by a slight growth delay of the infected cells, which produce large amounts of viral structural proteins. Plaques originating from these viruses are usually turbid, and some inoviruses do not form plaques at all. The difficulties in detecting inovirus infections have probably led to a drastic underestimation of the frequency of inoviruses in nature [51]. This assumption is supported by the fact that metagenomic analyses have shown that cryptic inoviruses are widespread in microbial genomes and can be detected in a variety of different biomes on Earth, indicating a major importance for global ecosystems [9]. However, considering the currently described phages, inoviruses have been described very rarely, with the majority of all bacteriophages (>95%) being tailed phages [48].

In this study, a new member of the viral family *Inoviridae* which infects selected *Shewanella* species was isolated and characterised. When analysing the genome of the newly described *Shewanella* phage Dolos, it is apparent that of the 11 known inoviral core genes [69, 156], the genes gIV, gX and gXI could not be identified. Gene gIV encodes the protein pIV, which is involved in pore formation and thus important for the extrusion process of virions. The absence of a pIV homologue is observed in a number of filamentous phages that infect Gram-negative bacteria [69]. The CTXφ phage that infects *V. cholerae* also lacks pIV and instead utilises the host's type II secretion system for pore formation [157]. It is therefore likely that phage Dolos also utilises host proteins to fully form the secretory pore. The viral gene gX, which is also missing in the predicted genome annotation, codes for a replication-associated protein and is an in-frame translational product that results from an internal start codon within gII [158]. The situation is similar with gXI, which codes for a protein important for virion assembly and export. gXI is an in-frame translational product within gI [69, 158, 159]. Because members of the family *Inoviridae* mutate rapidly, it is difficult to predict the exact position of gX within gII and gXI within gI. Normally, the assignment of the inoviral core genes is done by analysing the arrangement of the ORFs, the length of the ORFs and the protein domains found within the viral protein products [69]. In order to determine the translational start sites of gX and gXI, experiments such as an analysis of the entire viral proteome or pull-down assays should be performed. In the latter, the C-terminus of pI and pII should be tagged, followed by an MS analysis.
In addition, the ORFs 8 to 11 of Dolos are not essential for inoviruses. ORFs 8, 10 and 11 have unknown functions, while ORF 9 shares homologies with MazE-like antitoxins. In general, the presence of further ORFs which are not related to the inovirus core functions are common among this virus family. Inoviruses exhibit a high horizontal exchange of DNA, which among other things leads to the spread of virulence

factors and anti-phage defence systems like TA systems [9, 69, 117]. The putative antitoxin encoded by ORF 9 could be a possible remnant of a functional TA module, as ORF 9 is not part of a functional TA operon system. Moreover, the high horizontal DNA exchange of inoviruses leads to a high mutation frequency, resulting in low sequence homology within this family [69].

In an experiment, this high genetic variability could be demonstrated by the insertion of a chloramphenicol resistance cassette into different intergenic regions of Dolos (Dolos_Cm constructs). However, after electroporation into the host cells, the resistant cells were unable to produce infectious virions, which were expected to be larger than the native virions due to the increased genome size [160, 161]. By stopping the chloramphenicol exposure for one day, infectious virions were produced again. Genome analysis revealed that the chloramphenicol resistance gene as well as gene 11 and the promoter of gII had been removed within this day of cultivation, resulting in a functional virion-producing phage that utilised the promoter of the chloramphenicol resistance cassette for the transcription of gII. This drastic and rapid reversal of the cloning procedure has already been described for phage M13 [162]. However, this does not explain the complete lack of virion production of the Dolos_Cm constructs (~ 9,200 nt) under chloramphenicol pressure, since experiments with Dolos together with plasmid pDolos_KVL (~ 9,850 nt) result in pDolos_KVL particles that are larger than the native Dolos particles. A possible sensitivity of Dolos virions to the antibiotic chloramphenicol should therefore be tested, as it has been shown that some aminoglycosides have antiviral properties on phages of different viral orders. However, an antiviral effect of aminoglycosides against inovirus M13 or fd was not observed in this study [163]. There is also no evidence that the antibiotic chloramphenicol, an amphenicol, inhibits virion production of inoviruses. An fd-derived phage display system using a chloramphenicol resistance cassette for selection shows that fd-derived functional virions are produced in the presence of chloramphenicol [164]. How this observed viral phenotype came about and whether and how the Dolos phage can be genetically modified without impairing genetic stability must therefore be investigated in more detail.

When analysing the basic viral properties of the phage Dolos, the major pilin subunit MshA of the MSHA pilus was determined to be the adsorption receptor. According to current literature, all presently described inoviruses use a pilus as an adsorption receptor [45]. The Ff filamentous coliphages (M13, fd and f1), which are almost identical viruses as indicated by a genetic similarity of about 98%, but were discovered independently [73], are the best studied models and attach to the tip of the F-pilus of *E. coli* [73, 165]. Like Dolos, the *V. cholerae* phage VGJφ uses the MSHA pilus as adsorption receptor [166], but an infection of the VGJφ sensitive *V. cholerae* El Tor N16961 strain with Dolos was not possible. However, the MshA amino acid identities between *S. oneidensis* MR-1 and *V. cholerae* El Tor N16961 are only about 68%. In addition, no analysis of the exact adsorption receptor used by VGJφ was carried out, so it is not known whether VGJφ binds a minor pilin and thus attaches to the pilus tip like the Ff coliphages, or binds to the major pilin subunit MshA like the *Shewanella* phage Dolos.

The influence of the pilus activity on the transduction efficiency and infectivity of inoviruses has already been analysed by Floyd *et al.* 2020 using the VGJφ phage [104]. In this work, amino acid substitutions in

the pilus extension ATPase MshE (MshE$^{L10A/L54A/L58A}$) of *V. cholerae* led to a constitutively active and thus extended state of the MSHA pilus by preventing c-di-GMP binding. The quantity of surface-exposed MshA of the strain MshE$^{L10A/L54A/L58A}$ and the wt were similar, but the individual pili seemed to be longer in the MshE$^{L10A/L54A/L58A}$ strain [104]. This phenotype was not observed in *S. oneidensis* MR-1, in which substitutions in MshE (MshE$^{L9A/L53A/L57A}$) resulted in a significant reduction of surface exposed MshA. In addition, the study showed that VGJφ transduction is increased in the MshE$^{L10A/L54A/L58A}$ strain compared to the wt, indicating a hyperretractile state of the MSHA pilus in *V. cholerae* [104]. In contrast, the adsorption of inovirus Dolos to the *S. oneidensis* MR-1 MshE$^{L9A/L53A/L57A}$ strain is significantly reduced compared to the adsorption to the control strain. The intracellular c-di-GMP concentrations and the importance of the second messenger c-di-GMP for pilus activity, as well as the interaction of the protein components of the highly complex protein machinery "MSHA-Pilus", therefore most likely differ between *V. cholerae* and *S. oneidensis* MR-1.

Remarkably, changes in *S. oneidensis* MR-1 pilus activity do not seem to have a major impact on the fitness of phage Dolos. Thus, the adsorption time and the time from phage adsorption to injection of viral DNA do not appear to be crucial for viral fitness, as the viral output after 24 hours of Dolos infection is balanced in both the MshE$^{L9A/L53A/L57A}$ and the control strain. This effect could be due to the chronic infection caused by inoviruses. Once a cell is infected with a non-integrative inovirus, the cell constantly produces viral progenies. A slight increase in the time required for the injection of the inoviral DNA does not appear to have a significant effect on the quantity of progeny in long-term infections.

Compared to viruses which utilise the lytic life cycle, the general adsorption time of Dolos and other inoviruses to their hosts is very long and difficult to measure due to the long time period and constant growth of the host cells [167]. The lytic *Shewanella* phage Thanatos, for example, requires less than 3 minutes for 50% of the phages to adsorb to *S. oneidensis* MR-1 [72], while Dolos requires 60 minutes. As lytic phages lyse their host at the end of their life cycle, the predatory pressure on bacterial hosts is very high, leading to constant adaptation and predator-prey competition [168]. Competition between different phages within a host also increases the selection pressure on phages, so rapid infection and the quick production and release of numerous viral progeny are likely to increase the persistence of a lytic phage [168, 169]. A chronic lifestyle, as practised by inoviruses, is unlikely to lead to such a high predatory pressure on bacteria as is the case with lytic phages. Of course, like all MGEs, inoviruses also have to compete with other MGEs within a host, but the reproduction cycle does not depend on killing the host, which thus should reduce the viral pressure on the host. The comparatively long adsorption time of inoviruses could possibly even be a fitness advantage, as potential hosts that are already infected with a lytic phage are doomed to die; a massive and rapid adsorption of inovirus virions to such a host would be pointless and would only lead to a permanent blockade of the phage attachment proteins and thus render the attached virions useless for reproduction. Additionally, the diffusion-based spread of inovirus virions could be longer on average than that of most lytic phages. This is because the probability of adsorption to a relatively rare adsorption receptor is lower, which increases the likelihood of reaching an uninfected host. Inovirus virions therefore on average possibly

have to persist extracellularly longer than most lytic virions. This hypothesis could be supported by the fact that inovirus virions are usually extreme pH and thermostable [117, 170]. A pronounced pH stability from pH 4 to pH 12 has also been demonstrated for the newly described inovirus Dolos.
Since too fast adsorption and too fast DNA injection could be a disadvantage for the inoviral fitness, the use of the MSHA pilus as adsorption receptor seems to be highly advantageous. Pili are not as abundant as the adsorption receptors often used by lytic phages, such as LPS structures and outer membrane proteins (OMPs) [171]. In addition, the MSHA pilus must be retracted to allow the virus to reach the secondary receptor in the inner membrane. Apparently, rapid infection does not seem to be crucial for the successful persistence and spread of inoviruses such as Dolos, as it is the case with lytic phages, but rather the right timing, as the host's MSHA pilus activity depends on factors such as the host's c-di-GMP level, which influences the host's growth phase and lifestyle. [96, 104, 172, 173].

The present study investigated the Dolos-dependent influence on planktonic cells and biofilms of *S. oneidensis* MR-1. As described for inoviruses, a slight phage-dependent growth delay of planktonic cells can also be observed when cells are infected with Dolos, which is probably caused by the massive production of viral structural proteins. In addition, Dolos-infected planktonic cells presumably exhibit increased capsule production. Bacterial capsule production is an efficient mechanism for covering surface structures and blocking the attachment step of phages [174–176]. Thus, a phage-dependent increase in capsule production could be a virus-mediated anti-phage system that likely protects both the host *S.oneidensis* MR-1 and the phage Dolos from infection with other phages. To clarify this possible connection, a capsule staining of the bacteria should be performed to confirm the phenotype observed by negative staining of infected cells with subsequent EM analysis, as negative staining on a grid is very irregular. In addition, a phage adsorption test with other *Shewanella* phages (e.g. Thanatos) should be performed by using cells long-term infected with Dolos as host to elucidate differences in adsorption time.

The analysis of the sessile lifestyle of infected cells shows that Dolos has a negative effect on biofilm formation, whereas most studies have shown a positive effect of inoviruses on biofilm formation [177, 178]. *Pseudomonas* Pf prophages are the best-known models used to investigate the influence of inoviruses on biofilms. These phages, for example, positively influence biofilm formation and the stability of mature biofilms through the accumulation of virions, which act as an important structural component of the extracellular matrix [177]. The *Pseudomonas* prophage Pf4 was also found to enhance the release of eDNA, leading to an increase of the overall biofilm biomass [64, 128]. In addition, it has been shown that the integrative *Vibrio* phage CTXφ has a positive effect on the transcription of genes involved in biofilm formation [178].
The presented study on the influence of phage Dolos on *S. oneidensis* MR-1 biofilm formation is of great importance as data on the influence of non-integrative inoviruses on biofilm formation is currently underrepresented. It was shown that the biofilm formation of long-term Dolos-infected cells was reduced compared to the uninfected control. This result was observed for both static and flow chamber grown

biofilms. In addition, it appears that the amount of dead cells within a biofilm is reduced when cells are infected with Dolos. Thus, Dolos strongly influences the sessile lifestyle of its host.
Another study also showed an extreme effect of a filamentous phage on the lifestyle of its host. The inovirus φRSS1 increases the type IV pilus pilin production of its host *Ralstonia solanacearum* and thus influences the hosts twitching ability, which is important for bacterial movement over solid surfaces [179]. Therefore, it is necessary to investigate whether Dolos affects crucial factors of biofilm formation, such as MSHA pilus activity or matrix production. To investigate how Dolos affects its host *S. oneidensis* MR-1 in detail, especially in relation to biofilm formation, a first approach could be to analyse the transcriptome of infected cells.

3.1.2 Characterization of satellite plasmid pDolos

In this study, a second MGE was co-isolated with the phage Dolos, which based on the data obtained was named "satellite plasmid pDolos". In the following, this newly described MGE is viewed both in the plasmid and phage satellite context in order to classify the reproduction strategy and the parasitic behaviour of this genetic element.

Analysis of pDolos in a plasmid context

In this study, an extrachromosomal, circular, ssDNA-based genetic element with a length of 2,926 nt was co-isolated together with the phage Dolos from a freshwater sediment sample. The newly described MGE was identified as a plasmid consisting of 5 ORFs, one of which was predicted to encode a Rep protein. Rep proteins are HUH endonucleases that contain a HUH motif consisting of a histidine followed by an undefined hydrophobic amino acid and a second histidine [30]. HUH endonucleases are ubiquitous proteins involved in replication, conjugation and recombination [30, 38]. The conserved HUH motif is crucial for the binding of divalent cations that are involved in the catalytic activity of these endonucleases [30, 180, 181]. These proteins can be categorised into two replicative (Rep) protein families and six mobility (Mob) protein families with the categorization depending on the motifs present, the order of the motifs as well as the amount and order of the catalytic tyrosine residues [39]. Based on an AlphaFold [131] structure prediction with subsequent Foldseek [132] analysis, it was shown that the Rep protein of pDolos is very similar to RepA from the plasmid pBAA1 of *Bacillus sp.*, which is likely to be replicated via rolling-circle replication (RCR) [182]. RepA is a member of the Rep_1 family, whose main function is the replication and not the mobilisation of plasmids [39]. Looking at the 17 RCR plasmid families described so far, pDolos could be assigned to the well-described pC194 family [38, 40]. This plasmid family characteristically has a RepA protein and a leading-strand nick site with the sequence 5'-cttgata-3' upstream of the Rep protein [38, 40, 183]. The isolation of pDolos as an ssDNA plasmid and the exclusive occurrence of circular ssDNA as an intermediate of the RCR of plasmids support the assumption that pDolos could be an RCR plasmid

[19]. Furthermore, unlike plasmids that carry out strand-displacement replication, RCR plasmids require only a single Rep protein [19, 36]. Therefore, it is very likely that pDolos belongs to the pC194 family of RCR plasmids.

Since pDolos appears to be an RCR plasmid the question arises regarding the exact replication differences between these types of plasmids and inoviruses, since non-integrative inoviruses persist in a host as RCR plasmids [69, 184]. Even though the mechanisms of inoviral replication are very similar to the replication of pC194-like plasmids, there are significant differences. The most important point to note is that the replication protein (pII) of inoviruses lacks a HUH motif, which is a conserved motif of RepA proteins [38]. Nevertheless, the nicking of the DNA also depends on divalent cations that interact with pII via a so far unknown mechanism [184]. Since a HUH motif is conserved in the pC194 plasmid family and the absence of such a motif is a feature of inoviral pII proteins, it is unlikely that pDolos originates from an inovirus that has lost all phage structural genes and adapted to other inoviruses. It seems more likely that pDolos is a RCR plasmid that adapted to inoviruses by mimicking the viral packaging signal, an approximately 80 nt long ssDNA hairpin [156, 185]. By mimicking the packaging signal, the DNA of pDolos can be transported to the inner membrane and interact with the pVII/pIX complex, which initiates virion assembly [156, 185].

There are also differences between pII and Rep proteins in the mechanism of RCR. The Rep-mediated plasmid RCR terminates after each completed cycle, whereas the pII tetramers for inoviral replication are recycled two to three times before the pII complex dissociates from the (-)-strand. This leads to the production of two to three ssDNA copies per replication cycle, which can then be packaged [184]. Members of the *Microviridae* family, which are also circular ssDNA viruses but undergo the lytic life cycle, recycle the (-)-strand up to 20 times, resulting in a large number of ssDNA progeny before the replication complex dissociates from the (-)-strand [184]. This comparison of the replication complexes used for RCR leads to the conclusion that the ratio of the infectious form ((+)-ssDNA) to the replicative form (dsDNA) differs drastically depending on the replication strategy. Microviruses that carry out lytic infection need to produce many progeny in a short time, whereas inoviruses that carry out chronic infection do not depend on a high release of progeny in a brief time. However, plasmids usually do not depend at all on the production of ssDNA for packaging and release of virions. The (+)-ssDNA of RCR plasmids is typically an intermediate of RCR, followed by (-)-strand synthesis, resulting in a circular dsDNA plasmid [38]. Thus, the circular ssDNA intermediate of RCR plasmids should be less abundant compared to the circular ssDNA genome of inoviruses. The ratio of (+)-stranded ssDNA to dsDNA of the plasmid pDolos should therefore be analysed and compared with the ssDNA to dsDNA ratio of the phage Dolos. For this purpose, it is recommended to use cells infected with pDolos_K and to isolate the plasmids from these cells. By following enzymatic cutting of the plasmid dsDNA, the exact ratio of ssDNA plasmid to dsDNA plasmid can be determined after electroporation and selection on kanamycin plates. This experiment could demonstrate a possible replicative adaptation of the satellite plasmid pDolos to the helper phage Dolos.

Looking at the coding genes of RCR plasmids, it is noticeable that antibiotic resistance genes are frequently present [38]. Such genes are often discovered on MGEs such as plasmids on which they are thought to ensure genetic stability [29, 186]. The reason for this is that, under normal conditions, the presence of a plasmid reduces the fitness of bacteria by slowing down the proliferation of the host cell, which suffers from the plasmid-dependent consumption of cellular resources. Plasmids are therefore just cellular invaders, genetic parasites, that consume cellular resources for their selfish propagation [187, 188]. Consequently, plasmids often carry genes that provide the host with a fitness advantage under certain conditions, such as antibiotic resistance genes [189].

Harbouring TA modules is also a mechanism for ensuring genetic stability, hence these modules are very commonly found on plasmids and other MGEs [190]. Removal of a plasmid harbouring a TA system usually leads to post-segregational killing of the host cell, as toxins are more stable than antitoxins [191]. Without constitutive production of the antitoxin, the toxin will become free after a certain period of time and will therefore no longer be bound in a TA complex. This then allows the toxin to exert its toxic function within the cell [192, 193]. The assumption that ORF 4 and ORF 5 could encode a TA system is based on the fact that no other ORFs are considered for the genetic stability of the plasmid pDolos. This is supported by the fact that, with the exception of ORF 4, the ORFs of pDolos appear to encode nucleic acid-binding proteins, which could therefore have regulatory functions at the DNA or RNA level, whereas known systems for ensuring plasmid stability, such as antibiotic resistance systems, all function at the protein level [194]. Moreover, the pDolos ORFs 4 and 5 are part of an operon system that is structurally similar to known type II TA modules [193, 195]. Additionally, it is likely that the pDolos protein 4 and 5 form a complex, however, no evidence of pDolos protein 5 having a toxic function has been demonstrated. Remarkably, the operon described appears to contribute to the long-term stability of the plasmid, despite lacking any toxic function. It could therefore be possible that this operon has a regulatory function on the host or pDolos itself.

The functional characterisation of the different pDolos proteins, including protein 4 and 5, should be the main goal to understand the life cycle and the interaction of pDolos with the phage Dolos and its host *S. oneidensis* MR-1, as most of the pDolos protein products seem to interact with nucleic acid and thus could have a regulatory function.

Assuming that pDolos has no known stability assurance system, the question arises how it can exist at all. This described phenomenon is called the "plasmid paradox" [27, 186, 196]. Various models for the distribution and stability of plasmids show that plasmids cannot theoretically exist [197, 198]. This is due to the fact that the maintenance of a plasmid is associated with fitness costs for the host cell. Furthermore, the segregation of plasmids is imperfect, which should lead to plasmid-containing cells being removed from bacterial populations by selection, as plasmid-free cells outcompete cells harbouring a plasmid [186, 197]. Nevertheless, plasmids are extremely common and are considered to be important drivers of bacterial evolution [186, 199, 200]. In addition, there are often plasmids in nature that do not contain known genes that provide the host with a fitness advantage under certain conditions (e.g. antibiotic resistance genes) or

a fitness disadvantage when the plasmid is disposed of (e.g. TA systems) [201]. Again, models predict that even if plasmids are able to outweigh the cellular costs of their persistence (e.g. through antibiotic resistance genes) or even if they increase the pressure on bacteria by carrying toxic properties (e.g. TA systems), bacteria would capture these genes and then dispose the reduced plasmids [186, 197]. Plasmids which contain no known stability genes, are referred to as cryptic plasmids. These are usually small plasmids that carry only replication genes and a few genes of unknown function [1, 12]. It is therefore quite possible that pDolos has no known stability genes at all and therefore likely belongs to the group of cryptic plasmids.

Analysis of pDolos in a phage satellite context

Since the newly described plasmid pDolos can be transferred into cells by transduction, the question arises as to whether pDolos is really (just) a plasmid. According to the definition coined by Joshua Lederberg in 1952, a plasmid is a *mobile* or at least self-transmissible*, extrachromosomal, circular* genetic element that is transferred as *unpacked* DNA [26, 202]. The newly described plasmid pDolos appears to have extended the horizontal transfer through the use of transduction, which means that it is not (only) transferred as *unpacked* DNA. The genetic transfer by transduction is typically carried out by viruses and by MGEs of the satellite group [203, 204]. Satellites are genetic elements that parasitize viruses and can therefore be considered as the viruses of viruses. MGEs of this type are ubiquitous and parasitize viruses that infect organisms from all domains of life [83, 205, 206].

Phage satellites are satellites that utilise bacteriophages for their own horizontal transfer. Currently, five families of phage satellites are characterised and described in more detail: the P4-like phage satellites, the phage-inducible chromosomal islands (PICIs), the capsid-forming PICIs, the phage-inducible chromosomal minimalist islands (PICMIs) and the phage-inducible chromosomal island-like elements (PLEs) [2, 83, 85, 86]. In all cases, the types of phage satellites described are integrative elements that possess phage genes [207]. In most cases, the satellite reduces the fitness of the helper phage by capturing the structural proteins. An exception is when a PLE hijacks the ICP1 phage, which leads to a total loss of virion production of the helper phage [208]. A regulatory influence of satellites on their helpers is also described. For example, satellite P4 manipulates the gene expression of helper P2 in a way that leads to a smaller P2 capsid size, matching the comparatively smaller P4 satellite genome [83, 209].

When analysing the plasmid pDolos, it is noticeable that pDolos uses the phage Dolos like a satellite. The production of Dolos virions is drastically reduced in the presence of pDolos. The observed virion distribution of many smaller, satellite-containing virions compared to phage-containing virions is also a frequently described phenomenon [209–211]. Furthermore, it is also often reported that isolation of satellites by single plaque isolation is not successful [10, 210]. This could be due to the fact that without the helper phage, a local distribution of virions leading to a visible plaque is not possible. pDolos thus appears to be a plasmid behaving like a phage satellite, which is referred in this work as "satellite plasmid". Possible regulatory interactions between the satellite plasmid pDolos and helper phage Dolos should be analysed in

the future, as the proteins of pDolos seem to interact with DNA. Furthermore, a regulatory function of pDolos on *S. oneidensis* MR-1 should also be analysed, as pDolos together with the phage Dolos strongly influences the sessile lifestyle of the host. Initial indications of interactions could be provided by analysing the transcriptome of Dolos and pDolos infected cells.

Since phage satellites are referred to as integrative elements, satellite-encoded genes such as integrases are found very frequently [83, 212]. Some phage satellites that exploit inoviruses are an exception: The phage satellite TLCφ as well as the helper phage CTXφ use the host's XerCD recombination system instead of own encoded integrases in order to integrate into the host chromosome. To do this, they mimic the *dif* recognition site of the host, a conserved DNA sequence to which the XerCD recombination complex binds [213, 214]. Such described mechanisms can be excluded for pDolos, since a sequencing analysis of the chromosomal DNA of infected *S. oneidensis* cells did not reveal any indication of a possible integration into the host chromosome as well as neither genes for integration nor a *dif*-like sequence were found.

Recent studies have shown that the diversity of satellites is probably underestimated, as, for example, sequence analysis of marine virions resulted in the description of satellites lacking genes for integration [212]. This observation led to the suggestion that some satellites may not need to be integrative elements in order to interact in a beneficial way with their helper phages [210, 212]. Furthermore, in October 2023, deCarvalho *et al.* published the first observation of a non-integrative satellite system in which smaller satellite virions bind to the neck of tailed helper phage virions [210]. The satellite DNA of this system enters the host cell during phage infection via an unknown mechanism. Intracellular, the phage satellite appears to utilises the tRNA reservoir and the lysis system of the helper phage for successful propagation. The helper phage as well as the phage satellite of this newly described system seem to follow the lytic life cycle. In addition, the plasmid pSSVx was described in Archaea as a hybrid between a plasmid and a virus [10]. This MGE was characterised as a cryptic plasmid of the pRN family that exhibits properties and ORF similarities of viruses. It has also been described that this plasmid is packaged in the presence of SSV helper viruses, resulting in a mixed virion-containing supernatant with a significantly higher proportion of virions containing pSSVx.
pDolos does not have ORFs similar to the ORFs of inoviruses, however, the packaging signal, an approximately 80 nt long ssDNA hairpin structure just upstream of the origin of replication, must be present on the ssDNA plasmid to be transported to the inner membrane and packaged by inoviral structural proteins [156, 185]. Therefore, pDolos seems more likely to be a plasmid that happens to have a packaging hairpin structure, or it could be a plasmid that co-opt the packaging signal from a phage. Hence, the packaging signal of both Dolos and pDolos needs to be identified in the future. Selective single base exchanges that alter the structure of individual hairpins in this region should clarify the exact position of the packaging signal.

All these studies, including the latest characterisation of pDolos, indicate that integrativity should not be included in the definition of phage satellites. It is quite possible that we have overlooked many non-

integrative satellite types, since infection with a satellite does not usually lead to plaque formation. Classical phage isolation protocols always use single plaque purification steps and thus presumably exclude the isolation of satellite virions [215]. It should therefore come as no surprise that the currently well-described phage satellite families are all integrative elements, as such elements are comparatively easy to detect and describe. Theories of satellite evolution suggest that these elements could have evolved, for example, from other types of MGEs that co-opt phage components to extend horizontal transfer. Additionally, these elements could have evolved through the reduction of phages, resulting in cryptic phages that were able to hijack functional phages [83]. It is therefore questionable why only integrative prophages should be able to reduce themselves and exploit other phages. Furthermore, extrachromosomal MGEs and thus plasmids, should be able to acquire phage properties as well as integrative elements.

This work thus supports the hypothesis that phage satellite systems are likely to be much more diverse than previously thought. It is therefore likely that several pDolos-like systems will be found in the future.

Categorisation of the newly described MGE pDolos

Recent discoveries of new MGEs suggest a smooth transition from one MGE group to another. However, this should not really come as a surprise considering that each selfish genetic element must compete with other elements within a host in order to persist. Moreover, replicons already existed in pre-cellular times, so that the described intracellular competition between genetic elements has existed since the beginning of life and has probably shaped life in a unique way [216, 217]. Therefore, strictly adhering to all the criteria used to define a MGE group may be difficult and sometimes even disadvantageous. In the case of the term plasmid as being a *mobile* or self-transmissible, *circular*, *extrachromosomal* genetic element that is transmitted as *unpackaged* DNA, exceptions could be observed for all the criteria described [26, 202]. In 2017, Erdmann *et al.* discovered the plasmid pR1SE in an haloarchaeon that encodes proteins which are part of vesicles [218]. When a cell is infected with this plasmid, it begins to produce vesicles containing the plasmid. Since the term virus is mainly characterised by the fact that these MGEs are transduced by an own encoded packaging system, this discovery was extraordinary. In addition, the term phage-plasmid was introduced because some MGEs are both, phages and plasmids [219, 220]. Phage-plasmids are non-integrative temperate phages that are transmitted horizontally as phages during the lytic cycle and vertically as plasmids during the lysogenic cycle.

Interestingly, the *mobile* criterion for defining a plasmid raises many questions. Plasmids are categorised into three groups depending on their mobility [26]. Mobile plasmids encode genes for their own conjugation, such as genes encoding a type IV secretion system as well as mobility genes (*mob* genes), which are involved in DNA processing for conjugational transfer [26]. Mobilizable plasmids only possess *mob* genes and are therefore dependent on mobile plasmids in order to be transferred by conjugation [26]. Mobilizable plasmids thus represent plasmids that exploit other plasmids. On the other hand, non-mobilizable plasmids

are plasmids, for which it is unclear how they can be transmitted horizontally, as they have neither genes for conjugation nor *mob* genes. Interestingly, about half of the currently described plasmids are non-mobilizable [26, 28]. pDolos is also categorised as non-mobilizable, since the HUH endonuclease of pDolos belongs to the Rep family and not to the Mob family.

When considering the currently known mechanisms of horizontal transfer of non-mobilizable plasmids, reference is usually made to the transformation of free plasmid DNA, although this mechanism can only explain the mobility of some non-mobilizable plasmids [26]. In 2021, Humphrey *et al.* demonstrated that non-mobilizable *S. aureus* plasmids can be transduced by prophages or phage satellites with a similar genome size to the plasmid genomes [221]. The transduction of these plasmids nevertheless is a rare event that did not affect the virion count of the phages or phage satellites used. This described event seems to be a rather random and rare occurrence, which is exclusively determined by the genome size of the plasmids and not by the adaption of plasmids to helper phages. However, the plasmid pDolos described in this study seems to have evolved towards the active utilisation of a phage, since the presence of virions containing pDolos outnumbers those containing Dolos by far. This work has therefore revealed a way in which a non-mobilizable plasmid can be transmitted horizontally in high numbers. It is thus conceivable that many other non-mobilisable plasmids act as satellite plasmids, like pDolos, and thus spread on a large scale through transduction.

The discovery of pDolos is the first description of a satellite system, which is a plasmid without recognisable phage genes that hijacks a phage belonging to the family *Inoviridae*.

It is interesting to note that pDolos could be described as a natural phagemid in a certain sense. Phagemids are vectors used for phage display, a technique that is important to generate so-called phage libraries to identify protein-protein, protein-peptide or protein-DNA interactions [81, 222]. These vectors produce recombinant virions holding the vector DNA instead of the helper phage DNA. To summarise, phagemids are simple plasmids that replicate by RCR. Packaging of the phagemid ssDNA is initiated by an inoviral packaging signal that is part of the phagemid vector. This signal allows the phagemid to utilise a helper phage for self-packaging.

The requirements for a plasmid to hijack an inovirus are therefore very simple.

3.1.3 Satellite plasmid pDolos propagation hypothesis

The described satellite plasmid pDolos seems to be a cryptic, non-mobilizable plasmid that likely replicates by RCR. pDolos is very stable in the host *S. oneidensis* MR-1 and maintain itself vertically within a species by host cell segregation, as shown in **Figure 31**. When a helper phage infects a cell harbouring the satellite plasmid pDolos, the plasmid hijacks the phage components and can thus be horizontally transferred to other species, such as the *S. baltica* isolates described in this work. A hypothesis of how pDolos virions might be produced is illustrated in **Figure 31**.

The data indicates that initially the helper phage replicates, which probably leads to a stabilisation of the helper phage within a population. In later stages of replication, the satellite plasmid pDolos seems to increasingly exploit the helper phage. This appears to be achieved by exploiting the viral segregation system as well as viral structural proteins to produce virions containing the satellite.

The observed reduction in the replication of inoviruses in later stages of infection is a generally described phenomenon. Usually, the production of inoviral virions decreases in later stages of viral infection, leading to a steady state of virion production that is likely to spare the host in the long term [45, 223]. The steady state is regulated by the accumulation of the viral protein pV within the infected cell, which directly inhibits the synthesis of the viral (-)-strand and thus the further production of the replicative form (dsDNA), as well as it inhibits the translation of the for replication important pII and pX proteins. [45, 224, 225]. Hence, progeny production of inoviruses is slowed down in above a certain quantity of pV.

It is quite possible that during this viral stable state, the satellite plasmid pDolos exerts a regulatory effect on the helper phage Dolos, leading to the production of more viral structural proteins to package pDolos instead of the phage Dolos. Possible regulatory effects of pDolos on Dolos as well as the probability of using other inoviruses as helper phages should be analysed in the future.

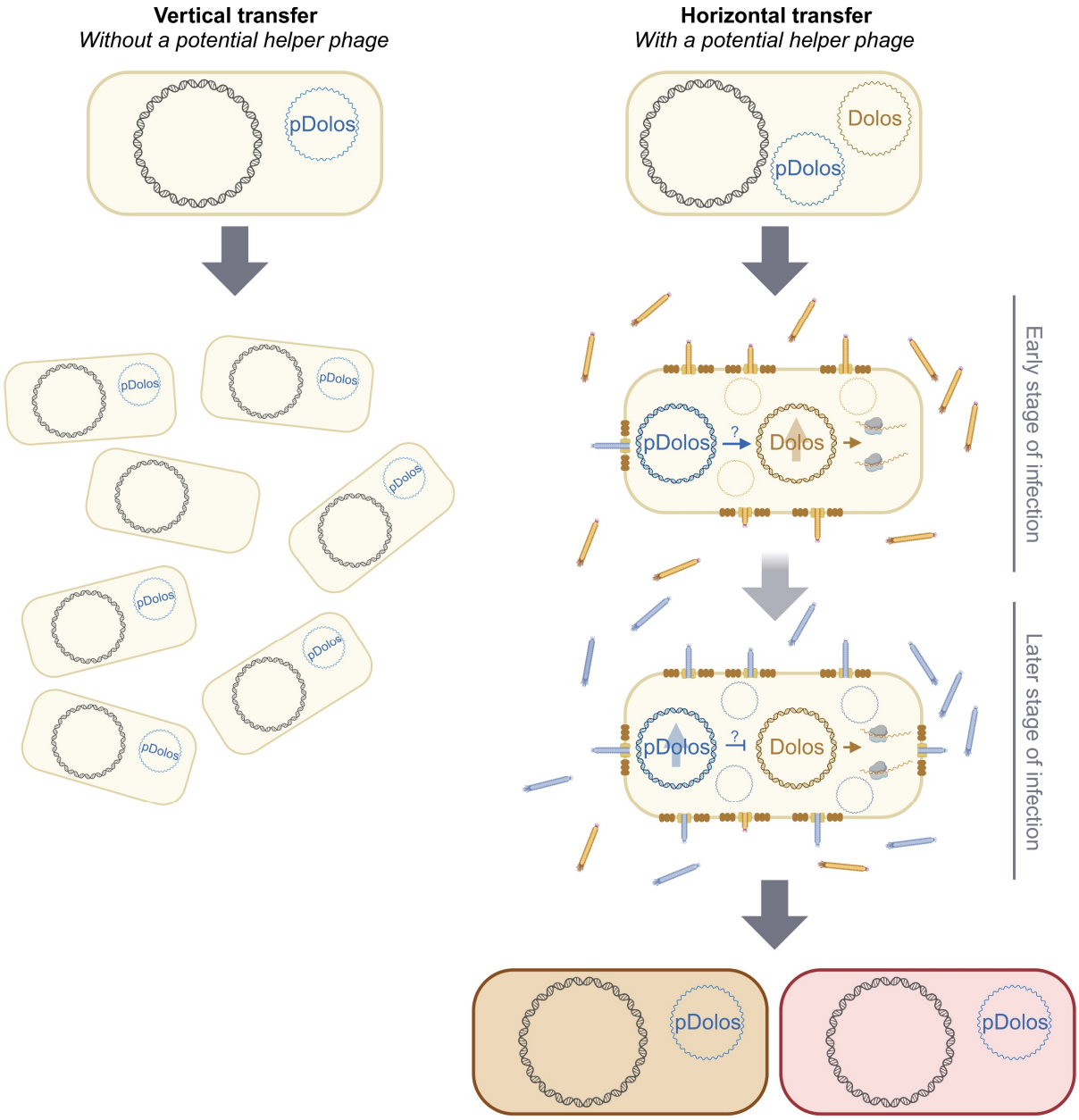

Figure 31: Reproduction hypothesis of satellite plasmid pDolos. Without a helper phage, the satellite plasmid pDolos spreads vertically via cell segregation. If a cell containing the satellite plasmid pDolos is infected by a potential helper phage (Dolos), pDolos can spread horizontally through transduction by exploiting the helper phage. At an early stage of phage infection, structural and segregational proteins of the phage are produced that package the phage, probably leading to an establishment of the phage within a population. In later stages of the infection, the proliferation of the helper phage is reduced whereas the reproduction of the satellite plasmid pDolos is increased, leading to the production of numerous pDolos virions. It is likely that pDolos regulates the replication and gene expression of the helper phage Dolos during all stages of infection.

3.2 Analysis of *Shewanella* phage Thanatos ADP-ribosyltransferases Alt1 and Alt2

Bacteriophages hijack their hosts for their own propagation. Lytic phages in particular hijack host components such as the cellular gene expression system and reprogram the host quickly as well as in a time-regulated manner [226, 227]. To reprogram the cell into a virion-producing factory, phage-related host acquisition factors (HAFs) must be expressed early in the infection or injected into the host as active proteins along with the DNA [55, 228]. Known HAFs among others include transcription factors that alter the host transcriptional profile, nucleoid disruption proteins that digest the host chromosome, nucleases that digest host DNA or mRNA, and ADP-ribosyltransferases (ARTs) that alter host proteins properties [56, 57, 149]. The mechanisms by which lytic phages reprogram bacterial hosts, thereby exerting significant predatory pressure on their hosts, are of current scientific interest.

To analyse the host acquisition mechanisms of the lytic *Shewanella* phage Thanatos, a Thanatos virion proteomics analysis was performed, which revealed 72 proteins as part of the Thanatos particles. In addition to typical structural proteins, a nucleoid disruption protein (TH1_046), a ssDNA-binding protein (TH1_037) and two ARTs (TH1_028, TH1_029), homologues of the phage T4 ART Alt, were found to be part of the Thanatos virion.
The focus of this study was on the phage T4 Alt homologues, referred to as Alt1 (TH1_028) and Alt2 (TH1_029). These proteins were found to be extremely abundant in the phage particle.

ARTs catalyse the transfer of one or more ADP-ribose units from NAD^+ to target proteins, thereby modifying them post-translationally and with this presumably changing their properties [229]. These enzymes are ubiquitous in nature and are found in all three domains of life as well as in MGEs such as viruses [230]. How ART-dependent ADP-ribosylation alters protein properties is still unclear and therefore of current interest, as their functions are wide-ranging. Eukaryotic ARTs have specific functions in the cellular stress response [231]. In contrast, bacterial ARTs act as toxins and modify eukaryotic proteins, making them bacterial virulence factors [232]. Some archaeal ARTs are involved in the RNA processing machinery [233] and the viral ARTs described so far are associated with host reprograming and hijacking of the host's gene expression machinery [234].

The *E. coli* phage T4, a virus closely related to the *Shewanella* phage Thanatos, reprograms its host *E. coli* among others through the ARTs Alt, ModA and ModB. The T4 ART Alt is a component of the T4 particle and is injected into the host along with the DNA. Alt then performs ADP-ribosylation on various proteins, including the RNA polymerase [149]. This described modification is believed to affect the activity of the polymerase, resulting in preferential transcription of early phage genes, including ModA and ModB [150, 151]. It is known that ModA further modifies the RNA polymerase and ModB modifies among others the ribosomal protein 1 (rS1) and likely changes with this the translational profile of the cell [152].

Thanatos harbours two Alt homologues, both of which, like the T4 Alt, are part of the virion and are injected immediately along with the viral DNA. After injection of these Thanatos-ARTs, the target proteins are immediately labelled with ADP-ribose units, as a time-serial analysis of the infection clearly showed. Homologues of T4 ModA and ModB are not present in Thanatos. Therefore, the function of Thanatos ARTs and the host remodelling they cause likely occurs differently than the host remodelling caused by phage T4. Interestingly, analysis of the ADP-ribosylation profile of Thanatos Alt1 and Alt2 reveals differences in the activity of Alt1 and Alt2. The ADP-ribosylation reaction of Alt2 is much stronger compared to Alt1. Furthermore, it appears that Alt1 and Alt2 carry out ADP-ribosylation on different target proteins. Compared to T4 Alt, it is also interesting that proteins of varying sizes are modified, whereas Alt of phage T4 seems to mainly modify proteins < 70 kDa [57]. Furthermore, an autocatalytic activity of both enzymes was demonstrated through further analysis of the purified Alt1 and Alt2 proteins. A autocatalytic activity could also be demonstrated for T4 ARTs [152]. How this autocatalytic reaction affects the activity of the ARTs is currently unknown.

Since the Thanatos ART-dependent remodelling of the host appears to function differently, the proteins that interact with Alt1 and Alt2 were analysed. Six proteins interacting with Alt1 and eight proteins interacting with Alt2 were identified by co-IP. Overall, the proteins identified by co-IP could be categorised into three groups. Thus, potential anti-phage defence systems, proteins that are probably involved in regulation of biofilm formation and proteins that are involved in metabolic pathways were identified as potential interaction partners of Alt1 and Alt2.
Proteins interacting with Alt1 are likely involved in anti-phage defence and in regulation of biofilm formation. For example, the toxin RelE and the deoxyguanosinetriphosphate triphosphohydrolase-like protein (dGTPase-like protein) could function in anti-phage defence. In addition, the identified bifunctional diguanylate cyclase (DGC)/phosphodiesterase (PDE) SO_0427 and the identified NAD-dependent epimerase/dehydratase SO_0768 could function in the regulation of biofilm formation.
Proteins interacting with Alt2 are probably mostly involved in anti-phage defence and in metabolic pathways. For instance, the toxin HipA could function in anti-phage defence. The identified molybdopterin-molybdenum transferase MoeA, the glutamine synthetase GlnB, the cyclopropane-fatty acyl-phospholipid synthase CfaS as well as the 4-hydroxybenzoyl-CoA thioesterase are metabolic enzymes.

In the following, some of these Alt1- and Alt2-interacting proteins are contexed to possible functions during phage infection. It is important to note that the proteins identified through co-IP have not been verified as interacting proteins by other methods, such as two-hybrid assays. Moreover, the method used identifies only interaction partners and with this does not provide any information about potential targets of Alt1 and Alt2. Hence, Alt1- and Alt2-dependent ADP-ribosylated proteins could not be identified. To determine proteins modified by Alt1 or Alt2, a more specific MS analysis focussing on ADP-ribosylated proteins should be performed [235]. Furthermore, a possible interaction and influence directed by *S. oneidensis* MR-1 proteins cannot be excluded. Therefore, it is also possible that the identified proteins are *S. oneidensis* MR-1 proteins affecting the Thanatos ARTs.

When analysing the data obtained via co-IP, it is noticeable that Alt1 and Alt2 interact with bacterial toxins of TA systems. Both RelE and HipA are toxins of type II TA systems, but their toxic function is very different. The toxin RelE has been described as a ribosome-dependent endoribonuclease that cleaves strictly translating mRNA [236]. The toxin HipA, on the other hand, is a kinase that is known to inhibit protein synthesis [237]. In both cases, the toxic function causes the translation of mRNAs to be interrupted, which leads to a halt in cell growth. The function of bacterial TA systems is currently implicated in persister cell formation [238], biofilm formation [239, 240], the general stress response [240] and bacterial anti-phage defence [241]. A function in anti-phage defence has been demonstrated, for example, in the case of the toxin MazF, which suppresses lytic multiplication of the lysogenic phage SPbeta of *Bacillus subtilis* by inducing a regulated cell growth arrest. This described mechanism is an anti-phage defence system known as abortive infection [142]. MazF is a toxin that cleaves sequence-specific mRNA, which leads to cellular growth arrest. In addition, the type II toxins RnlA, a RNase [242], and LsoA, a mRNA endoribonuclease [243], have also been shown to have a function in anti-phage defence. Since toxins of TA systems function in anti-phage defence, rapid phage-dependent modification of toxins could be advantageous for phage propagation. In the case of the phage T4, it was shown that the ART Alt negatively regulates the toxin MazF, leading to a reduced enzymatic activity of MazF [244]. Based on this study, a Thanatos Alt1- and Alt2-dependent ADP-ribosylation of the *S. oneidensis* toxins RelE and HipA should be elucidated.
In addition to the two toxins of the TA system, a dGTPase-like protein was also identified that possibly interacts with Alt1. dGTPases are enzymes that cleave deoxyguanosine triphosphate (dGTP) into phosphate-free deoxyguanosine (dG) and inorganic triphosphate (PPPi) [245]. Recent research has shown that dGTPases function in anti-phage defence, as the cells use these enzymes to break down an essential building block for DNA synthesis and thus stop phage replication [153]. An antiviral effect of nucleotide depletion is not only observed in prokaryotes, but appears to be a widespread antiviral strategy, as such systems have long been known in eukaryotes [153, 246]. Since ARTs of bacteriophages are known to interact with anti-phage defence mechanism, it is quite possible that Thanatos Alt1 manipulates this GTPase via ADP-ribosylation.
Therefore, ARTs of phages could also be considered as anti-defence proteins, as these enzymes seem to be able to manipulate anti-phage defence systems, which makes the coevolution of these systems very intriguing. Recent studies show that the degradation of NAD^+ is a bacterial anti-phage defence mechanism carried out by the widespread anti-phage defence system named Thoeris [247]. Since NAD^+ is the donor that ARTs use for their catalytic reaction, one could speculate that Thoeris-mediated anti-phage defence is a bacterial mechanism to attack the phage encoded anti-defence proteins.

In addition, proteins that probably have regulatory functions in *S. oneidensis* MR-1 biofilm formation were found to interact with Alt1 or Alt2. The NAD-dependent epimerase/dehydratase SO_0768 is an enzyme that requires NAD and could therefore be a potential target of ARTs as it utilises the same donor. Beyond that, a function of this protein family in *E. coli* and *Pectobacterium carotovorum* in the biosynthesis of exopolysaccharides, important for biofilm formation, has been demonstrated [248, 249].

Furthermore, a bifunctional DGCs/PDEs appears to interact with Alt1. Enzymes of this family regulate the c-di-GMP level of the cells [173, 250]. C-di-GMP is an important second messenger that is involved in bacterial lifestyle changes. An increasing intracellular c-di-GMP level has been shown to promote biofilm formation [105]. Interestingly, an interaction of virulent PB1-like phages with DGCs of their host *Pseudomonas aeruginosa* has already been demonstrated. Here, phage-encoded proteins interact directly with the DGC YfiN and increase the c-di-GMP production of this enzyme, which leads to increased biofilm formation of *P. aeruginosa* [251].
Additionally, Alt2 likely interacts with RsmI, the ribosomal RNA methyltransferase I. In *Pseudomonas putida* KT2440, overexpression of RsmI reduces bacterial attachment to surfaces and thus influences biofilm formation [252].
Since so many proteins potentially involved in biofilm formation are likely to interact with Thanatos Alt1 or Alt2, the Thanatos-mediated increase in biofilm formation of *S. oneidensis* MR-1 observed in a previous study may not be solely due to phage-mediated cell lysis [72].

The protein RsmI has also been associated with other regulatory functions. For example, rRNA methylation performed by Rsm proteins has a verifiable effect on the *E. coli* gene expression quantity. In addition, a defect in rRNA methylation increases the efficiency of suboptimal protein biosynthesis in *E. coli* [253]. Thus, an Alt2-dependent modification of RsmI could possibly influence the translation profile of the cell.
Furthermore, the ART Alt1 appears to interact with the ribosome rescue factor YfcN. YfcN cuts mRNAs upstream of blocked ribosomes [254]. A study showed that the prophage CP4-57 switches the ribosome rescue of *E. coli* during phage excision and thereby alters the proteome landscape of the host [255]. A regulatory function of Alt1 is therefore also conceivable here.
It was also found that Alt1 likely interacts with the tryptophan synthase TrpA. A recent study showed that inactivation of TrpA in *Staphylococcus aureus* sensitises the bacteria to phage infection [256]. The authors speculated that this effect is due to the accumulation of the intermediate indole glycerol phosphate, but the exact mechanism of the observed sensitivity to phages is currently unclear.
Furthermore, Alt2 likely interacts with a periplasmic metalloprotease of the M23B family. Proteins of this family are peptidoglycan hydrolases, which are responsible for the remodelling of peptidoglycan and are important for cell growth, cell division and shape determination of bacteria [257]. In addition, some of these bacterial M23B proteases are exoenzymes that act as bacteriocins by digesting the peptidoglycan of other bacteria [257]. Phages also harbour enzymes from this family; phage-encoded endolysins are M23B proteases, which are essential for the lysis of the host cell [257].
When *S. oneidensis* MR-1 cells are infected with Thanatos, an interesting phenotype of rounded-up cells is observed at later stages of infection [72]. A possible altered function of the periplasmatic metalloprotease SO_2180 could potentially explain the observed phenotype of rounded-up cells.

Interestingly, several metabolic proteins appear to interact with Alt2. Since ARTs are factors for host acquisition, it is quite conceivable that a change in the host metabolic function is important for an efficient phage infection cycle.

In general, the proteins identified by co-IP analysis to interact with Thanatos Alt1 or Alt2 may play an important role in the course of phage infection. As previously mentioned, a proof of Alt-dependent ADP-ribosylation must be conducted to exactly determine the target proteins of Alt1 and Alt2.

When analysing the phenotypes of the different Thanatos variants, it is noticeable that the initial phage-dependent lysis is not affected by Alt1 or Alt2. Interestingly, long-term adaptation to the host seems to be favoured by Alt1 and Alt2. Therefore, the activity of Alt1 and Alt2 is probably not crucial for initial infection, but likely important for adaptation and evolutionary stability within a population after the emergence of resistance mechanisms against the phage Thanatos. To verify this, a long-term infection should be monitored over several days to provide insight into the stability of the Thanatos variants with inactive ARTs.

By analysing the phage output over time, it is noticeable that the inactivity of Alt2 reduces the amount of Thanatos virions. Interestingly, after 4 hours of infection, the total number of virions is lower than after 2 hours of infection. The virions must therefore either be attached, which means that a certain amount of virions is blocked, or the Thanatos virions must be degraded. Since the growth analysis of cells infected with different Thanatos variants shows no differences in cell density and the general lysis behaviour at these infection time points, a degradation of Thanatos Alt2^{E541A} is more likely. For example, the amino acid substitution in Alt2 may affect the stability of Alt2, which in turn could impact the stability of the virion, as Alt2 is the second most abundant protein of Thanatos particles. In order to investigate the virion stability of Thanatos Alt2^{E541A}, the phage concentration of a Alt2^{E541A} phage stock should be quantified over a longer period of time and compared to the phage concentration of a Thanatos wt stock. Since virion reduction started 4 hours after infection, it is also very likely that the degradation of Thanatos Alt2^{E541A} is an active and thus proteolytic degradation of the virions.

Interestingly, one of the proteins identified by co-IP analysis that interacts with Alt2 is a periplasmic metalloprotease of the M23B family. As already described, enzymes of this family have different functions, but all of them act in the cleavage of peptidoglycan [257]. These periplasmic proteases are presumably also released by phage-mediated lysis. Since the degradation of Thanatos is evident at the time of complete phage-dependent lysis, a possible activity of this protease in virion cleavage should be analysed.

To summarise, this study reveals first impressions of the Thanatos ART-dependent host acquisition of *S. oneidensis* MR-1. Future experiments should clarify whether the interacting *S. oneidensis* MR-1 proteins identified by co-IP are target proteins of ARTs and thus host proteins ADP-ribosylated by Thanatos Alt1 or Alt2. In addition, the function of the Alt1 and Alt2 modifications should be determined to understand the importance of Alt1 and Alt2 for infection.

While comparing the effect of the Thanatos ARTs with those of the T4 ARTs, it is evident that inactivity of the T4 ARTs is associated with stronger phenotypes. The inactivation of one of three T4 ARTs, ModB,

leads to a delayed lysis and an approximately 100-fold decrease in the amount of virions [152]. Moreover, in 2023 Wolfram-Schaute *et al.* showed that the T4 ART ModB modifies proteins not only by ADP-ribosylation but also by RNAylation, which is the transfer of selected RNAs from RNA-capped NAD to acceptor proteins, thereby altering the activity of the acceptor proteins [152]. The T4 ART Alt also RNAylates proteins, but to a lesser extent. A possible Thanatos Alt1- and Alt2-dependent RNAylation is therefore currently under investigation and may provide some more information about the Thanatos Alt1 and Alt2-dependent host acquisition.

4. Materials and methods

4.1 Materials

The reagents generally used in this study were purchased from Carl-Roth (Germany), Merck (Germany), Sigma-Aldrich (Germany), Thermo Fisher Scientific (USA) and New England Biolabs (NEB, USA).

A detailed list of materials is given below.

Table 5: Media used in this study.

Medium	Components		Reference
Myers and Myers Minimal Medium (4M)	NaCl Na_3PO_4 $(NH_4)2SO_4$ $MgSO_4$ $CaCl_2$ $MnSO_4$ $FeCl_2$ $CoCl_2$ $ZnSO_4$ $CuSO_4$ H_3BO_3 Na_2MoO_4 $NiCl_2$ Na_2SeO_4 HEPES Lactate casamino acids pH	150 mM 5 mM 10 mM 0.5 mM 50 mM 0.13 mM 0.54 mM 0.5 mM 0.1 mM 0.02 mM 5.66 mM 0.39 mM 0.5 mM 0.15 mM 25 mM 40 mM 0.5% (w/v) 7.5	[258]
Lysogeny Broth (LB) (Luria/Miller)	Tryptone Yeast Extract NaCl pH	10 g/l 5 g/l 10 g/l 7.0	[259]
Lactate Medium (LM)	Yeast Extract Peptone HEPES NaCl Lactate [85% (v/v)] pH	0.2 g/l 0.1 g/l 10 mM 10 mM 15 mM 7.5	[260]

Table 6: Antibiotics and other additives used in this study.

Antibiotic or additive	Stock concentration	Final concentration	Solvent
Chloramphenicol	10 mg/ml	10 µg/ml	96% (v/v) EtOH
Ampicillin-sodium salt	100 mg/ml	100 µg/ml	ddH_2O
Kanamycinsulfate	50 mg/ml	50 µg/ml	ddH_2O
L-Arabinose	20% (w/v)	0.2% (w/v)	ddH_2O
DAP (Meso-diaminopimelic acid)	60 mM	300 µM	ddH_2O
Sucrose	80% (w/v)	10% (w/v)	ddH_2O
IPTG (isopropyl-β-Dthiogalactopyranoside)	1 M	1 mM	ddH_2O

Table 7: Kits used in this study.

Kit	Application
E.Z.N.A. PCR Cleanup Kit (Omega Bio-tek, USA)	PCR purification
E.Z.N.A. Plasmid DNA Mini Kit (Omega Bio-tek, USA)	plasmid preparation
E.Z.N.A. Gel Extraction Kit (Omega Bio-tek, USA)	DNA extraction from agarose gels
E.Z.N.A Bacterial DNA Kit (Omega Bio-tek, USA)	Chromosomal DNA extraction
PowerUp™ SYBR™ Green Master Mix (Thermo Fisher Scientific, USA)	qPCR

Table 8: Antibodies used in this study.

Antibody	Dilution
Monoclonal Anti-FLAG M2, HRP coupled (Sigma-Aldrich, Germany)	1:1,000
Anti-pan-ADP-ribose binding reagent (MABE1016 – Merck, Germany)	1:10,000
V5 Tag Monoclonal Antibody (SV5Pk1 - Thermo Fisher Scientific, USA)	1:1,000
His-Tag Antibody HRP conjugate (Thermo Fisher Scientific, USA)	1:1,000
Anti-Mouse IgG from goat, AP coupled (Sigma-Aldrich, Germany)	1:5,000
Anti-Rabbit IgG, AP coupled (Sigma-Aldrich, Germany)	1:20,000

Table 9: Further chemical components and their application in this study.

Component	Application
Alexa Fluor™ 488 C5 maleimide dye (Thermo Fisher Scientific, USA)	MshA staining
Western Lightning® Plus-ECL (PerkinElmer, USA)	Western Blot (HRP conjugates)
CDP-Star (Sigma-Aldrich, Germany)	Western Blot (AP conjugates)
GeneRuler™ 1 kb DNA Ladder (Life Technologies, USA)	Ladder (agarose gel electrophoresis)
BLUeye Prestained Protein Ladder (GeneDireX Inc., USA)	Ladder (SDS Page)

Table 10: Enzymes and their application in this study.

Enzyme	Application
EcoRV (Fast digest – Thermo Fisher Scientific, USA)	Linearization of pNPTS
SmaI (Fast digest – Thermo Fisher Scientific, USA)	Linearization of pBAD
BamHI (Fast digest – Thermo Fisher Scientific, USA)	Linearization of BACTH plasmids
XhoI (Fast digest – Thermo Fisher Scientific, USA)	Linearization of pET24c(+)
NdeI (Fast digest – Thermo Fisher Scientific, USA)	Linearization of pET24c(+)
Phusion DNA Polymerase (in-house production)	PCR
Taq polymerase (in-house production)	PCR
DNAseI (PanReac AppliChem, Germany)	Virion DNA isolation
RNase A (Omega Bio-Tek, USA)	Virion DNA isolation
Proteinase K (Omega Bio-Tek, USA)	Virion DNA isolation

Buffers and relevant solutions used in this study are listed in the following.

Acrylamide gels:

- 30% acrylamide/ bisacrylamide-solution 37.5: 1 – Rotiphorese, Carl-Roth (Germany).
- APS: 10% (w/v) in ddH_2O.
- SDS-solution: 10% (w/v) in ddH_2O.
- 4x lower buffer (SDS-PAGE stacking gel buffer): 0.4% SDS, 1.5 M Tris-HCl, pH 8.8.
- 4x upper buffer (SDS-PAGE separating gel buffer): 0.4% SDS, 0.5 M Tris-HCl, pH 6.8.
- 10x SDS-PAGE running buffer: 250 mM Tris-Base, 1.92 M glycine, 0.25% (w/v) SDS, pH 8.3.
- SDS-PAGE sample buffer (2 x): 125 mM Tris, 4% SDS, 20% glycerol, 10% β-mercaptoethanol, 0.02% bromophenol blue, pH 6.8.

- Coomassie staining solution: 0.1% (w/v) Coomassie, 200 ml methanol, 50 ml acetic acid, 250 ml H_2O.
- Fixing solution: 25% (v/v) ethanol, 5% (v/v) acetic acid, 70% (v/v) H_2O.

Western Blot:

- 10x Western transfer buffer: 0.25 M Tris Base, 1.92 M glycine.
- 1x Western transfer buffer: 100 ml 10x Western transfer buffer, 100 ml methanol (100%), add ddH_2O up to one litre.
- 10x PBS: 80 g NaCl, 2 g KCl, 17.8 g Na_2HPO_4 x 2 H_2O, 2.4 g KH_2PO_4, add ddH_2O up to one litre, pH 7.4.
- 1x PBS-T: 100 ml 10x PBS, 1 ml Tween 20, add ddH_2O up to one litre.
- Blocking solution: 5% milk powder in PBS-T.
- Antibody solution (primary): 5% milk powder in 1x PBS-T.
- Antibody solution (secondary): 2.5% milk powder in 1x PBS-T.

Agarose gel electrophoresis:

- 1x TBE-buffer: 89 mM Tris-Base, 89 mM boric acid (100%), 1 mM EDTA, pH 8.0
- 6x Agarose gel electrophoresis loading buffer: 0.5% (w/v) xylene cyanole, 0.5 % (w/v) bromophenol blue, 30% (w/v) glycerine.

Chromatography:

- Lysis buffer: 50 mM Tris-HCl (pH 7.4), 400 mM NaCl, 50 mM KCl, 5 mM $MgCl_2$, 0.3 mg/l DNase, 20 mM AEBSF, 4 mM Benzamidine.
- Buffer A: 50 mM Tris-HCl (pH 7.4), 400 mM NaCl, 50 mM KCl, 5 mM $MgCl_2$, 10% Glycerol, 20 mM Imidazole.
- Buffer B: 50 mM Tris-HCl (pH 7.4), 400 mM NaCl, 50 mM KCl, 5 mM $MgCl_2$, 10% Glycerol, 600 mM Imidazole.
- GeFi buffer: 50 mM Tris-HCl (pH 7.4), 400 mM NaCl, 50 mM KCl, 5 mM $MgCl_2$, 5% Glycerol.

Further solutions:

- 5x isothermal reaction buffer: 25% (w/v) PEG 8000, 500 mM Tris HCl pH 7.5, 50 mM $MgCl_2$, 50 mM DTT, 5 mM NAD, 1 mM of every dNTP, fill up to 1 ml with ddH_2O.
- Gibson Assembly master mix: 320 µl 5x isothermal reaction buffer, 0.64 µl T5 exonuclease, 20 µl Phusion DNA polymerase (2 U/µl), 160 µl Taq DNA ligase (40 U/µl), 699,36 µl ddH_2O.

Table 11: Laboratory equipment and its use in this study.

Equipment	Usage
Mastercycler nexus gradient (Eppendorf, Germany)	PCR cycler
NanoDrop 1000 Spectrophotometer (PEQLAB, Germany)	Spectrophotometer
Leica DMI6000 B microscope (Leica AG, Germany)	Fluorescence microscopy
Intas Photo imager (INTAS science imaging, Germany)	Chemiluminescence imaging
TE77 ECL Semi-Dry Transfer Unit (Amersham Biosciences Corp., UK)	Blotting
Tecan INFINITE M NANO+ (Tecan, CH)	Microplate reader (growth curves)
Äkta pure 25 (Cytiva, USA)	Chromatography
TCS SP8 microscope (Leica AG, Germany)	Confocal microscopy
JEM-1400 electron microscope (JEOL, Japan)	Electron microscopy
QuantStudio3 (Thermo Fisher Scientific, USA)	qPCR

Table 12: Software and its use in this study.

Software	Usage
Leica LAS X (Leica, Germany)	Confocal microscopy
"Design & Analysis" software (QuantStudio™)	qPCR analysis
BiofilmQ [129]	Biofilm analysis
Fiji (ImageJ)	Image analysis
Benchling (Benchling Inc., USA)	Primer design, AlphaFold prediction, plasmid construction
GraphPad Prism 10 (GraphPad Software, Inc, USA)	Graph design, statistics
Unicorn™ 7 (Cytiva, USA)	Chromatography
iControl 2.0 (Tecan, CH)	Tecan measurements
Visiview (Visitron, Germany)	Fluorescence microscopy
BioRender (BioRender)	Illustration (Fig. 1, 3, 4, 5, 6, 8, 31)
Affinity Designer / Affinity Photo (Serif Europe Ltd.)	Figure design
Microsoft Excel (Microsoft Corporation, USA)	Data management
Foldseek (Foldseek Search)	Alignment / search of protein PDB structures
BLAST (ncbi)	Alignment searching

Table 13: Bacterial strains used in this study.

Strain	Relevant genotype or description	Source or reference
***Shewanella oneidensis* MR-1 strains**		
S79	Wild type	[261]
S2828	*Tn7:::egfp* (Cm^r)	[63]
S176	*Tn7:::ecfp* (Cm^r)	[63]
S6608	ΔLambdaSo	[63]
S1381	ΔMuSo2	[63]
S6593	ΔLambdaSo ΔMuSo2	[72]
S882	Δ*mshA*	[262]
S6758	Δ*mshA:::mshA*	[263]
S7290	ΔLambdaSo ΔMuSo2 $MshA^{S69C}$ $MshE^{L9A/L53A/L57A}$	This study
S6896	ΔLambdaSo ΔMuSo2 $MshA^{S69C}$	This study
S7413	ΔLambdaSo ΔMuSo2 $MshA^{S69C}$ $PilT^{K136A}$	This study
Further *Shewanella* strains		
S. oneidensis Isolate S52	Unspecified isolate	[264]
S. oneidensis Isolate S54	Unspecified isolate	[264]
S. oneidensis Isolate S62	Unspecified isolate	[264]
S. oneidensis Isolate S63	Unspecified isolate	[264]
S. oneidensis Isolate S66	Unspecified isolate	[264]
S. oneidensis Isolate S69	Unspecified isolate	[264]
S. oneidensis Isolate S74	Unspecified isolate	[264]
S. baltica Isolate S4	Unspecified isolate	[264]
S. baltica Isolate S44	Unspecified isolate	[264]
S. baltica Isolate S37	Unspecified isolate	[264]
S. baltica Isolate S38	Unspecified isolate	[264]
S. baltica Isolate S50	Unspecified isolate	[264]
S. amazonensis SB2B	Wild type	[265]
S. seohaensis Isolate S8	Unspecified isolate	[264]
S. seohaensis Isolate S10	Unspecified isolate	[264]
S. seohaensis Isolate S11	Unspecified isolate	[264]
S. seohaensis Isolate S31	Unspecified isolate	[264]
S. seohaensis Isolate S32	Unspecified isolate	[264]
S. putrefaciens CN-32	Wild type	[266]
S. putrefaciens CN-32	Δ*cas1_2*	[267]
S. putrefaciens W3-18-1	Wild type	[268]
S. sp. ANA-3	Wild type	[269]
S. sp. MR-4	Wild type	[270]
S. sp. MR-7	Wild type	[270]

***Escherichia coli* strains**		
E. coli MG1655	K12 Wild type	[271]
E. coli DH5α λpir	φ80d*lacZ* ΔM15 Δ(*lacZYA-argF*) U169 *recA1 hsd*R17 *deo*R *thi-l supE44 gyrA96 relA1*/λpir	[272]
E. coli BL21 (DE3)	*fhuA2 [lon] ompT gal (λ DE3) [dcm]* Δ*hsdS λ DE3 = λ sBamHIo* Δ*EcoRI-B int::(lacI::PlacUV5::T7 gene1) i21* Δ*nin5*	NEB
E. coli WM3064	*thrB1004 pro thi rpsL hsdS lacZ* Δ*M15* RP4-1360 Δ(*araBAD*) 567Δ*dapA* 1341: [*erm pir*(wt)]	W. Metcalf, University of Illinois, Urbana-Champaign
E. coli BTH101	*F, cya-99, araD139, galE15, galK16, rpsL1 (Str^r), hsd*R2, *mcrA1, mcrB1.*	Euromedex, France
Further strains		
P. putida KT2440	Wild type	[273]
V. cholerae El Tor N16961	Wild type	[274]

Table 14: Plasmids used in this study.

Plasmid	Description	Source or reference
pNPTS138-R6KT	mobRP4+, R6K ori, *sacB*, Km^R (suicide vector for in-frame deletions or integrations)	[275]
pNPTS_MshA^{S69C}	aa substitution (MshA^{S69C})	this study
pNPTS_MshE$^{L9A/L53A/L57A}$	aa substitution (MshE$^{L9A/L53A/L57A}$)	this study
pNPTS_PilT^{K136A}	aa substitution (PilT^{K136A})	this study
pNPTS_Δ*mshE*	Deletion of *mshE*	this study
pNPTS_Δ*pilT*	Deletion of *pilT*	this study
pBAD33	P15A, araBp, Cm^r (expression vector)	[276]
pBAD_V5_Alt1	Expression of V5_Alt1	this study
pBAD_V5_Alt2	Expression of V5_Alt2	this study
pBAD_Alt1^{E521A}	Expression of Thanatos Alt1^{E521A}	this study
pBAD_Alt2^{E541A}	Expression of Thanatos Alt2^{E541A}	this study
pBAD_ORF5	Expression of pDolos protein 5	this study
pBAD_ORF5_3xFLAG	Expression of pDolos protein 5_3xFLAG	this study
pBAD_Alt1^{E521A}_for engineering	Vector used for phage engineering	this study
pBAD_Alt2^{E541A}_for engineering	Vector used for phage engineering	this study

pKT25	*plac*, P15A, MCS downstream from T25 fragment encoding region, Kan^r (vector for protein-protein interaction analysis)	[277]
pKT25_*mshA*	Fusion with *mshA*	this study
pKT25_gIII	Fusion with Dolos gIII	this study
pKNT25	*plac*, P15A, MCS upstream from T25 fragment encoding region, Kan^r (vector for protein-protein interaction analysis)	[277]
pKNT25_*mshA*	fusion with *mshA*	this study
pKNT25_gIII	fusion with Dolos gIII	this study
pUT18C	*plac*, Col E1, MCS upstream from T18 fragment encoding region, Amp^R (vector for protein-protein interaction analysis)	[277]
pUT18C_*mshA*	Fusion with *mshA*	this study
pUT18C_gIII	Fusion with Dolos gIII	this study
pUT18	*plac*, Col E1, MCS downstream from T18 fragment encoding region, Amp^R (vector for protein-protein interaction analysis)	[277]
pUT18_*mshA*	Fusion with *mshA*	this study
pUT18_gIII	Fusion with Dolos gIII	this study
pET24c(+)	lac promotor, Kan^r (expression vector)	[278]
pET24c_Alt1_His	Alt1_His expression	this study
pET24c_Alt2_His	Alt2_His expression	this study
pDolos	Isolated from a virion sample	this study
pDolos_K	Kan^r	this study
pDolos_KV	*venus* (Kan^r)	this study
pDolos_KVL	*venus*, *lacZ´* (Kan^r)	this study
pDolos_ΔORF4-5	Gene deletion of pDolos ORF4-5	this study

Table 15: Bacteriophages used in this study.

Phage	Description	Reference
Phonos	Native	[279]
Dolos	Native	This study
Thanatos	Native	[72]
Thanatos Alt1^{E521A}	Alt1^{E521A}	This study
Thanatos Alt2^{E541A}	Alt2^{E541A}	This study
Thanatos double mutant	Alt1^{E521A} Alt2^{E541A}	This study

Table 16: Oligonucleotides used in this study.

ID	Name	Sequence (5´→ 3`)
Check primer		
M13 FWD		TGTAAAACGACGGCCAGTCC
M13 REV		CAGGAAACAGCTATGAC
AD214	pBAD FWD	GCACGGCGTCACACTTTGCTATG
AD215	pBAD REV	GCCAGGCAAATTCTGTTTTATCAG
JH460	pKT25-for	CACTGACGGCGGATATCGACATGTT
JH461	pKT25-rev	CCGCCGGACATCAGCGCCATTC
JH462	pUT18-for	CCAGGCTTTACACTTTATGCTTCC
JH463	pUT18-rev	GACGCGCCTCGGTGCCCACTGC
JH464	pKNT25-for	CCCAGGCTTTACACTTTATGCTTCC
JH465	pKNT25-rev	GTTTTTTTCCTTCGCCACGGCCTTG
JH466	pUT18C-for	CGGCGTGCCGAGCGGACGTTCG
JH467	pUT18C-rev	TCAGCGGGTGTTGGCGGGTGTC
pDolos constructs		
NES476	pDolos_179 cut FWD	CTAGAGGCTTGCAGAGCGA
NES477	pDolos_179 cut REV	AGGCCGCGCCCCGCCT
NES610	pDolos _Venus FWD	AATTCGAGCTCGGTACCCTTACTTGTACAGCTCGTCCATG
NES611	pDolos _Venus REV	ATCGAATTCCTGCAGCCCAGGAGGGCAAATATGGTGAGCAAGGGCG AG
NES612	pDolos _pBBR Promotor FWD	CTCGCCCTTGCTCACCATATTTGCCCTCCTGGGCTGCAGGAATTCGA T
NES613	pDolos _pBBR Promotor REV	GCGATGGCCCACTACGTGTCATGCCGTTTGTGATGG
NES614	pDolos _Kan FWD	AAGCCATCACAAACGGCATGAGGAGCGCCTGAAGCCC
NES615	pDolos _Kan REV	GAATGATGTAGCCGTCAAGTTGTCATAACCTGAATCGCCAGCGG
NES616	pDolos _pBAD Promotor FWD	AATATGGTATTGATAATCCTTATGACAACTTGACGGCTAC
NES617	pDolos _pBAD Promotor REV	AGTGAATCCGTAATCATGGTCATATTTGCCCTCCTGGGTACCGAGCT CGAATT

NES618	pDolos _LacZ FWD	CGAGCTCGGTACCCAGGAGGGCAAATATGACCATGATTACGGATTC A
NES619	pDolos _LacZ REV	CGACTCTAGAGGATCCCCTTATTTTTGACACCAGACCAA
NES620	pDolos _Kan no_LacZ REV	GCCTGCAGGTCGACTCTAGAGGATCCCCGGATTATCAATACCATATT TTTGAAA
NES486	pDolos _Kan Insert 179 FWD	TCAGGCGGGGCGCGGCCTCACGTAGTGGGCCATCG
NES487	pDolos _Kan Insert 179 REV	GCTCTGCAAGCCTCTAGGGATTATCAATACCATATTTTTGAAA
NES654	Venus insertion pDolos _179 FWD	AGGCGGGGCGCGGCCTTTACTTGTACAGCTCGTCCATG
NES655	LacZ insertion pDolos _179 REV	ATCGCTCTGCAAGCCTCTAGTTATTTTTGACACCAGACCAACT
NES657	no lacZ pDolos_179 REV	ATCGCTCTGCAAGCCTCTAGCCTGAATCGCCAGCGG
NES681	pDolos _Kan ORF4-5 KO FWD	TCAGGCGGGGCGCGGCCTGGAGCGCCTGAAGCCCGT
NES682	pDolos _Kan ORF4-5 KO REV	TAGCCAAAAGGTAAAATCCCTGAATCGCCAGCGGCA

qPCR

NES581	pDolos qPCR FWD	CAGTTGGCCATTCATGGT
NES582	pDolos qPCR REV	GCAAGCAGATGATGAAACG
NES583	MR-1 qPCR FWD	CTGTCTGAAACTCAACGGC
NES584	MR-1 qPCR REV	CATGCCATTACTCTATCTCTACTGC
NES464	Dolos qPCR FWD	TAGAACGATTCTCATGCTTCG
NES447	Dolos qPCR REV	GGCTCGGTCTTTACTAAATGG

BACTH

NES400	pKT_mshA new FWD	CAGGGTCGACTCTAGAGTTTACCTTAATCGAATTAGTCGTAGT
NES401	B2H_mshA new FWD	CTGCAGGTCGACTCTAGAGTTTACCTTAATCGAATTAGTCGTAGT
NES384	B2H_pKT_mshA REV	TTAGTTACTTAGGTACCCGGGGTTAACAACCACTATCTGTAATAACA TACTT
NES383	B2H_mshA REV	GAGCTCGGTACCCGGGGACAACCACTATCTGTAATAACATACTTAGG
NES374	B2H_D_pIII FWD	CTGCAGGTCGACTCTAGAGATGGCTTTTAGTCCTTTTGGTA
NES375	B2H_D_pIII REV	GAGCTCGGTACCCGGGGGTGATATTTAACAATCATTAAGCCA
NES376	B2H_pKT_D_pIII FWD	CAGGGTCGACTCTAGAGATGGCTTTTAGTCCTTTTGGTA

NES377	B2H_pKT_D_pIII REV	TTAGTTACTTAGGTACCCGGGGCTAGTGATATTTAACAATCATTAAG CC

V5 tagged Alt1 and Alt2

NES597	pBAD TH1_28-V5 REV	ACCGGTGCTATCCAGGCCCAGCAGAGGGTTCGGAATCGGTTTGCCA ATTCCTTTAGCTGTTATAGGTCTAGG
NES598	pBAD_TH1_28_29-V5 V5 Tag FWD	GCTGGGCCTGGATAGCACCGGTGGCAAACCGATTCCGAACCCTCTG CTGGGCCTGGATAGCACCTAAGGGGATCCTCTAGAGTCGAC
NES599	pBAD_TH1_28_29-V5 V5 Tag REV	GTCGACTCTAGAGGATCCCCTTAGGTGCTATCCAGGCCCAGCAGAG GGTTCGGAATCGGTTTGCCACCGGTGCTATCCAGGCCCAGC
NES600	pBAD V5-TH1_28 FWD	TAGCACCGGTGGCAAACCGATTCCGAACCCTCTGCTGGGCCTGGAT AGCACCTCAGAAGAATTAATGTTATGTGAAGTT
NES601	pBAD_V5-TH1_28_29 V5 Tag FWD	AGCGAATTCGAGCTCGGTACCCAGGAGGGCAAATATGGGCAAACCG ATTCCGAACCCTCTGCTGGGCCTGGATAGCACCGGTGGCAAACCGA T
NES602	pBAD_V5-TH1_28_29 V5 Tag REV	ATCGGTTTGCCACCGGTGCTATCCAGGCCCAGCAGAGGGTTCGGAA TCGGTTTGCCCATATTTGCCCTCCTGGGTACCGAGCTCGAATTCGCT
NES603	pBAD_TH1_29-V5 REV	ACCGGTGCTATCCAGGCCCAGCAGAGGGTTCGGAATCGGTTTGCCA TACAAATAATCTGCTGTTTCTGG
NES604	pBAD_V5-TH1_29 FWD	ATAGCACCGGTGGCAAACCGATTCCGAACCCTCTGCTGGGCCTGGA TAGCACCTCAGAAGAATTAATGTTATGCGA

Construction of pDolos protein 5 expression vectors

NES492	pBAD_ORF5 FWD	AATTCGAGCTCGGTACCCATGAGCATGCTAACCATGA
NES684	pBAD_ORF5 3xFLAG REV	TCGACTCTAGAGGATCCCCCTATTTATCATCATCATCTTTATAATCAA TATCATGATCTTTATAATCGCCATCATGATCTTTATAATCGAGGCTTG CAGAGCGATTC
NES493	pBAD_ORF5 REV	CGACTCTAGAGGATCCCCCTAGAGGCTTGCAGAGCG

Construction of pBAD based Alt1 and Alt2 expression vectors

NES514	pBAD_TH1_028 FWD	AATTCGAGCTCGGTACCCAGGAGGGCAAATATGTCAGAAGAATTAA TGTTATGTGAAG
NES515	pBAD_TH1_028 REV	CGACTCTAGAGGATCCCCTTAAATTCCTTTAGCTGTTATAGGTC
NES516	pBAD_TH1_029 FWD	AATTCGAGCTCGGTACCCAGGAGGGCAAATATGTCAGAAGAATTAA TGTTATGCG
NES517	pBAD_TH1_029 REV	CGACTCTAGAGGATCCCCTTAATACAAATAATCTGCTGTTTCTG
NES518	TH1-028 E to A FWD	CAAGATGAATCAGCAATTATTTTACCTAGA
NES519	pBAD_TH1-028 E to A REV	TCTAGGTAAAATAATTGCTGATTCATCTTG
NES520	pBAD_TH1-029 E to A FWD	AGCTCAGAACAGGCAGTTATTTTACCTA

NES521	pBAD_TH1-029 E to A REV	TAGGTAAAATAACTGCCTGTTCTGAGCT

Construction of pET24c(+) based Alt1 and Alt2 expression vectors

NES436	pET_T028-His FWD	GGTGGTGGTGGTGCTCGATTAATGGTGATGGTGATGGTGAATTCCTTTAGCTGTTATAGGTCTAG
NES437	pET_T028-His REV	TTAAGAAGGAGATATACATAATGTCAGAAGAATTAATGTTATGTGAAG
NES440	pET_T029-His FWD	GGTGGTGGTGGTGCTCGATTAATGGTGATGGTGATGGTGATACAAATAATCTGCTGTTTCTGG
NES441	pET_T029-His REV	AAGAAGGAGATATACATAATGTCAGAAGAATTAATG

Thanatos phage engineering

NES589	pBAD_TH1_28 E to A 1 FWD	AATTCGAGCTCGGTACCCTTTTTATTAGGTAGAGATGAATTTGC
NES519	TH1-028 E to A 1 REV	TCTAGGTAAAATAATTGCTGATTCATCTTG
NES518	TH1-028 E to A 2 FWD	CAAGATGAATCAGCAATTATTTTACCTAGA
NES571	TH1_28 Tag 2 REV	TATCATGATCTTTATAATCGCCATCATGATCTTTATAATCTTAAATTCCTTTAGCTGTTATAGGTC
NES572	TH1_28 Tag 3 FWD	ATTATAAAGATCATGATATTGATTATAAAGATGATGATGATAAATAAACCGAAAAAGGAGGCTAA
NES590	pBAD_TH1_28 E to A 3 REV	CGACTCTAGAGGATCCCCTTTAGGATGGATGCCTCTG
NES591	pBAD_TH1_29 E to A 1 FWD	AATTCGAGCTCGGTACCCTAGATTGCCTCTTTTAGCGA
NES575	TH1_29 E to A new 1 REV	TAAAGATCATGATATTGATTATAAAGATGATGATGATAAATAAATTAAGGAGACTTCGGTCTCC
NES576	TH1_29 Tag 2 FWD	CAATATCATGATCTTTATAATCGCCATCATGATCTTTATAATCTTAATACAAATAATCTGCTGTTTCTG
NES521	TH1-029 Tag 2 REV	TAGGTAAAATAACTGCCTGTTCTGAGCT
NES520	TH1-029 E to A 3 FWD	AGCTCAGAACAGGCAGTTATTTTACCTA
NES592	pBAD_TH1_29 E to A 3 REV	CGACTCTAGAGGATCCCCAAAAAGGCTATGGGGTACG

4.2 Methods

4.2.1 Microbiological methods

Cultivation of *Shewanella* strains

Shewanella strains were incubated overnight at RT with shaking (120 rpm). Unless otherwise stated, overnight cultures were diluted (OD_{600} 0.02) for experiments and then incubated in liquid medium at 30 °C and 180 rpm until mid-exponential phase was reached. If necessary, the liquid media or the agar plates were supplemented with antibiotics or other additives (see Table 6). Incubation of *S. oneidensis* MR-1 strains was performed in LB medium. Incubation of unspecified *Shewanella* isolates [264] was always performed in 4M medium.

Cultivation of *E. coli* strains

E. coli strains were incubated in LB medium at 37 °C. Liquid incubation was performed on a shaker at 180 rpm. If necessary, liquid media or LB agar plates were supplemented with antibiotics/additives (see Table 6).

Storage of strains

For long-term storage of bacteria, strains were grown to OD_{600} 1 and supplemented with DMSO to a final concentration of 10% (v/v). The strains were then stored at -70°C.

Static biofilm assay

The influence of Dolos and Dolos as well as pDolos on the biofilm formation and mature biofilms of *S. oneidensis* MR-1 was investigated by carrying out static biofilm assays.

For this purpose, cultures were diluted to an OD_{600} of 0.15 in LB medium. A transparent, flat bottom 96-well plate (Sarstedt, Germany) was then inoculated with these diluted cultures (200 µl/well) and statically incubated at 30°C for 24 h. For short-term tests, Dolos or Dolos + pDolos (10^8 PFU/ml) were added to the wells 0, 3, 6 and 22 hours after inoculation to investigate the effects of these MGEs on developing *S. oneidensis* MR-1 biofilms. For long-term testing, the inoculated 96-well plate was incubated at 30°C for 24 h without the addition of MGEs. After 24 hours, the mature biofilm was infected (10^8 PFU/ml) and incubated for a further 2, 6, 9 or 24 h. To test the influence of long-term infected cells (infected 24 h before

the start of the static assay) on *S. oneidensis* MR-1 biofilm formation, infected cells were inoculated (200 µl/well) and statically incubated for 24 h.

After the static incubation was completed, the OD_{600} was determined to measure bacterial growth. The surface-associated biomass was then stained with 12 µl of 0.5% (w/v) crystal violet per well for 10 min at RT. The supernatant was then removed and the wells were washed with 200 µl ddH_2O. Following, 200 µl 96% (v/v) ethanol was added to dissolve the retained crystal violet. Following, the surface-associated biomass was quantified by measuring the absorbance at 580 nm. The absorbance at 580 nm was then normalised to the absorbance at 600 nm and the biofilm biomass percentage of infected cultures compared to untreated cultures (addition of an equal volume of LB medium) was calculated. All experiments were repeated three times independently.

Cultivation of biofilms grown within flow cells

To analyse *S. oneidensis* MR-1 biofilms developed under hydrodynamic conditions, biofilms were grown at RT in LB medium in a three-chamber flow system. The size of each chamber was 1 x 4 x 40 mm. Coverslips (Carl-Roth, Germany) were used as colonisation surfaces for the bacteria. The coverslips were attached to the channels with silicone (Aquasil, JBL, Germany).

Pre-infected *S. oneidensis* MR-1 *tn7:::egfp* cells (infected 24 h before the start of the static test) were used for biofilm analysis. The flow chamber system was sterilized and set up as described in [96]. For the experiments, overnight cultures were diluted in LB medium (OD_{600} 0.05) and injected (~500 µl) into the system. After a short pre-incubation of about 20 min without flow, flow was started (0.75 rpm). The cells were incubated in these flow cells for 24 h. Biofilms were then observed by confocal microscopy (TCS SP8 microscope (Leica AG, Germany)) and analysed using the software tools Fiji (ImageJ) and BiofilmQ [129]. The biofilm analyses were performed in triplicates in at least two independent experiments.

Measurement of planktonic growth

To generate growth curves, cell cultures with set OD_{600} were inoculated into a transparent, flat bottom 96-well plate (Sarstedt, Germany). Each well was filled with 200 µl of culture. The plate was following inserted into a microplate reader (INFINITE M NANO+, Tecan, CH). The OD_{600} was then measured every 10 min for at least 10 h. Shaking incubation conditions and 30 °C were used inside the device. Finally, growth curves were generated with these data points using Microsoft Excel and GraphPad PRISM. All growth experiments were conducted in biological triplicates.

Plasmid stability assay

The stability of the plasmid pDolos was analysed by incubating *S. oneidensis* MR-1 ΔLambdaSo ΔMuSo2 cells containing the plasmid pDolos_K over six consecutive regrowth phases (over three days). At mid-exponential growth during the last regrowth without kanamycin in the medium, cells were diluted and plated on LB agar plates with or without kanamycin. Colony forming units (cfu) were counted after 48 h of growth. The experiment was performed in biological triplicates.

Electron microscopy of infected cells

For electron microscopy of infected cells, *S. oneidensis* MR-1 ΔLambdaSo ΔMuSo2 cells at mid-exponential growth were infected for 2.5 h with Dolos or a mixed virion-containing supernatant (Dolos and pDolos) at a MOI of 5. Cells were then fixed by addition of glutaraldehyde (final concentration: 1.25% (v/v)). After 15 min incubation, the cells were washed once with LM medium and concentrated by centrifugation at 13,000 rpm (initial volume: 500 µl; final volume: 50 µl). Subsequently, 5 µl of the cell suspension was spotted onto carbon-coated copper grids (400 square mesh; Plano, Germany). After 5 min of incubation, the grids were washed twice with ddH_2O and negatively stained with the UA zero stain (Plano, Germany) for 45 sec. The grids were examined using a JEM-1400 electron microscope (JEOL, Japan) at 100 kV.

The microscopy was carried out thanks to the support of Anke Treuner-Lange from the Søgaard-Andersen group at the MPI Marburg.

MSHA pili staining

For MSHA pili staining, mid-exponential *S. oneidensis* MR-1 ΔLambdaSo ΔMuSo2 $MshA^{S69C}$ cells were harvested by centrifugation of 1 ml at 3,000 × g for 5 min at RT. Following, the pellets were washed with 50 µl 1 x PBS. A total of 1.5 µl of Alexa Fluor™ 488 C5 maleimide dye (Thermo Fisher Scientific, USA) was added to reach a final concentration of 25 µg/ml. The cells were then incubated in the dark for 15 minutes. Subsequently, the cells were sedimented by centrifugation at 3,000 × g for 5 min at RT and washed with 500 µl PBS. Washing was repeated and cells finally resuspended in 950 µl LM medium. 3 µl of the stained culture was spotted onto a 1% (w/v) LM agar pad for microscopy.

Fluorescence microscopy

For microscopic analysis of cells, 3 µl of a mid-exponential cell culture was spotted onto an agarose pad (1% (w/v) agarose in LM medium) and images were taken using a DMI 6000 B (Leica AG, Germany) inverted microscope equipped with an sCMOS camera and HCX PL APO 100x/1.4 objective. VisiView

software (Visitron Systems, Germany) was used for image acquisition. Image processing was performed using Fiji (ImageJ).

To verify horizontal gene transfer by fluorescence microscopy, cells transduced with different pDolos constructs were analysed. For this purpose, mid-exponential *S. oneidensis* MR-1 ΔLambdaSo ΔMuSo2 cells were infected with a mixed virion-containing supernatant (containing different pDolos variants) at a MOI of 2. 24 h after infection, regrown mid-exponential infected cells were analysed by microscopy.

4.2.2 Virological methods

Virion isolation of aquatic or freshwater sediment samples

Virions were isolated and enriched from aquatic and freshwater sediment samples by incubation with a liquid culture of *S. oneidensis* MR-1 ΔLambdaSo ΔMuSo2 (1:1). After 24 h of incubation at RT and 120 rpm, the cells were harvested and the supernatants were filtered using a polyethersulfone (PES) 0.2 μm filter. The presence of phages in the filtrates was assessed by spot assays (see 4.2.2 (phage spot and plaque assay)). The supernatants were stored at 4 °C in the phage-collection.

Phage working stock preparation and single plaque incubation

Virion-containing working stocks were prepared by infecting a 10 ml mid-exponential *S. oneidensis* MR-1 ΔLambdaSo ΔMuSo2 culture with 100 μl phage-containing supernatant (from the phage collection). 24 h after infection, the cells were harvested and the supernatants were filtered through a PES (0.2 μm) filter. Working stocks were stored at 4 °C.

To generate phage-containing supernatants resulting from a single plaque, a plaque assay was performed (see 4.2.2 (phage spot and plaque assay)). Using a sterile pipette tip, a single plaque was isolated and following incubated with a mid-exponential *S. oneidensis* MR-1 ΔLambdaSo ΔMuSo2 culture. 24 h after infection, the cells were harvested and the supernatants were filtered using PES (0.2 μm) filter.

Phage spot and plaque assay

Plaque and spot assays were performed to analyse the infectivity of Phages. For both assays, 400 μl of stationary cell culture was mixed with 7 ml of 47 °C warm soft agar [agar: 0.5% (w/v)], vortexed and poured onto an agar plate [agar: 1.5% (w/v)] (agar overlay method). For a plaque assay, 100 μl of diluted phage-containing supernatant was mixed with the soft agar before being poured onto the agar plate. For a spot assay, phage-containing supernatants were spotted onto a hardened overlay plate. Plaque and spot formation were assessed after 24 h (Thatatos) or 48 h (Dolos) of incubation.

Virion temperature and pH stability assay

In order to investigate the pH stress resistance of phage Dolos, 10 µl of a supernatant containing phage Dolos (10^9 PFU/ml) were incubated with 90 µl of LB medium that had been adjusted to different pH values at RT. The phages were incubated in these media of different pH values for 24 h at RT. In order to test the thermal stability of Dolos, supernatants containing phage Dolos (10^9 PFU/ml) were incubated for 24 h at different temperatures using a thermal cycler (Mastercycler nexus gradient, Eppendorf, Germany). The supernatants were then serially diluted with LB medium and 1.5 µl of each dilution was spotted onto agar overlay plates. Plaque formation was assessed after two days of incubation. pH and temperature sensitivity were determined in three independent biological replicates.

Dolos adsorption assay

To test the adsorption of Dolos on host cells, mid-exponential *S. oneidensis* MR-1 ΔLambdaSo ΔMuSo2 cells were infected at a MOI of 0.1. At various times after infection, samples were collected, filtered through a PES filter (0.2 µm) and a plaque assay was performed to calculate the PFU/ml of these samples. As a control, phage Dolos was also added to LB medium. The percentage of extracellular phages was estimated by normalisation to the calculated PFU/ml of the control.

Transduction assay

To determine whether the horizontal transfer of pDolos is predominantly transduction, mid-exponential *S. oneidensis* MR-1 cultures harbouring pDolos_K were infected with Dolos at a MOI of 0.1. 24 h post infection, these as well as uninfected cells were diluted to an OD_{600} of 0.02 and following incubated to an OD_{600} of 0.2. These early-exponential cells were then mixed with early-exponential *S. oneidensis* MR-1 *Tn7:::ecfp* (Cm^r) cells. The dilution factor for the co-incubation was 1:10. The cell mixture was plated on LB agar plates containing kanamycin, chloramphenicol or both after 24 h of co-incubation. Colony growth was monitored after 48 h of incubation. Experiment was conducted in biological duplicates.

Virion reproduction assay

To analyse phage reproduction, mid-exponential *S. oneidensis* MR-1 ΔLambdaSo ΔMuSo2 cells were infected at a MOI of 0.1. At various times after infection, samples were collected, filtered through a PES filter (0.2 µm) and subsequently a plaque assay was performed to calculate the PFU/ml of these samples.

Transfer of pDolos variants into different *Shewanella* species

For the transfer of different pDolos variants into bacteria, mixed virion-containing supernatants were prepared by infecting mid-exponential *S. oneidensis* MR-1 ΔLambdaSo ΔMuSo2 cell cultures harbouring different pDolos variants with a Dolos-containing supernatant (MOI 0.1). 24 h after infection, virion-containing supernatants were harvested like described in 4.2.2 (Virion stock preparation). These virion-containing supernatants were then used to transduce the different pDolos variants into several *Shewanella* strains. For this purpose, mid-exponential cells were infected with these supernatants at a MOI of 2. 24 h after addition of the supernatants, cells (OD_{600} 1) were plated on kanamycin-containing agar plates. Depending on the medium used, colony growth was imaged after 24 h (LB medium) or 48 h (4M medium) of incubation.

4.2.3 Molecular biological methods

Polymerase chain reaction (PCR)

PCR was performed either to generate DNA fragments for cloning (Phusion PCR) or to control genotypes (Taq PCR). The used PCR components and the programs are described in **Table 17**. For the reaction the Mastercycler nexus gradient (Eppendorf, Germany) was used.

Table 17: Programmes and components for Taq and Phusion PCR.

Cycle	Temperature	Time
1	Taq: 95 °C Phusion: 98 °C	5 min 30 sec
30	Taq: 95 °C Phusion: 98 °C	30 sec 30 sec
	56-60 °C	30 sec
	72 °C	diverse
1	72 °C	10 min

Component	Taq PCR	Phusion PCR
ddH_2O	19.4 µl	36.65 µl
Reaction buffer	2.5 µl	10 µl
dNTPS	0.5 µl	1.5 µl
FWD primer (50 µm)	0.3 µl	0.3 µl
REV primer (50 µm)	0.3 µl	0.3 µl
Polymerase	1 µl	0.25 µl
Template	1 µl	1 µl
Total volume	25 µl	50 µl

Gel electrophoresis

PCR products were analysed by agarose gel electrophoresis. For this purpose, 2 µl or 10 µl (Phusion or Taq) of the PCR product was mixed with an appropriate volume of sample buffer and loaded onto a 1% (w/v) TBE agarose gel containing 0.05 µg/ml ethidium bromide and immersed in 0.5 x TBE buffer. 5 µl of the GeneRulerTM 1 kb DNA Ladder (Life Technologies, USA) was loaded onto the gel and used to determine the size of the PCR products. The gels were run at 140 V for 20 min at RT. At the end of the run, the DNA products within the agarose gel were detected by using UV light.

Purification of plasmid, chromosomal and PCR-generated DNA

Plasmid DNA, chromosomal DNA and PCR products were purified using E.Z.N.A Kits (Plasmid DNA Mini Kit, Bacterial DNA Kit, PCR Cleanup Kit; Omega Bio-tek, USA). Finally, the DNA was eluted in ddH_2O.
The DNA concentration of the eluate was then measured using a spectrophotometer (NanoDrop).

DNA sequencing

DNA sequencing was carried out to check whether the products are free of point mutations. Microsynth Seqlab GmbH (Göttingen, Germany) was used for this purpose. A plasmid concentration of at least 30 ng/µl was required to obtain a sequencing result.

Restriction enzyme digest

Restriction enzyme digestion was used to linearise plasmids for plasmid cloning. Digestion was performed according to the FastDigest protocol (Thermo Fisher Scientific, USA).

Gibson assembly

The Gibson assembly was used for plasmid cloning [280]. Using this assembly method, DNA inserts were ligated into a linearised vector. The required amount of DNA inserts was calculated according to the following formula:

$$Amount\ of\ insert\ DNA\ required = \frac{\text{Vector (ng)}\ x\ Insert\ (bp)}{\text{Vector (bp)}}$$

1 µl of linearised vector containing 25 ng/µl DNA was used for Gibson assembly. Calculated insert and vector volumes were added to 15 µl Gibson Assembly Mix, filled to 20 µl with ddH_2O and incubated at 50°C for 1 h.

Transformation

To perform transformation of bacterial cells, 1 µl of plasmid DNA or a complete Gibson assembly mix containing the ligated plasmid (20 µl) was added to 50 µl of chemically competent *E. coli* DH5α λpir, *E. coli* BL21, *E. coli* WM3064 or *E. coli* BTH101 cells and incubated on ice for 20 min. Heat shock was then applied at 42 °C for 45 seconds, after which 1,000 µl of LB medium was added to the sample. The bacteria were then regenerated on a thermoblock shaker at 37 °C (30 °C for BTH101) and 600 rpm for 1 h, after which the bacterial cells were precipitated by centrifugation (9,000 x g for 2 min) and 900 µl of the supernatant

was discarded. The pellet was then resuspended in the remaining supernatant and plated on an agar plate containing selective additives. The plates were following incubated for 24 h at 37 °C. The cultured bacterial colonies were then checked using Taq-PCR (see Table 17) to confirm the presence of ligated plasmids containing the insert of interest. For this, no DNA template was added to the PCR mixture, but some cell material was added using a toothpick.

Generation of *S. oneidensis* MR-1 mutants by conjugation and subsequent homologous recombination

Conjugation was carried out to transfer pNPTS into *S. oneidensis* MR-1. For this, 1 ml of a stationary culture of *E. coli* WM3064 containing the pNPTS plasmid of interest and 1 ml of a stationary culture of *S. oneidensis* MR-1 were washed twice with LB medium and centrifuged at 9,000 x g for 2 min. The cells were then combined in 200 µl and spotted (50 µl spots) onto LB-DAP plates. DAP was required as an essential additive to ensure the growth of *E. coli* WM3064, as this strain is DAP auxotroph. After an overnight incubation at 30 °C, the cells were washed from the plate with 2 ml LB + Kan medium. To remove DAP, the harvested cells were washed twice with 1 ml LB + Kan medium before being resuspended in 1 ml LB + Kan medium and diluted 1:10 and 1:50. From these dilutions 100 µl were plated onto individual LB + Kan agar plates. After these plates were incubated overnight at 30 °C, 25 Kan-resistant colonies were restreaked individually first onto an LB + Suc plate and then onto an LB + Kan plate using the same toothpick. These plates were then incubated overnight at 30 °C. Colonies resistant to Kan and sensitive to Suc were identified. For the loop out, 3 colonies with the above-mentioned characteristics were selected and co-inoculated into a single flask containing 10 ml of LB medium. The inoculated culture was then incubated for 3.5 h at 30 °C on a shaker at 180 rpm and then plated onto LB + Suc plates at 1:10 and 1:50 dilutions. Following an overnight incubation at 30 °C, a total of 25 colonies were individually restreaked first onto an LB + Kan agar plate and then onto an LB + Suc agar plate, followed by another overnight incubation at 30 °C. A colony PCR using the Taq polymerase was performed on colonies that were both sensitive to Kan and insensitive to Suc to determine whether the required mutation had been achieved.

Electroporation

pBAD and pDolos plasmids were transferred into *S. oneidensis* MR-1 via electroporation. For this purpose, 1 ml of a S. *oneidensis* culture (OD_{600} 1) was centrifuged for 3 min at 8,000 rpm and following resuspended in 1 ml of ice-cold sorbitol (1 M). From this step onwards, the cells were always kept on ice. The washing was repeated and the cells were finally resuspended in 50 µl of sorbitol. Approximately 100 ng of the plasmid to be transformed was added to the cells. The whole preparation was then transferred to an electroporation cuvette and electroporation was performed by applying a pulse of 2.5 kV for 4-5 ms. 1 ml of LB medium was pipetted into the sample before the cells were allowed to regenerate for 1-2 h at 30 °C. The preparation was then centrifuged and the bacterial pellet was then resuspended in 100 µl of LB medium.

Following, the entire volume was plated onto LB plates containing selective additives and incubated at 30 °C for 1-2 days.

Native gel electrophoresis assay

To determine differences in virion size depending on the packaged genome, the native agarose gel electrophoresis method developed by Bennett *et al.* 2011 [160] was used. For this purpose, a virion-containing supernatant was incubated with 0.1 mg/ml DNAse I for 15 min at 37 °C to digest the free DNA of the supernatant. For separation of virion DNA, 10 µl of virion-containing supernatant was incubated with 2 µl of DNA loading dye (30% glycerol (v/v), 0.25% bromophenol blue dye (w/v) and 0.25% xylene cyanol FF dye (w/v) in 1x TBE) and a final concentration of 1% (w/v) SDS and following heat-inactivated at 80 °C for 15 min. To separate virions, 2 µl DNA loading dye was added to the 10 µl supernatant. Samples were loaded onto a 0.6% (w/v) TBE agarose gel. Virions and DNA were separated by electrophoresis at 2.5 V/cm for 14.5 h. Visualisation of free DNA was achieved by incubating the gel with ethidium bromide (1 µg/ml) for 15 min. To visualise packaged DNA, the particles were degraded in a 0.2 M NaOH bath for 45 min. The gel was then neutralised in a 0.45 M Tris-HCl (pH 7.2) bath for 15 min. A second ethidium bromide stain and UV light analysis revealed then the DNA of the virions that had passed through the gel.

Bacterial-adenylate cyclase two-hybrid assay (BACTH)

The bacterial adenylate cyclase two-hybrid (BACTH) assay was used in this study to determine a protein interaction between Dolos pIII and the *S. oneidensis* MR-1 protein MshA. Plasmids containing the proteins of interest genetically fused to either the N- or C-terminus of the T18 or T25 fragment of the adenylate cyclase catalytic domain were used to test various protein interaction constellations. For the assay, 1 µl T18 and T25 fragment containing plasmids were co-transformed into 20 µl of *E. coli* BTH101. After regeneration at 30 °C for 1 h, the total transformation reaction mixture was transferred to 5 ml of LB medium containing Kan and Amp. The subsequent incubation step was performed overnight at 30 °C. After incubation, 10 µl of each co-transformation culture was dropped onto an LB agar plate containing Kan, Amp, IPTG and X-gal and incubated for 24 h at 30 °C. Following, the plates were checked for the interaction phenotype of each colony drop (blue colour) and scanned.

Cloning of pDolos plasmid variants

For the creation of pDolos variants, the plasmid was linearised by PCR by generating forward and reverse primers adjacent to each other at the same position in the plasmid. The PCR was conducted with the Phusion Polymerase (Thermo Fisher Scientific, USA). Constructs of pDolos were made using the Gibson assembly method (see 4.2.3 (Gibson assembly)). The resulting constructs were purified by using the E.Z.N.A. DNA Probe Purification Kit (Omega Bio-tek, USA) and then electroporated into *S. oneidensis* MR-1 strains (see 4.2.3 (Electroporation)).

Thanatos phage engineering

A method based on Shitrit *et al.* 2022 [155] was used to generate recombinant Thanatos phages. For this purpose, cloning vectors (pBAD33 based) containing a short Tag (~70 bp) and 2 x 500 bp homologue overhangs upstream and downstream of the Tag were generated by the Gibson assembly method (see 4.2.3 (Gibson assembly)). In one of these homologous overhangs, point mutations were present that led to Alt1^{E521A} or Alt2^{E541A}. After vector generation, mid-exponential *S. oneidensis* MR-1 ΔLambdaSo ΔMuSo2 cells carrying such a phage engineering vector were infected with Thanatos at a MOI of 0.01. 24 h after infection, the supernatant was filtered through a 0.2 µm PES filter. Phusion PCR was then performed to verify the presence of recombinant phages in the supernatant. One of the primers used for the PCR annealed within the inserted Tag and the other primer annealed outside of the 500 bp overhang region. This step was followed by an enrichment step in which mid-exponential *S. oneidensis* MR-1 ΔLambdaSo ΔMuSo2 cells were divided into 4 x 96-well plates (200 µl per well) and infected with 10 phages per well. After 24 h of infection, each well was screened for recombinant phages by PCR. Supernatants from wells containing recombinant phages were collected and plaque assays were performed (see 4.2.2 (Plaque assay)). Subsequently, 50 plaques were isolated and incubated with *S. oneidensis* MR-1 ΔLambdaSo ΔMuSo2 for 24 h. These 50 cultures were then screened by PCR for the presence of single plaque-purified recombinant phages. Finally, positive PCR products were sequenced to ensure the presence of the point mutations and the filtered supernatants containing single plaque-purified recombinant phages were stored at 4°C.

Density centrifugation, staining and electron microscopy of virions

The density centrifugation, staining and electron microscopy of phage Dolos was kindly conducted by Clara Rolland, Mathias Müsken and Johannes Wittmann (Leibniz Institute DSMZ, Braunschweig, Germany).

For virion enrichment and purification, 300 ml of a Dolos-containing supernatant (~10^{11} PFU/ml) was centrifuged for 2 h at 16,000 rpm (Sorvall RC6Plus, F21S 8 × 50Y) to concentrate the phages. Phages were following resuspended in 4 ml LB medium and purified by ultracentrifugation in a discontinuous CsCl gradient (0.5 mL CsCl solution with densities 1.6, 1.5, 1.4 and 1.3) for 2 h at 4°C and 35,000 rpm (SW 60

Ti rotor). The phage bands were then isolated and dialysed against SM buffer (100 mM NaCl, 8 mM $MgSO_4$ and 50 mM Tris-HCL (pH 7.5).

For TEM analysis, the phages were prepared as described previously [281]. For this, phages were allowed to adsorb onto thin carbon support films. Negative staining was then performed with 2% (w/v) aqueous uranyl acetate, pH 5.0. Samples were examined in a Zeiss EM 910 or Zeiss Libra120 Plus transmission electron microscope (Carl Zeiss, Germany) at an acceleration voltage of 80 kV/120 kV at calibrated magnifications using a crossed line grid replica. ITEM software (Olympus Soft Imaging Solutions, Germany) was used for size determination.

Virion enrichment by PEG precipitation and virion DNA isolation

Virion enrichment and DNA isolation were essentially performed using a variation of an established protocol (Phage DNA Extraction - Traditional. Texas A&M University, College Station, TX 77843 Rev. 21.9.2018). To enrich the virions, PEG precipitation was performed. For this, 10 ml of a virion-containing supernatant was incubated overnight at 4°C with 5 ml of 30% (w/v) PEG 8000 in 3M NaCl. Following, the samples were centrifuged at 10,000 x g for 90 min to precipitate the virions. The sediments were resuspended in 5 mM $MgSO_4$ for DNA extraction or in LB medium for a simple enrichment of the virions.

For virion DNA extraction, free DNA and RNA in the samples were first digested with DNAse I and RNase A (final concentration: 0.1 mg/ml) for 1 h at 37 °C. A final concentration of 20 mM EDTA was then added for DNAse inactivation. For the subsequent digestion of the virions, the samples were incubated for 1 h at 60 °C with a final concentration of 20 µg of Proteinase K and 10% (w/v) SDS. A phenol-chloroform extraction was following performed to isolate the DNA encapsulated in virions. For this, an equal volume of phenol:chloroform (1:1) was added and the samples were inverted several times. The water phase containing the DNA was separated after centrifugation at 6,000 x g for 5 min and the phenol-chloroform step was repeated with the separated water phase. An equal volume of chloroform was then added to the samples, which were gently mixed by inversion. Following, the water phases were again separated by pipetting after centrifugation. DNA precipitation was performed by adding 1/10 volume of 3M sodium acetate (pH 7.5) and 2.5 volumes of 96% (v/v) ice cold ethanol. After storing overnight at -20°C, the DNA was precipitated by centrifuging at 10,000 x g for 30 min. The DNA pellets were then washed twice by half filling the tubes with 70% (v/v) ethanol followed by centrifugation at 10,000 x g for 3 minutes. The tubes were then opened to disperse the final amount of ethanol and the DNA was dissolved in 50 µl of water and stored at 4°C.

qPCR

qPCR was performed to determine the amount of pDolos in comparison to the amount of Dolos. In biological triplicates, virion DNA was isolated (see 4.2.3 (virion DNA isolation)) from Dolos-containing supernatants and from Dolos- and pDolos-containing supernatants. Chromosomal DNA from cells at different stages of infection was also isolated. For this, *S. oneidensis* MR-1 ΔLambdaSo ΔMuSo2 cells were infected during mid-exponential growth phase at a MOI of 0.1 with Dolos or with a mixed supernatant containing Dolos and pDolos. DNA from biological triplicates was isolated at 2 h, 4 h, 6 h, 8 h and 24 h post-infection. For DNA isolation of infected cells, the protocol of the E.Z.N.A Bacterial DNA Kit (Omega Bio-tek, USA) up to the column step was then performed, followed by phenol-chloroform DNA extraction. qPCR was performed using PowerUp™ SYBR™ Green Master Mix (Thermo Fisher Scientific, USA), the qPCR cycler QuantStudio3 (Thermo Fisher Scientific, USA) and the Design & Analysis software (QuantStudioTM). In order to determine the reproduction rates of Dolos and pDolos, the ΔCt values of Dolos and pDolos were calculated by subtracting the Ct values of the host genome from the Ct values of Dolos and pDolos. The temporal reproduction rate was determined by normalising these values using the formula 2-ΔCt [126], followed by a calculation of the ratio between different time points.

Genome sequencing, assembly and annotation of a mixed virion-containing supernatant

Dolos and pDolos genome sequencing, assembly and annotation was kindly conducted by David Brandt and Jörn Kalinowski (CeBiTec, Bielefeld University, Germany).

The extracted virion DNA was sequenced using Illumina (San Diego, USA) and Oxford Nanopore (Oxford, UK) technology. For Oxford Nanopore sequencing, the Rapid Barcoding Kit (SQK-RBK004) and an R9.4.1 flow cell were used. Sequencing was performed on a GridION machine. A MiSeq machine was used to prepare Illumina libraries using the NanoLT workflow. After sequencing, hybrid genome assembly was performed using Unicycler v0.4.6 [282]. The assembled contigs were annotated using prokka v1.14.5 [111], supplemented with HMMs from the PHROG database and refined using AlphaFold structure predictions [131, 283, 284]. Unless otherwise stated, tools were used with default settings. Annotated genome sequences were made available on Genbank.

4.2.4 Biochemical methods

SDS-PAGE

Protein samples were separated by sodium dodecyl sulphate polyacrylamide gel electrophoresis (SDS-PAGE) as described by Laemmli [285]. Protein samples were obtained from exponentially growing cultures unless otherwise stated. Cells were sedimented by centrifugation so that the resuspension of the cell pellet in 2x SDS sample buffer would reach an OD_{600} of 10. The cells were then boiled for 5 minutes and stored at -20°C. Frozen samples were boiled again for 5 minutes before loading onto an SDS gel consisting of a 5% stacking gel and an 12.5% resolving gel (see **Table 18**). 5 µl of a molecular weight marker was loaded as a standard (BLUeye Prestained Protein Ladder (GeneDireX Inc., USA)). Electrophoresis was performed in a Tris/glycine-based buffer system at 80 V. The protein bands were then visualised by Coomassie staining overnight at RT and a subsequent incubation in fixative solution for 6 hours. Another SDS-PAGE was used for Western Blot analysis (see next section).

Table 18: SDS-PAA gel recipe (for two gels).

12.5% SDS-PAGE	12.5% resolving gel	5 % stacking gel
ddH_2O	3.2 ml	2.8 ml
30% Acrylamide	4.2 ml	825 µl
4x upper buffer	--	1.25 ml
4x lower buffer	2.5 ml	--
10% APS	80 µl	50 µl
TEMED	6 µl	3.75 µl

Western Blot

Following SDS-PAGE Western Blot was conducted to detect proteins of interests or ADP-ribosylated proteins. For Western Blot, a semi-dry system (Electroblotter TE 77 ECL Semi Dry (Amersham Biosciences, Germany)) was used. Prior to the assembly, the PVDF membranes were first activated in 100% methanol for 20 s, washed in ddH2O for 2 min and equilibrated in Western transfer buffer for 5 min. According to the manufacturer's instructions, the activated PVDF membrane and the SDS gel were sandwiched between blotting paper (2x 3 blotting paper) soaked in 1 x Western transfer buffer. Proteins were blotted onto the PVDF membrane by applying an electric field of 2 mA/cm^2 for 45 min. The membrane was then blocked in 5% (w/v) milk powder dissolved in PBS-T for 1 h at RT. Subsequently, primary antibody was added to the blocking solution and incubated over night at 4 °C. After antibody incubation the membrane was washed three times with PBS-T for 10 min each time. If a secondary antibody was needed, it was dissolved in 2.5% (w/v) milk powder solution. The washed membrane incubated with

the secondary antibody for 1 h at RT. Afterwards, the membrane was washed again as described before and depending on the conjugate, Western Lightning® Plus-ECL (PerkinElmer, USA) for HRP conjugates or CDP-Star (Sigma-Aldrich, Germany) for AP conjugates was used for visualisation. Chemiluminescent signals were then visualised by the Intas Photo imager (INTAS science imaging, Germany).

Co-Immunoprecipitation and LC-MS analysis

Co-IP was carried out in cooperation with Prof. Dr. Lienhard Schmitz (JLU Giessen) and the subsequent LC-MS analysis was kindly performed by Aleksandra Bogucka (Lochnit group, JLU Giessen).

To analyse protein interaction partners of Alt1 and Alt2, *S. oneidensis* MR-1 cells harbouring plasmid pBAD_V5_Alt1 or pBAD_V5_Alt2 were used. At mid-exponential phase, 0.2% L-arabinose was added to the cultures and 2 h after induction, 20 ml of each culture was harvested and the pellets were dissolved in 5 ml of ice-cold lysis buffer (50 mM Tris-HCl (pH 7.4), 400 mM NaCl, 50 mM KCl, 5 mM MgCl2, 0.3 mg/l DNase, 20 mM AEBSF, 4 mM benzamidine). Cells were disrupted using a French pressure cell (2 cycles at 1000 psi) and the resulting lysates were cleared by centrifugation at 13,000 x g for 20 min at 4 °C. Protein concentrations were adjusted and 1 µg anti-V5 AB (Thermo Fisher Scientific, USA) or anti-mouse AB (Sigma-Aldrich, Germany) was added to the samples (10 mg of protein (dissolved in 1.7 ml)). Samples were incubated for 3 h at 4°C with gentle shaking. 25 µl protein A/G agarose beads (Sigma-Aldrich, Germany) were then added and the samples were again incubated (3 h, 4 °C, gentle shaking). After incubation, the beads were washed 3 times with lysis buffer and 3 times with PBS (13,000 x g, 1 min). Finally, proteins were eluted in lysis buffer after incubation of the beads for 10 min at 70 °C.

For LC-MS analysis the samples were digested with trypsin using the Filter-Aided Sample Preparation (FASP) protocol [286]. All MS measurements were performed on the Orbitrap Eclipse Tribrid mass spectrometer coupled to the UltiMate 3000 RSLCnano system via the Advion source. Samples were dissolved in 0.1% Trifluoroacetic acid and the peptide concentration was measured using a spectrophotometer. 500 ng of the sample was injected onto the µPAC trapping precolumn washed with loading buffer (0.05% Trifluoroacetic acid, 1% acetonitrile) at a flow rate of 5 µl/min. The peptides were separated on a µPAC HPLC column (C18, 315µm, 50 cm) with a gradient of 0 to 55% buffer 2 (buffer 1: 0.1% formic acid; buffer 2: 80% acetonitrile, 0.1% formic acid). Spectra were acquired in positive mode using a data independent acquisition (DIA) method with a cycle time of 3 sec. The MS1 survey scan was performed in the range of 375-1500 m/z with the following settings: Automatic Gain Control (AGC) target of 400,000, 30% RF lens, Orbitrap resolution of 60,000 and a maximum injection time of 50 ms. MS2 was acquired in 40 overlapping acquisition windows of 15 m/z in the range of 375 to 975 m/z with the following settings: AGC target of 1000000, Orbitrap resolution of 30,000, 30% HCD collision energy, and 54 ms maximum injection time.

The raw files were processed using DIA-NN 1.8 software in a library-free mode using a FASTA file containing the *S. oneidensis* MR-1 reference proteome (UP000008186), including the sequences of the V5-tagged bait proteins: TH1_028 (Alt1) and TH1_029 (Alt2). Digestion was set to trypsin/P with 2 possible missed cleavages, methionine oxidation and N-terminal acetylation as variable modifications and cysteine carbamidomethylation as fixed modification. The precursor FDR was set to 1%. The resulting report file was further analysed using the autonomics package in RStudio. Experimental conditions were compared using a limma t-test and a p-value of 0.05 was used as the threshold for statistical significance.

Phage particle proteomics

Sucrose gradient purification was carried out in collaboration with Nadiia Pozhydaieva and Dr. Katharina Höfer from the MPI Marburg. LC-MS analysis was kindly conducted by Dr. Timo Glatter (MPI Marburg).

For Thanatos particle proteomics, the virions were first purified by sucrose gradient. For this, Thanatos lysate (10^{10} PFU/ml) was treated with 20 U DNase I (Thermo Fisher Scientific, USA) and 2 µL RNase A/T1 mix (4 µg RNase A, 10 U RNase T1, Thermo Fisher Scientific, USA) at 37 °C for 30 min to remove free nucleic acids. The phage was then purified in a 0-45% sucrose gradient (based on TM buffer (50 mM Tris-HCl, 10 mM MgCl2, pH 7.5)). For sucrose gradient purification, 500 µL of phage solution was added to the gradient and centrifuged at 70,000 x g for 20 minutes at 4°C. Following, the phage fraction was removed with a blunt cannula and transferred to a new centrifuge tube. Subsequently, 30 ml of ice-cold TM buffer was added and the phages were pelleted at 100,000 x g for 1 h at 4 °C. Pellets were finally resuspended in 500 µL TM buffer.

For particle proteomics (LC-MS analysis) an on-bead digestion [287] was performed and the dried peptides were reconstituted in 0.1% Trifluoroacetic acid. Following, a liquid-chromatography-mass spectrometry analysis was conducted on an Exploris 480 instrument connected to an Ultimate 3000 RSLC nano and a nanospray flex ion source (all instruments: Thermo Fisher Scientific, USA). Peptide separation was carried out on a reverse-phase HPLC column (75 µm x 42 cm) packed in-house with C18 resin (2.4 µm; Dr Maisch). For separation, the following gradient was used: 98% solvent A (0.15% formic acid) and 5% solvent B (99.85% acetonitrile, 0.15% formic acid). The flow was conducted over 45 min (flow rate: 300 nl/min). The data acquisition mode was set to generate a high-resolution MS scan at 60,000 full width at half maximum (at m/z 200). This was followed by MS/MS scans of the most intense ions within 1 s (cycle 1s). The charged state screening mode was enabled to exclude unassigned and single charged ions to increase the efficiency of MS/MS experiments. The dynamic exclusion duration was set to 14 sec. Ion accumulation time was set to 50ms (MS) and 50ms at 17,500 resolution (MS/MS). AGC was set to 3x106 for MS and 2x105 for MS/MS. For spectral based evaluation, MS raw files were searched using MSFragger embedded in Scaffold 4 (Proteome Software) with 20 ppm peptide and fragment tolerance with carbamidomethylation (C) as fixed and oxidation (M) as varying modification using a uniprot protein database.

Affinity chromatography and size exclusion chromatography

Affinity and size exclusion chromatography of Alt1 and Alt2 was conducted with the kind support of Svenja Thöneböhn (Thormann lab, JLU Giessen).

E. coli BL-21 cells containing the pET24c plasmid encoding the gene of interest were used. 1 l of BL-21 culture was incubated at 37°C with gentle shaking until an OD_{600} of 0.5 was reached. The culture was then cooled in an ice bath for 10 min before protein expression was induced by the addition of 1 mM IPTG. Protein expression was continued for 24 h at 16 °C with gentle shaking before the cells were harvested by centrifugation at 5,000 rpm for 10 min. The resulting cell pellet was frozen in liquid nitrogen and stored at -20°C until use.

The pellet was resuspended in lysis buffer (see 4.1 Materials) and lysed by sonication (Sono plus, Bandelin) through at least 3 cycles for 45 sec. The sample was centrifuged at 20,000 rpm for 20 min to remove cell debris and unlysed cells. The supernatant was then extracted and clarified by filtration through a 0.4 µm syringe filter. An affinity chromatography column was then attached to the ÄKTA PURE 25 system (Cytiva, USA) and a 150 ml Superloop (Cytiva, USA) was added. The sample was injected into the Superloop using an external peristaltic pump and the run was started. The programme started with washing the column with 5 column volumes (CV) of water (5 ml/min), followed by equilibration with 5 CV of buffer A (see 4.1 Materials). To ensure binding of the protein of interest to the NiNTA column (HisTrapHP 5 ml, GE Healthcare), the sample was applied at a slower rate (1 ml/min). At the end of this step, unspecific proteins are removed by washing at 10 CV with 5 ml/min lysis buffer supplemented with 10% buffer B (see 4.1 Materials). Proteins were eluted with 3 CV of a linear gradient from lysis buffer with 10%buffer B to 100% buffer B (3 ml/min). This step was followed by 3 CV of 100% Buffer B to ensure removal of the proteins. Proteins were following stored at – 70 °C. The column was then washed with 5 CV of water (5 ml/min) and 5 CV of 20% ethanol (5 ml/min). For the following SEC, Superdex200 PG column (GE Healthcare) was used. SEC run began with injection of the proteins onto the column, followed by isocratic elution for 1 CV (GeFi buffer (see 4.1 Materials)). Following use, the column was washed with 1.5 CV of water at maximum flow rate and 2 CV of 20% ethanol. Proteins were stored at – 70 °C.

Data processing and statistics were carried out using Microsoft Excel and GraphPad PRISM. Diagrams were created with GraphPad PRISM. Affinity Designer was used to compile figures, while schematic diagrams were created using Biorender (biorender.com).

5. Appendix

Supplementary Table 1: Protein analysis of the predicted Dolos ORFs using AlphaFold [131] (Benchling version (2023.4.MB.1)), Foldseek (web search version) [132], Protein BLAST (standard web version) [112] and InterPro (version: 96.0) [118]. The primary UniProt [140] access number of the Foldseek hits is shown in brackets. aa: amino acids, TM: transmembrane domain, S: signalling domain.

Phage Dolos						
						
ORF No.	**Protein structure (AlphaFold *)**	**aa**	**Foldseek analysis**	**Protein BLAST**	**InterPro**	**Assignment**
1	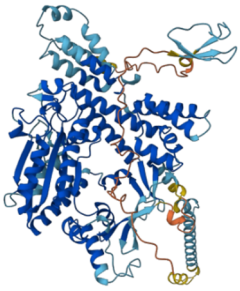	714		Replication protein	-	pII
2	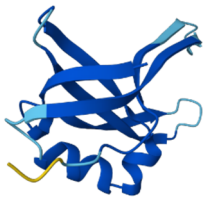	104		-	-	pV
3	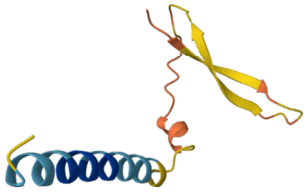	76		-	TM	pVII / pIX
4	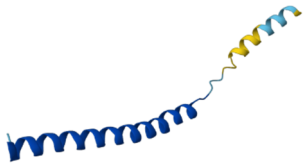	67		Coat protein B	TM	pVIII
5	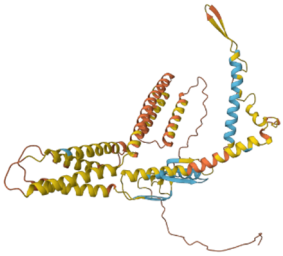	468		Attachment protein	TM, S	pIII

ORF No.	Protein structure (AlphaFold *)	aa	Foldseek analysis	Protein BLAST	InterPro	Assignment
6	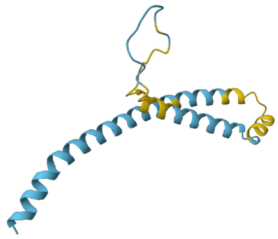	115		gp6	TM, S	pVI
7	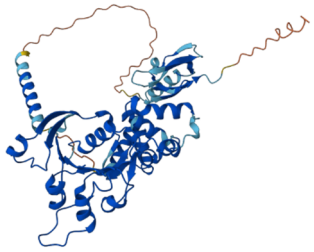	442		Zot protein	Zot domain	pI
8	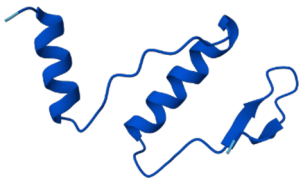	61	Protein of unknown function	Hypothetical protein	-	-
9	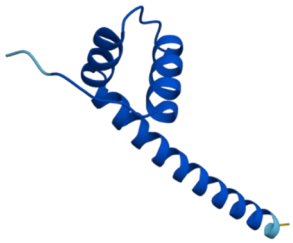	73	Potential antitoxin (MazE family) [P0CL61]	NikA	-	-
10	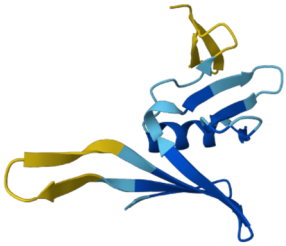	109	Protein of unknown function	-	coil domain	-
11	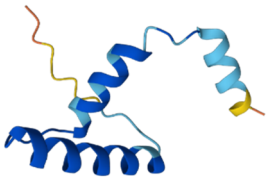	67	Protein of unknown function	Hypothetical protein	-	-

*** model confidence:** dark blue: very high (pLDDT > 90), blue: confident (< 90 pLDDT > 70), yellow: low (< 70 pLDDT > 50), orange: very low (pLDDT < 50)

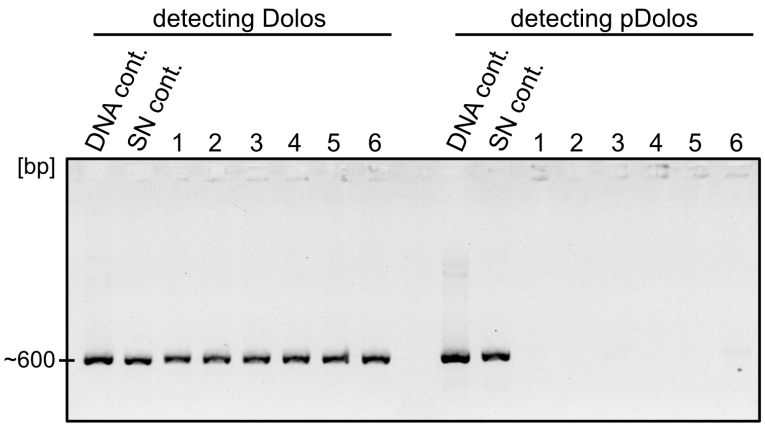

Supplementary Figure 1: The isolation of individual plaques from a supernatant containing mixed virions leads exclusively to the separation of the phage Dolos, not the satellite plasmid pDolos. A gel electrophoresis of PCRs of individual plaques from a supernatant containing mixed virions (Dolos and pDolos virions) is shown. SN cont: mixed virion-containing supernatant, DNA cont: Isolated virion DNA of a mixed-virion containing supernatant. Numbers 1 to 6: 6 different single plaques.

Supplementary Table 2: Host range of phage Dolos. Listed are strains that have been tested for phage infection. The strains that can be infected by phage Dolos are listed on the right. The host range was determined by a spot assay. *V. cholerae* El Tor N16961 was kindly tested by Susanne Brenziger (Brochado group, Universität Würzburg).

Not infected by Dolos	Infected by Dolos
S. oneidensis Isolate S17	*S. oneidensis* MR-1
S. oneidensis Isolate S52	*S. oneidensis* MR-1 ΔλSo ΔMuSoII
S. oneidensis Isolate S54	*S. baltica* Isolate S4
S. oneidensis Isolate S62	*S. baltica* Isolate S44
S. oneidensis Isolate S63	
S. oneidensis Isolate S66	
S. oneidensis Isolate S69	
S. oneidensis Isolate S74	
S. baltica OS195	
S. baltica Isolate S7	
S. baltica Isolate S37	
S. baltica Isolate S38	
S. baltica Isolate S50	
S. amazonensis SB2B	
S. seohaensis Isolate S8	
S. seohaensis Isolate S10	
S. seohaensis Isolate S11	
S. seohaensis Isolate S31	
S. seohaensis Isolate S32	
S. putrefaciens CN-32	
S. putrefaciens CN-32 ΔCas1_2	
S. putrefaciens W3-18-1	
S. sp. ANA-3	
S. sp. MR-4	
S. sp. MR-7	
E. coli MG1655	
P. putida KT2440	
V. cholerae El Tor N16961	

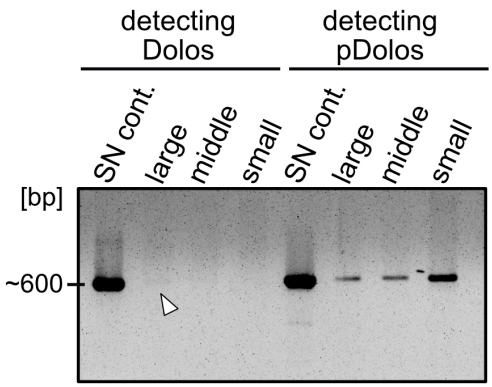

Supplementary Figure 2: The middle and small particle fractions shown in Figure 20 contain exclusive pDolos. Separated virion fractions from a supernatant containing mixed virions were tested for their packaged genomes by PCR. Shown is a gel electrophoresis of these PCRs. The white arrow indicates a weak DNA band. SN cont: mixed virion-containing supernatant.

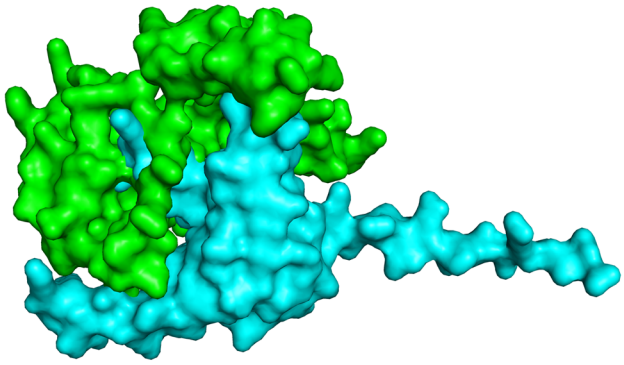

Supplementary Figure 3: Protein complex modelling of pDolos protein 4 and 5 by AlphaFold. Green: protein 4, blue: protein 5. pLDDT score (protein structure confidence score (scale: 0 to 100)): 64.2, pTM score (a model confidence score (scale: 0 to 1)): 0.45.

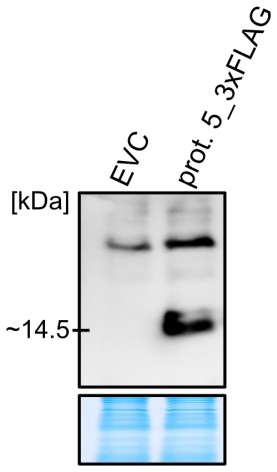

Supplementary Figure 4: Expression control of pDolos protein 5. Mid-exponential *S. oneidensis* ΔLambdaSo ΔMuSo2 cells containing pBAD expression vector systems were induced with 0.2 % L-Ara. 1 h after induction cells were sampled for Western Blot analysis. Upper panel: Western Blot using the anti-FLAG antibody, lower panel: Coomassie stain of total proteins. prot: protein

Supplementary Table 3: Thanatos phage particle proteomics. Listed are all 72 phage protein hits of an LC-MS proteomics analysis of sucrose gradient purified Thanatos phage particles. TH1_028 (Alt1) and TH1_029 (Alt2) are highlighted in bold. LFQ: label free quantification.

Number	Protein ID	Protein name	LFQ
1	TH1_010	Major capsid protein	1561
2	**TH1_029 (Alt2)**	RNA polymerase-ADP-ribosyltransferase	413
3	TH1_003	Tail sheath protein	318
4	TH1_011	Capsid vertex protein	258
5	TH1_058	Lipoprotein	167
6	TH1_204	Straight tail fiber protein	128
7	TH1_032	Tail fiber protein	121
8	TH1_005	Portal protein	107
9	**TH1_028 (Alt1)**	RNA polymerase-ADP-ribosyltransferase	103
10	TH1_205	Neck whiskers protein	95
11	TH1_004	Tail tube protein	90
12	TH1_170	Tail fibers protein	74
13	TH1_198	Baseplate wedge initiator	57
14	TH1_202	Baseplate wedge protein gp10	54
15	TH1_201	Baseplate wedge tail fiber connector	49
16	TH1_044	Transthyretin-like family protein	49
17	TH1_025	Tail tape measure protein	48
18	TH1_196	Baseplate wedge protein gp6	42
19	TH1_199	Baseplate wedge subunit	42
20	TH1_171	Tail connector protein	34
21	TH1_124	VWFA domain-containing protein	33
22	TH1_203	Baseplate wedge subunit	25
23	TH1_013	Head decoration protein	23
24	TH1_008	Prohead assembly (Scaffolding) protein	21
25	TH1_183	YugN-like family protein	21
26	TH1_057	Phage protein	20
27	TH1_026	Baseplate tail tube cap	19
28	TH1_206	Head completion, neck hetero-dimeric protein	19
29	TH1_186	Phage protein	19
30	TH1_027	Baseplate tail tube initiator	18
31	TH1_023	Baseplate hub subunit	16
32	TH1_059	Superinfection immunity protein	14
33	TH1_031	Tail connector protein	14
34	TH1_193	Lysozyme	12
35	TH1_189	Tail completion protein	11
36	TH1_046	Nucleoid disruption protein	10
37	TH1_037	Single-stranded DNA-binding protein	10
38	TH1_208	Tail completion protein	9
39	TH1_043	Valyl-tRNA synthetase modifier	9
40	TH1_075	dCTP pyrophosphatase	9
41	TH1_169	Holin	8
42	TH1_185	LytR_cpsA_psr domain-containing protein	7
43	TH1_207	Head completion, neck hetero-dimeric protein	7

Number	Protein ID	Protein name	LFQ
44	TH1_190	DNA end protector protein	6
45	TH1_051	Sliding clamp	6
46	TH1_103	Thymidylate synthase	6
47	TH1_192	Baseplate wedge subunit	6
48	TH1_146	Transposase	6
49	TH1_067	Recombination protein	5
50	TH1_009	Prohead assembly (Scaffolding) protein	5
51	TH1_085	Toxic anion resistance protein	5
52	TH1_145	TIR domain-containing protein	5
53	TH1_056	DNA-directed DNA polymerase	4
54	TH1_062	Deoxycytidylate 5-hydroxymethyltransferase	4
55	TH1_020	Baseplate wedge subunit / tail lysozyme	4
56	TH1_091	Anti-sigma facto	4
57	TH1_106	Ribonucleoside-diphosphate reductase	4
58	TH1_151	DUF4304 domain-containing protein	3
59	TH1_039	Lysozyme	3
60	TH1_065	Peptidase	3
61	TH1_105	Uncharacterised protein	3
62	TH1_187	Histone-like nucleoid-structuring protein	3
63	TH1_015	RNase_PH_C domain-containing protein	3
64	TH1_050	Uncharacterised protein	3
65	TH1_104	Ribonucleoside-diphosphate reductase	2
66	TH1_042	SLT domain-containing protein	2
67	TH1_162	HEPN domain-containing protein	2
68	TH1_143	AbiTii domain-containing protein	2
69	TH1_049	Recombination-related endonuclease	2
70	TH1_197	UDP-3-O-[3-hydroxymyristoyl] glucosamine N-acyltransferase	2
71	TH1_070	Recombination protein	2
72	TH1_097	Ovule protein	2

Alt1_His

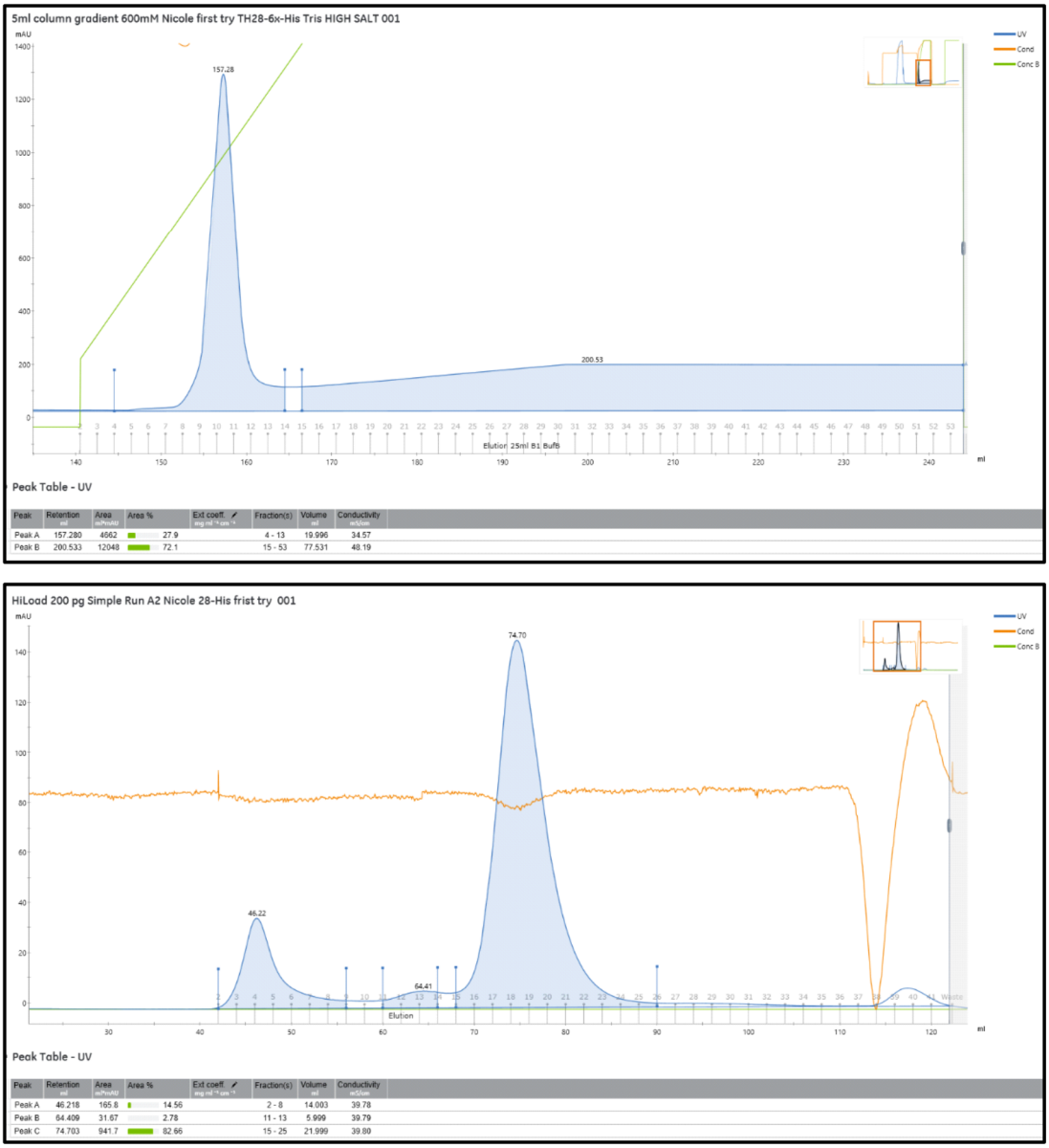

Supplementary Figure 5: Shown are the recordings of the affinity chromatography and the size exclusion chromatography of the Alt1_His purification. Äkta pure system (Cytiva, USA) was used.

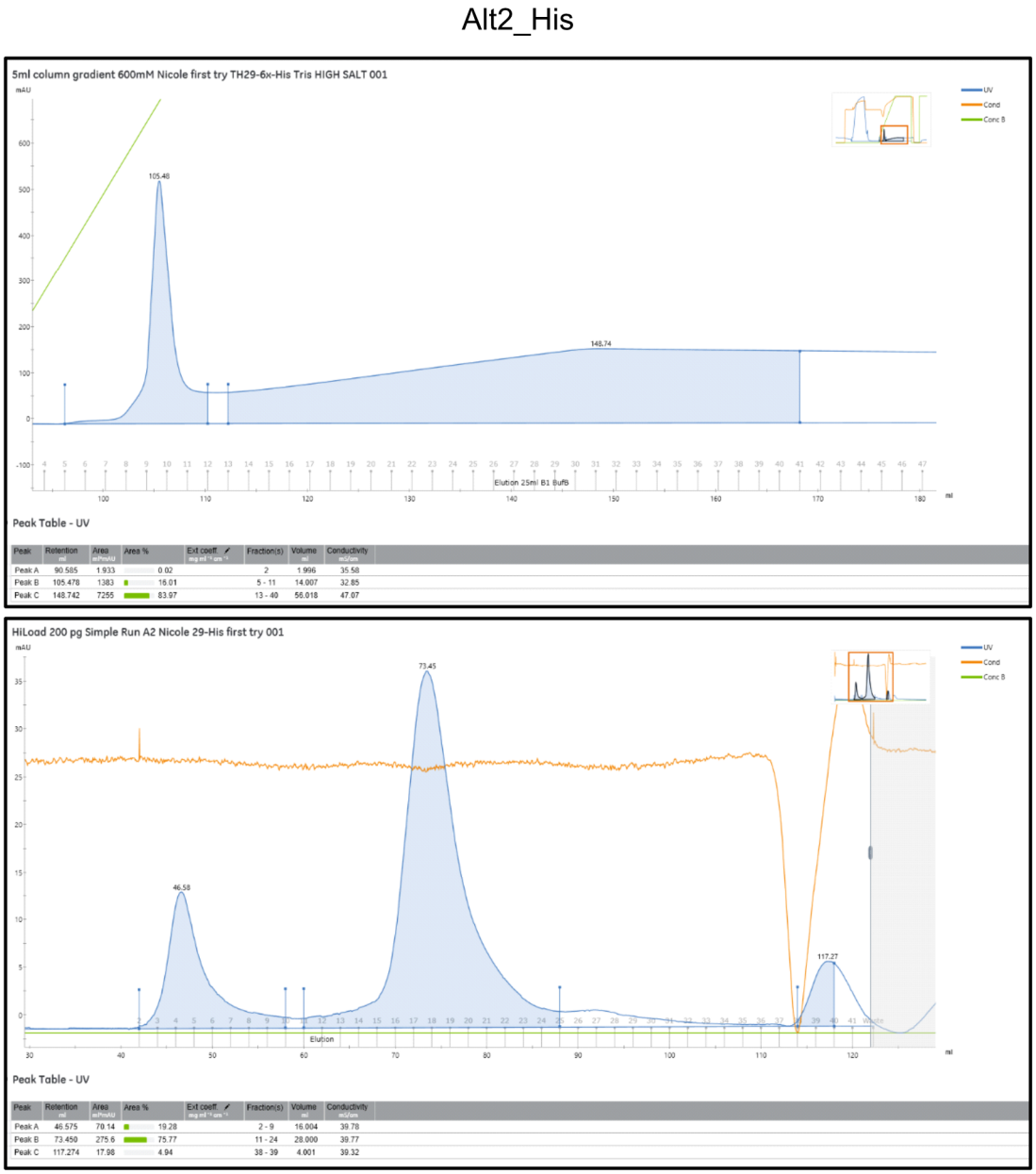

Supplementary Figure 6: Shown are the recordings of the affinity chromatography and the size exclusion chromatography of the Alt2_His purification. Äkta pure system (Cytiva, USA) was used.

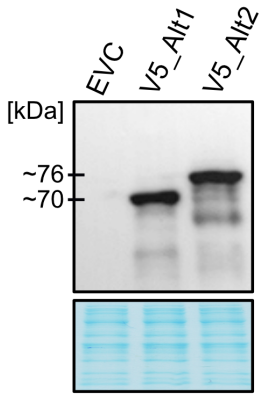

Supplementary Figure 7: Alt1 and Alt2 protein detection after cells were disrupted by a French pressure cell. Mid-exponential *S. oneidensis* ΔLambdaSo ΔMuSo2 cells containing pBAD expression vector systems were induced with 0.2 % L-Ara. 2 h after induction cells were diluted in lysis buffer and disrupted by a French pressure cell. The collected supernatant was used for Western Blot analysis. Upper panel: Western Blot using the anti-V5 antibody, lower panel: Coomassie stain of total proteins.

6. Abbreviations

A	alanine
aa	amino acids
AB	antibody
AP	alkaline phosphatase
Amp	Ampicillin
Ara	arabinose
ARTs	ADP-ribosyltransferases
a.u.	arbitrary units
BACTH	bacterial adenylate cyclase two-hybrid system
C	cysteine
cfu	colony forming units
Cm	Chloramphenicol
Ct	Cycle threshold
DAP	2,6-diaminopimelinic acid
ddH_2O	double distilled water
DMSO	dimethyl sulfoxide
DNA	desoxyribonucleic acid
E	glutamic acid
E. coli	*Escherichia coli*
EDTA	ethylenediaminetetraacetate
et al.	lat.: *et alii* (and others)
EM	electron microscopy
EPS	extracellular polymeric substances
EtBr	ethidium bromide

FWD	forward
HAFs	host acquisition factors
HRP	horseradish peroxidase
IF	infectious form
IM	inner membrane
IPTG	isopropyl-β-D-1-thiogalactopyranoside
K	lysine
Kan	Kanamycin
KI	knock in
KO	knock out
L	leucine
LB	lysogeny broth
LC	liquid chromatography
LPS	lipopolysaccharides
MCS	multiple cloning site
MGE	mobile genetic element
ml	millilitre
MOI	multiplicity of infection
MPI	Max-Planck-Institute
MS	mass spectrometry
NEB	New England Biolabs
OD	optical density
OM	outer membrane
ori	origin of replication
ORF	open reading frame
PAA	polyacrylamide

PCR	polymerase chain reaction
P. putida	*Pseudomonas putida*
PFU	plaque forming units
Primer	starter oligonucleotide
r	resistant
REV	reverse
RF	replicative form
RT	room temperature
S	serine
S.	*Shewanella*
Suc	sucrose
SDS	sodium dodecyl sulphate
SP	sequencing primer
Taq	*Thermus aquaticus*
TEM	Transmission electron microscopy
TEMED	tetramethyl ethylenediamine
TMD	transmembrane domain
V.	*Vibrio*
v/v	volume per volume
w/v	weight per volume
wt	wild type
X-Gal	5-bromo-4-chloro-3-indolyl-β-D-galactopyranoside
ΔΔ	ΔLambdaSo ΔMuSo2

7. Acknowledgments

As is so often the case, this work has only been possible thanks to the help of many people. Unfortunately, I cannot thank every single cooperation partner in detail, but without the active and/or informal support of Katharina Höfer, Nadiia Pozhydaieva, Clara Rolland, Mathias Müsken, Johannes Wittmann, David Brandt, Jörn Kalinowski, Anke Treuner-Lange, Jacqueline Böhme, Callypso Pellegri, Laetitia Houot, Lienhard Schmitz, Aleksandra Bogucka and Susanne Brenzinger this work would not have been realised to this extent.

I would like to express my gratitude to my supervisor Prof. Dr. Kai Thormann for his excellent supervision and support over the last four years. He always had confidence in me and given me plenty of room to develop myself and my scientific work. My academic career has been continuously promoted by him. I would like to thank him in particular for the warm and free working atmosphere in which I always felt very welcome.

I would like to thank the entire Institute of Microbiology and Molecular Biology. Thanks for the great atmosphere and cooperation.

I am very grateful to my thesis committee members PD Dr. Bork Berghoff, PD Dr. Oliver Roßbach and especially Prof. Dr. Julia Frunzke, who agreed without hesitation to be my second examiner.

I would also like to thank the former and current members of the Thorman lab for their excellent team spirit and help. So, thanks to Alina, Dorian, Svenja, Bubi, Alfi, Fred, Tim, John, Meike, Daniel, Lisa, Ulrike, Anja and Vanessa.

I would especially like to thank Ulrike, the best technical assistant on planet Earth for her support and her endlessly big heart. In addition, I want to thank my PhD sister, Vanessa, with whom I started my PhD together. I thank her for the support, the cooperation and the friendship I have gained.

I would also like to thank my whole family for their support, especially John, Kleo and Atalja for their emotional support and proofreading of this thesis.

8. References

[1] Frost LS, Leplae R, Summers AO, Toussaint A. Mobile genetic elements: the agents of open source evolution. Nat Rev Microbiol 2005; 3(9): 722–32
[https://doi.org/10.1038/nrmicro1235][PMID: 16138100]

[2] Haudiquet M, Sousa JM de, Touchon M, Rocha EPC. Selfish, promiscuous and sometimes useful: how mobile genetic elements drive horizontal gene transfer in microbial populations. Philos Trans R Soc Lond B Biol Sci 2022; 377(1861): 20210234
[https://doi.org/10.1098/rstb.2021.0234][PMID: 35989606]

[3] van Elsas JD, Bailey MJ. The ecology of transfer of mobile genetic elements. FEMS Microbiol Ecol 2002; 42(2): 187–97
[https://doi.org/10.1111/j.1574-6941.2002.tb01008.x][PMID: 19709278]

[4] Hall RJ, Whelan FJ, McInerney JO, Ou Y, Domingo-Sananes MR. Horizontal Gene Transfer as a Source of Conflict and Cooperation in Prokaryotes. Front Microbiol 2020; 11: 1569
[https://doi.org/10.3389/fmicb.2020.01569][PMID: 32849327]

[5] LEDERBERG J, TATUM EL. Gene recombination in Escherichia coli. Nature 1946; 158(4016): 558
[https://doi.org/10.1038/158558a0][PMID: 21001945]

[6] Zinder ND, LEDERBERG J. Genetic exchange in Salmonella. J Bacteriol 1952; 64(5): 679–99
[https://doi.org/10.1128/jb.64.5.679-699.1952][PMID: 12999698]

[7] Griffith F. The Significance of Pneumococcal Types. J Hyg (Lond) 1928; 27(2): 113–59
[https://doi.org/10.1017/s0022172400031879][PMID: 20474956]

[8] Wang H, Peng N, Shah SA, Huang L, She Q. Archaeal extrachromosomal genetic elements. Microbiol Mol Biol Rev 2015; 79(1): 117–52
[https://doi.org/10.1128/MMBR.00042-14][PMID: 25694123]

[9] Roux S, Krupovic M, Daly RA*, et al.* Cryptic inoviruses revealed as pervasive in bacteria and archaea across Earth's biomes. Nat Microbiol 2019; 4(11): 1895–906
[https://doi.org/10.1038/s41564-019-0510-x][PMID: 31332386]

[10] Arnold HP, She Q, Phan H*, et al.* The genetic element pSSVx of the extremely thermophilic crenarchaeon Sulfolobus is a hybrid between a plasmid and a virus. Mol Microbiol 1999; 34(2): 217–26
[https://doi.org/10.1046/j.1365-2958.1999.01573.x][PMID: 10564466]

[11] Koning APJ de, Gu W, Castoe TA, Batzer MA, Pollock DD. Repetitive elements may comprise over two-thirds of the human genome. PLoS Genet 2011; 7(12): e1002384
[https://doi.org/10.1371/journal.pgen.1002384][PMID: 22144907]

[12] Fogarty EC, Schechter MS, Lolans K*, et al.* A highly conserved and globally prevalent cryptic plasmid is among the most numerous mobile genetic elements in the human gut. bioRxiv 2023
[https://doi.org/10.1101/2023.03.25.534219][PMID: 36993556]

[13] Hall JPJ, Harrison E, Baltrus DA. Introduction: the secret lives of microbial mobile genetic elements. Philos Trans R Soc Lond B Biol Sci 2022; 377(1842): 20200460
[https://doi.org/10.1098/rstb.2020.0460][PMID: 34839706]

[14] Koonin EV. Viruses and mobile elements as drivers of evolutionary transitions. Philos Trans R Soc Lond B Biol Sci 2016; 371(1701)
[https://doi.org/10.1098/rstb.2015.0442][PMID: 27431520]

[15] Mu X, Ahmad S, Hur S. Endogenous Retroelements and the Host Innate Immune Sensors. Adv Immunol 2016; 132: 47–69
[https://doi.org/10.1016/bs.ai.2016.07.001][PMID: 27769507]

[16] Gautreau G, Bazin A, Gachet M*, et al.* Correction: PPanGGOLiN: Depicting microbial diversity via a partitioned pangenome graph. PLoS Comput Biol 2021; 17(12): e1009687
[https://doi.org/10.1371/journal.pcbi.1009687][PMID: 34890406]

[17] Koonin EV, Dolja VV, Krupovic M. Origins and evolution of viruses of eukaryotes: The ultimate modularity. Virology 2015; 479-480: 2–25
[https://doi.org/10.1016/j.virol.2015.02.039][PMID: 25771806]

[18] Griffiths AJ. Natural plasmids of filamentous fungi. Microbiol Rev 1995; 59(4): 673–85
[https://doi.org/10.1128/mr.59.4.673-685.1995][PMID: 8531891]

[19] Del Solar G, Giraldo R, Ruiz-Echevarría MJ, Espinosa M, Díaz-Orejas R. Replication and control of circular bacterial plasmids. Microbiol Mol Biol Rev 1998; 62(2): 434–64
[https://doi.org/10.1128/MMBR.62.2.434-464.1998][PMID: 9618448]

[20] Zillig W, Kletzin A, Schleper C*, et al.* Screening for Sulfolobales, their Plasmids and their Viruses in Icelandic Solfataras. Systematic and Applied Microbiology 1993; 16(4): 609–28
[https://doi.org/10.1016/S0723-2020(11)80333-4]

[21] Keen EC. A century of phage research: bacteriophages and the shaping of modern biology. Bioessays 2015; 37(1): 6–9
[https://doi.org/10.1002/bies.201400152][PMID: 25521633]

[22] Comeau AM, Hatfull GF, Krisch HM, Lindell D, Mann NH, Prangishvili D. Exploring the prokaryotic virosphere. Res Microbiol 2008; 159(5): 306–13
[https://doi.org/10.1016/j.resmic.2008.05.001]

[23] Khedkar S, Smyshlyaev G, Letunic I*, et al.* Landscape of mobile genetic elements and their antibiotic resistance cargo in prokaryotic genomes. Nucleic Acids Res 2022; 50(6): 3155–68
[https://doi.org/10.1093/nar/gkac163][PMID: 35323968]

[24] Morales G, Abelson B, Reasoner S*, et al.* The Role of Mobile Genetic Elements in Virulence Factor Carriage from Symptomatic and Asymptomatic Cases of Escherichia coli Bacteriuria. Microbiol Spectr 2023; 11(3): e0471022
[https://doi.org/10.1128/spectrum.04710-22][PMID: 37195213]

[25] Salmond GPC, Fineran PC. A century of the phage: past, present and future. Nat Rev Microbiol 2015; 13(12): 777–86
[https://doi.org/10.1038/nrmicro3564][PMID: 26548913]

[26] Wein T, Dagan T. Plasmid evolution. Curr Biol 2020; 30(19): R1158-R1163
[https://doi.org/10.1016/j.cub.2020.07.003][PMID: 33022260]

[27] Carroll AC, Wong A. Plasmid persistence: costs, benefits, and the plasmid paradox. Can J Microbiol 2018; 64(5): 293–304
[https://doi.org/10.1139/cjm-2017-0609][PMID: 29562144]

[28] Smillie C, Garcillán-Barcia MP, Francia MV, Rocha EPC, La Cruz F de. Mobility of plasmids. Microbiol Mol Biol Rev 2010; 74(3): 434–52
[https://doi.org/10.1128/MMBR.00020-10][PMID: 20805406]

[29] Norman A, Hansen LH, Sørensen SJ. Conjugative plasmids: vessels of the communal gene pool. Philos Trans R Soc Lond B Biol Sci 2009; 364(1527): 2275–89 [https://doi.org/10.1098/rstb.2009.0037][PMID: 19571247]

[30] Chandler M, La Cruz F de, Dyda F, Hickman AB, Moncalian G, Ton-Hoang B. Breaking and joining single-stranded DNA: the HUH endonuclease superfamily. Nat Rev Microbiol 2013; 11(8): 525–38 [https://doi.org/10.1038/nrmicro3067][PMID: 23832240]

[31] Garcillán-Barcia MP, Francia MV, La Cruz F de. The diversity of conjugative relaxases and its application in plasmid classification. FEMS Microbiol Rev 2009; 33(3): 657–87 [https://doi.org/10.1111/j.1574-6976.2009.00168.x][PMID: 19396961]

[32] Frank AC, Alsmark CM, Thollesson M, Andersson SGE. Functional divergence and horizontal transfer of type IV secretion systems. Mol Biol Evol 2005; 22(5): 1325–36 [https://doi.org/10.1093/molbev/msi124][PMID: 15746011]

[33] Silverman PM, Clarke MB. New insights into F-pilus structure, dynamics, and function. Integr Biol (Camb) 2010; 2(1): 25–31 [https://doi.org/10.1039/b917761b][PMID: 20473409]

[34] Oakley AJ. A structural view of bacterial DNA replication. Protein Sci 2019; 28(6): 990–1004 [https://doi.org/10.1002/pro.3615][PMID: 30945375]

[35] Lilly J, Camps M. Mechanisms of Theta Plasmid Replication. Microbiol Spectr 2015; 3(1) [PMID: 26005599]

[36] Kim JW, Bugata V, Cortés-Cortés G, Quevedo-Martínez G, Camps M. Mechanisms of Theta Plasmid Replication in Enterobacteria and Implications for Adaptation to Its Host. EcoSal Plus 2020; 9(1) [https://doi.org/10.1128/ecosalplus.ESP-0026-2019][PMID: 33210586]

[37] Loftie-Eaton W, Rawlings DE. Diversity, biology and evolution of IncQ-family plasmids. Plasmid 2012; 67(1): 15–34 [https://doi.org/10.1016/j.plasmid.2011.10.001][PMID: 22037393]

[38] Ruiz-Masó JA, MachóN C, Bordanaba-Ruiseco L, Espinosa M, Coll M, Del Solar G. Plasmid Rolling-Circle Replication. Microbiol Spectr 2015; 3(1): PLAS-0035-2014 [https://doi.org/10.1128/microbiolspec.PLAS-0035-2014][PMID: 26104557]

[39] Wawrzyniak P, Płucienniczak G, Bartosik D. The Different Faces of Rolling-Circle Replication and Its Multifunctional Initiator Proteins. Front Microbiol 2017; 8: 2353 [https://doi.org/10.3389/fmicb.2017.02353][PMID: 29250047]

[40] Novick RP. Staphylococcal plasmids and their replication. Annu Rev Microbiol 1989; 43: 537–65 [https://doi.org/10.1146/annurev.mi.43.100189.002541][PMID: 2679362]

[41] Garcillán-Barcia MP, Pluta R, Lorenzo-Díaz F, Bravo A, Espinosa M. The Facts and Family Secrets of Plasmids That Replicate via the Rolling-Circle Mechanism. Microbiol Mol Biol Rev 2022; 86(1): e0022220 [https://doi.org/10.1128/MMBR.00222-20][PMID: 34878299]

[42] Stern A, Sorek R. The phage-host arms race: shaping the evolution of microbes. Bioessays 2011; 33(1): 43–51 [https://doi.org/10.1002/bies.201000071][PMID: 20979102]

[43] Koskella B, Brockhurst MA. Bacteria-phage coevolution as a driver of ecological and evolutionary processes in microbial communities. FEMS Microbiol Rev 2014; 38(5): 916–31 [https://doi.org/10.1111/1574-6976.12072][PMID: 24617569]

[44] Yirmiya E, Leavitt A, Lu A*, et al.* Phages overcome bacterial immunity via diverse anti-defence proteins. Nature 2024; 625(7994): 352–9
[https://doi.org/10.1038/s41586-023-06869-w][PMID: 37992756]

[45] Hay ID, Lithgow T. Filamentous phages: masters of a microbial sharing economy. EMBO Rep 2019; 20(6)
[https://doi.org/10.15252/embr.201847427][PMID: 30952693]

[46] Luque A, Benler S, Lee DY, Brown C, White S. The Missing Tailed Phages: Prediction of Small Capsid Candidates. Microorganisms 2020; 8(12)
[https://doi.org/10.3390/microorganisms8121944][PMID: 33302408]

[47] Hatfull GF, Hendrix RW. Bacteriophages and their genomes. Curr Opin Virol 2011; 1(4): 298–303
[https://doi.org/10.1016/j.coviro.2011.06.009][PMID: 22034588]

[48] Ackermann H-W. 5500 Phages examined in the electron microscope. Arch Virol 2007; 152(2): 227–43
[https://doi.org/10.1007/s00705-006-0849-1][PMID: 17051420]

[49] Ackermann HW. Tailed bacteriophages: the order caudovirales. Adv Virus Res 1998; 51: 135–201
[https://doi.org/10.1016/s0065-3527(08)60785-x][PMID: 9891587]

[50] Turner D, Kropinski AM, Adriaenssens EM. A Roadmap for Genome-Based Phage Taxonomy. Viruses 2021; 13(3)
[https://doi.org/10.3390/v13030506][PMID: 33803862]

[51] Mäntynen S, Laanto E, Oksanen HM, Poranen MM, Díaz-Muñoz SL. Black box of phage-bacterium interactions: exploring alternative phage infection strategies. Open Biol 2021; 11(9): 210188
[https://doi.org/10.1098/rsob.210188][PMID: 34520699]

[52] Romantschuk M, Bamford DH. phi 6-resistant phage-producing mutants of Pseudomonas phaseolicola. J Gen Virol 1981; 56(Pt 2): 287–95
[https://doi.org/10.1099/0022-1317-56-2-287][PMID: 7310377]

[53] Jansson E, Backman A, Hakkarainen K, Miettinen A. Viruses of mycoplasmas and spiroplasmas. Med Biol 1982; 60(3): 125–31
[PMID: 7050553]

[54] Rakonjac J. Filamentous Bacteriophages: Biology and Applications. In: Encyclopedia of life sciences. Chichester: Wiley 2005.

[55] Ueno H, Yonesaki T. Phage-induced change in the stability of mRNAs. Virology 2004; 329(1): 134–41
[https://doi.org/10.1016/j.virol.2004.08.001.][PMID: 15476881]

[56] Wolfram-Schauerte M, Pozhydaieva N, Viering M, Glatter T, Höfer K. Integrated Omics Reveal Time-Resolved Insights into T4 Phage Infection of E. coli on Proteome and Transcriptome Levels. Viruses 2022; 14(11)
[https://doi.org/10.3390/v14112502][PMID: 36423111]

[57] Depping R, Lohaus C, Meyer HE, Rüger W. The mono-ADP-ribosyltransferases Alt and ModB of bacteriophage T4: target proteins identified. Biochem Biophys Res Commun 2005; 335(4): 1217–23
[https://doi.org/10.1016/j.bbrc.2005.08.023][PMID: 16112649]

[58] Guan J, Bondy-Denomy J. Intracellular Organization by Jumbo Bacteriophages. J Bacteriol 2020; 203(2)
[https://doi.org/10.1128/JB.00362-20][PMID: 32868402]

[59] Souther A, Bruner R, Elliott J. Degradation of Escherichia coli chromosome after infection by bacteriophage T4: role of bacteriophage gene D2a. J Virol 1972; 10(5): 979–84
[https://doi.org/10.1128/JVI.10.5.979-984.1972][PMID: 4564588]

[60] Wang X, Kim Y, Ma Q*, et al.* Cryptic prophages help bacteria cope with adverse environments. Nat Commun 2010; 1: 147
[https://doi.org/10.1038/ncomms1146][PMID: 21266997]

[61] Nanda AM, Thormann K, Frunzke J. Impact of spontaneous prophage induction on the fitness of bacterial populations and host-microbe interactions. J Bacteriol 2015; 197(3): 410–9
[https://doi.org/10.1128/JB.02230-14][PMID: 25404701]

[62] Pant A, Das B, Bhadra RK. CTX phage of Vibrio cholerae: Genomics and applications. Vaccine 2020; 38 Suppl 1: A7-A12
[https://doi.org/10.1016/j.vaccine.2019.06.034][PMID: 31272871]

[63] Gödeke J, Paul K, Lassak J, Thormann KM. Phage-induced lysis enhances biofilm formation in Shewanella oneidensis MR-1. ISME J 2011; 5(4): 613–26
[https://doi.org/10.1038/ismej.2010.153][PMID: 20962878]

[64] Rice SA, Tan CH, Mikkelsen PJ*, et al.* The biofilm life cycle and virulence of Pseudomonas aeruginosa are dependent on a filamentous prophage. ISME J 2009; 3(3): 271–82
[https://doi.org/10.1038/ismej.2008.109][PMID: 19005496]

[65] Webb JS, Thompson LS, James S*, et al.* Cell death in Pseudomonas aeruginosa biofilm development. J Bacteriol 2003; 185(15): 4585–92
[https://doi.org/10.1128/JB.185.15.4585-4592.2003][PMID: 12867469]

[66] Secchi E, Savorana G, Vitale A, Eberl L, Stocker R, Rusconi R. The structural role of bacterial eDNA in the formation of biofilm streamers. Proc Natl Acad Sci U S A 2022; 119(12): e2113723119
[https://doi.org/10.1073/pnas.2113723119][PMID: 35290120]

[67] Carrolo M, Frias MJ, Pinto FR, Melo-Cristino J, Ramirez M. Prophage spontaneous activation promotes DNA release enhancing biofilm formation in Streptococcus pneumoniae. PLoS One 2010; 5(12): e15678
[https://doi.org/10.1371/journal.pone.0015678][PMID: 21187931]

[68] Shen M, Yang Y, Shen W*, et al.* A Linear Plasmid-Like Prophage of Actinomyces odontolyticus Promotes Biofilm Assembly. Appl Environ Microbiol 2018; 84(17)
[https://doi.org/10.1128/AEM.01263-18][PMID: 29915115]

[69] Mai-Prochnow A, Hui JGK, Kjelleberg S, Rakonjac J, McDougald D, Rice SA. 'Big things in small packages: the genetics of filamentous phage and effects on fitness of their host'. FEMS Microbiol Rev 2015; 39(4): 465–87
[https://doi.org/10.1093/femsre/fuu007][PMID: 25670735]

[70] Knezevic P, Adriaenssens EM, Ictv RC. ICTV Virus Taxonomy Profile: Inoviridae. J Gen Virol 2021; 102(7)
[https://doi.org/10.1099/jgv.0.001614][PMID: 34227934]

[71] Rajagopala SV, Casjens S, Uetz P. The protein interaction map of bacteriophage lambda. BMC Microbiol 2011; 11: 213
[https://doi.org/10.1186/1471-2180-11-213][PMID: 21943085]

[72] Kreienbaum M, Dörrich AK, Brandt D*, et al.* Isolation and Characterization of Shewanella Phage Thanatos Infecting and Lysing Shewanella oneidensis and Promoting Nascent Biofilm Formation. Front Microbiol 2020; 11: 573260
[https://doi.org/10.3389/fmicb.2020.573260][PMID: 33072035]

[73] Rasched I, Oberer E. Ff coliphages: structural and functional relationships. Microbiol Rev 1986; 50(4): 401–27
[https://doi.org/10.1128/mr.50.4.401-427.1986][PMID: 3540571]

[74] LOEB T. Isolation of a bacteriophage specific for the F plus and Hfr mating types of Escherichia coli K-12. Science 1960; 131(3404): 932–3
[https://doi.org/10.1126/science.131.3404.932][PMID: 14417842]

[75] Hofschneider PH. Untersuchungen über „kleine" E. coli K 12 Bakteriophagen. Zeitschrift für Naturforschung B 1963; 18(3): 203–10
[https://doi.org/10.1515/znb-1963-0306]

[76] MARVIN DA, HOFFMANN-BERLING H. Physical and Chemical Properties of Two New Small Bacteriophages. Nature 1963; 197(4866): 517–8
[https://doi.org/10.1038/197517b0]

[77] Rakonjac J, Russel M, Khanum S, Brooke SJ, Rajič M. Filamentous Phage: Structure and Biology. Adv Exp Med Biol 2017; 1053: 1–20
[https://doi.org/10.1007/978-3-319-72077-7_1][PMID: 29549632]

[78] Sanger F, Coulson AR, Barrell BG, Smith AJ, Roe BA. Cloning in single-stranded bacteriophage as an aid to rapid DNA sequencing. J Mol Biol 1980; 143(2): 161–78
[https://doi.org/10.1016/0022-2836(80)90196-5][PMID: 6260957]

[79] Kunkel TA, Bebenek K, McClary J. Efficient site-directed mutagenesis using uracil-containing DNA. Methods Enzymol 1991; 204: 125–39
[https://doi.org/10.1016/0076-6879(91)04008-c][PMID: 1943776]

[80] Qi H, Lu H, Qiu H-J, Petrenko V, Liu A. Phagemid vectors for phage display: properties, characteristics and construction. J Mol Biol 2012; 417(3): 129–43
[https://doi.org/10.1016/j.jmb.2012.01.038][PMID: 22310045]

[81] Hoogenboom HR. Overview of antibody phage-display technology and its applications. Methods Mol Biol 2002; 178: 1–37
[https://doi.org/10.1385/1-59259-240-6:001][PMID: 11968478]

[82] Saw PE, Song E-W. Phage display screening of therapeutic peptide for cancer targeting and therapy. Protein Cell 2019; 10(11): 787–807
[https://doi.org/10.1007/s13238-019-0639-7][PMID: 31140150]

[83] Ibarra-Chávez R, Hansen MF, Pinilla-Redondo R, Seed KD, Trivedi U. Phage satellites and their emerging applications in biotechnology. FEMS Microbiol Rev 2021; 45(6)
[https://doi.org/10.1093/femsre/fuab031][PMID: 34104956]

[84] Sousa JAM de, Fillol-Salom A, Penadés JR, Rocha EPC. Identification and characterization of thousands of bacteriophage satellites across bacteria. Nucleic Acids Res 2023; 51(6): 2759–77
[https://doi.org/10.1093/nar/gkad123][PMID: 36869669]

[85] Alqurainy N, Miguel-Romero L, Moura de Sousa J*, et al.* A widespread family of phage-inducible chromosomal islands only steals bacteriophage tails to spread in nature. Cell Host Microbe 2023; 31(1): 69-82.e5
[https://doi.org/10.1016/j.chom.2022.12.001][PMID: 36596306]

[86] Barcia-Cruz R, Goudenège D, Moura de Sousa JA*, et al.* Phage-inducible chromosomal minimalist islands (PICMIs), a novel family of small marine satellites of virulent phages. Nat Commun 2024; 15(1): 664
[https://doi.org/10.1038/s41467-024-44965-1][PMID: 38253718]

[87] Moura de Sousa JA, Rocha EPC. To catch a hijacker: abundance, evolution and genetic diversity of P4-like bacteriophage satellites. Philos Trans R Soc Lond B Biol Sci 2022; 377(1842): 20200475 [https://doi.org/10.1098/rstb.2020.0475][PMID: 34839713]

[88] Kizziah JL, Rodenburg CM, Dokland T. Structure of the Capsid Size-Determining Scaffold of "Satellite" Bacteriophage P4. Viruses 2020; 12(9) [https://doi.org/10.3390/v12090953][PMID: 32867300]

[89] Rousset F, Depardieu F, Miele S*, et al.* Phages and their satellites encode hotspots of antiviral systems. Cell Host Microbe 2022; 30(5): 740-753.e5 [https://doi.org/10.1016/j.chom.2022.02.018][PMID: 35316646]

[90] Fillol-Salom A, Rostøl JT, Ojiogu AD*, et al.* Bacteriophages benefit from mobilizing pathogenicity islands encoding immune systems against competitors. Cell 2022; 185(17): 3248-3262.e20 [https://doi.org/10.1016/j.cell.2022.07.014][PMID: 35985290]

[91] Fredrickson JK, Romine MF, Beliaev AS*, et al.* Towards environmental systems biology of Shewanella. Nat Rev Microbiol 2008; 6(8): 592–603 [https://doi.org/10.1038/nrmicro1947][PMID: 18604222]

[92] Hau HH, Gralnick JA. Ecology and biotechnology of the genus Shewanella. Annu Rev Microbiol 2007; 61: 237–58 [https://doi.org/10.1146/annurev.micro.61.080706.093257][PMID: 18035608]

[93] Myers CR, Nealson KH. Bacterial manganese reduction and growth with manganese oxide as the sole electron acceptor. Science 1988; 240(4857): 1319–21 [https://doi.org/10.1126/science.240.4857.1319][PMID: 17815852]

[94] Deutschbauer A, Price MN, Wetmore KM*, et al.* Evidence-based annotation of gene function in Shewanella oneidensis MR-1 using genome-wide fitness profiling across 121 conditions. PLoS Genet 2011; 7(11): e1002385 [https://doi.org/10.1371/journal.pgen.1002385][PMID: 22125499]

[95] Thormann KM, Duttler S, Saville RM*, et al.* Control of formation and cellular detachment from Shewanella oneidensis MR-1 biofilms by cyclic di-GMP. J Bacteriol 2006; 188(7): 2681–91 [https://doi.org/10.1128/JB.188.7.2681-2691.2006][PMID: 16547056]

[96] Thormann KM, Saville RM, Shukla S, Pelletier DA, Spormann AM. Initial Phases of biofilm formation in Shewanella oneidensis MR-1. J Bacteriol 2004; 186(23): 8096–104 [https://doi.org/10.1128/JB.186.23.8096-8104.2004][PMID: 15547283]

[97] Teal TK, Lies DP, Wold BJ, Newman DK. Spatiometabolic stratification of Shewanella oneidensis biofilms. Appl Environ Microbiol 2006; 72(11): 7324–30 [https://doi.org/10.1128/AEM.01163-06][PMID: 16936048]

[98] Sauer K, Stoodley P, Goeres DM*, et al.* The biofilm life cycle: expanding the conceptual model of biofilm formation. Nat Rev Microbiol 2022; 20(10): 608–20 [https://doi.org/10.1038/s41579-022-00767-0][PMID: 35922483]

[99] Flemming H-C, Wuertz S. Bacteria and archaea on Earth and their abundance in biofilms. Nat Rev Microbiol 2019; 17(4): 247–60 [https://doi.org/10.1038/s41579-019-0158-9][PMID: 30760902]

[100] Penesyan A, Paulsen IT, Kjelleberg S, Gillings MR. Three faces of biofilms: a microbial lifestyle, a nascent multicellular organism, and an incubator for diversity. NPJ Biofilms Microbiomes 2021; 7(1): 80 [https://doi.org/10.1038/s41522-021-00251-2][PMID: 34759294]

[101] Yin W, Wang Y, Liu L, He J. Biofilms: The Microbial "Protective Clothing" in Extreme Environments. Int J Mol Sci 2019; 20(14)
[https://doi.org/10.3390/ijms20143423][PMID: 31336824]

[102] Sutherland IW. The biofilm matrix--an immobilized but dynamic microbial environment. Trends Microbiol 2001; 9(5): 222–7
[https://doi.org/10.1016/s0966-842x(01)02012-1][PMID: 11336839]

[103] Craig L, Forest KT, Maier B. Type IV pili: dynamics, biophysics and functional consequences. Nat Rev Microbiol 2019; 17(7): 429–40
[https://doi.org/10.1038/s41579-019-0195-4][PMID: 30988511]

[104] Floyd KA, Lee CK, Xian W*, et al.* c-di-GMP modulates type IV MSHA pilus retraction and surface attachment in Vibrio cholerae. Nat Commun 2020; 11(1): 1549
[https://doi.org/10.1038/s41467-020-15331-8][PMID: 32214098]

[105] Valentini M, Filloux A. Biofilms and Cyclic di-GMP (c-di-GMP) Signaling: Lessons from Pseudomonas aeruginosa and Other Bacteria. J Biol Chem 2016; 291(24): 12547–55
[https://doi.org/10.1074/jbc.R115.711507][PMID: 27129226]

[106] Lucas Binnenkade. Molecular Control of Extracellular DNA Release and Degradation in Shewanella Oneidensis MR-1 Biofilms: The Role of Phages and Nucleases. Philipps-Universität Marburg 2015.

[107] Heidelberg JF, Paulsen IT, Nelson KE*, et al.* Genome sequence of the dissimilatory metal ion-reducing bacterium Shewanella oneidensis. Nat Biotechnol 2002; 20(11): 1118–23
[https://doi.org/10.1038/nbt749][PMID: 12368813]

[108] Zeng Z, Liu X, Yao J*, et al.* Cold adaptation regulated by cryptic prophage excision in Shewanella oneidensis. ISME J 2016; 10(12): 2787–800
[https://doi.org/10.1038/ismej.2016.85][PMID: 27482926]

[109] Selva L, Viana D, Regev-Yochay G*, et al.* Killing niche competitors by remote-control bacteriophage induction. Proc Natl Acad Sci U S A 2009; 106(4): 1234–8
[https://doi.org/10.1073/pnas.0809600106][PMID: 19141630]

[110] Eisenstein M. Oxford Nanopore announcement sets sequencing sector abuzz. Nat Biotechnol 2012; 30(4): 295–6
[https://doi.org/10.1038/nbt0412-295][PMID: 22491260]

[111] Seemann T. Prokka: rapid prokaryotic genome annotation. Bioinformatics 2014; 30(14): 2068–9
[https://doi.org/10.1093/bioinformatics/btu153][PMID: 24642063]

[112] Altschul SF, Madden TL, Schäffer AA*, et al.* Gapped BLAST and PSI-BLAST: a new generation of protein database search programs. Nucleic Acids Res 1997; 25(17): 3389–402
[https://doi.org/10.1093/nar/25.17.3389][PMID: 9254694]

[113] Murugaiyan S, Bae JY, Wu J*, et al.* Characterization of filamentous bacteriophage PE226 infecting Ralstonia solanacearum strains. J Appl Microbiol 2011; 110(1): 296–303
[https://doi.org/10.1111/j.1365-2672.2010.04882.x][PMID: 21054700]

[114] Mauritzen JJ, Castillo D, Tan D, Lo Svenningsen S, Middelboe M. Beyond Cholera: Characterization of zot-Encoding Filamentous Phages in the Marine Fish Pathogen Vibrio anguillarum. Viruses 2020; 12(7)
[https://doi.org/10.3390/v12070730][PMID: 32640584]

[115] Smith RS, Trzaskoma S, editors. The Oxford handbook of Greek and Roman mythography. New York: Oxford University Press; 2022.

[116] Green MR, Sambrook J. Plating Bacteriophage M13. Cold Spring Harb Protoc 2017; 2017(10): pdb.prot093427
[https://doi.org/10.1101/pdb.prot093427][PMID: 28974654]

[117] Inoviridae. In: Virus Taxonomy. Elsevier 2012; 375–83.

[118] Paysan-Lafosse T, Blum M, Chuguransky S*, et al.* InterPro in 2022. Nucleic Acids Res 2023; 51(D1): D418-D427
[https://doi.org/10.1093/nar/gkac993][PMID: 36350672]

[119] Heidelberg JF, Eisen JA, Nelson WC*, et al.* DNA sequence of both chromosomes of the cholera pathogen Vibrio cholerae. Nature 2000; 406(6795): 477–83
[https://doi.org/10.1038/35020000][PMID: 10952301]

[120] Nishimura Y, Yoshida T, Kuronishi M, Uehara H, Ogata H, Goto S. ViPTree: the viral proteomic tree server. Bioinformatics 2017; 33(15): 2379–80
[https://doi.org/10.1093/bioinformatics/btx157][PMID: 28379287]

[121] Jonson G, Holmgren J, Svennerholm AM. Identification of a mannose-binding pilus on Vibrio cholerae El Tor. Microb Pathog 1991; 11(6): 433–41
[https://doi.org/10.1016/0882-4010(91)90039-d][PMID: 1686631]

[122] Marsh JW, Taylor RK. Genetic and transcriptional analyses of the Vibrio cholerae mannose-sensitive hemagglutinin type 4 pilus gene locus. J Bacteriol 1999; 181(4): 1110–7
[https://doi.org/10.1128/JB.181.4.1110-1117.1999][PMID: 9973335]

[123] Jones CJ, Utada A, Davis KR*, et al.* C-di-GMP Regulates Motile to Sessile Transition by Modulating MshA Pili Biogenesis and Near-Surface Motility Behavior in Vibrio cholerae. PLoS Pathog 2015; 11(10): e1005068
[https://doi.org/10.1371/journal.ppat.1005068][PMID: 26505896]

[124] Roelofs KG, Jones CJ, Helman SR*, et al.* Systematic Identification of Cyclic-di-GMP Binding Proteins in Vibrio cholerae Reveals a Novel Class of Cyclic-di-GMP-Binding ATPases Associated with Type II Secretion Systems. PLoS Pathog 2015; 11(10): e1005232
[https://doi.org/10.1371/journal.ppat.1005232][PMID: 26506097]

[125] Ellison CK, Kan J, Dillard RS*, et al.* Obstruction of pilus retraction stimulates bacterial surface sensing. Science 2017; 358(6362): 535–8
[https://doi.org/10.1126/science.aan5706][PMID: 29074778]

[126] Schmittgen TD, Livak KJ. Analyzing real-time PCR data by the comparative C(T) method. Nat Protoc 2008; 3(6): 1101–8
[https://doi.org/10.1038/nprot.2008.73][PMID: 18546601]

[127] Whitchurch CB, Tolker-Nielsen T, Ragas PC, Mattick JS. Extracellular DNA required for bacterial biofilm formation. Science 2002; 295(5559): 1487
[https://doi.org/10.1126/science.295.5559.1487][PMID: 11859186]

[128] Okshevsky M, Meyer RL. The role of extracellular DNA in the establishment, maintenance and perpetuation of bacterial biofilms. Crit Rev Microbiol 2015; 41(3): 341–52
[https://doi.org/10.3109/1040841X.2013.841639][PMID: 24303798]

[129] Hartmann R, Jeckel H, Jelli E*, et al.* Quantitative image analysis of microbial communities with BiofilmQ. Nat Microbiol 2021; 6(2): 151–6
[https://doi.org/10.1038/s41564-020-00817-4][PMID: 33398098]

[130] Schindelin J, Arganda-Carreras I, Frise E*, et al.* Fiji: an open-source platform for biological-image analysis. Nat Methods 2012; 9(7): 676–82
[https://doi.org/10.1038/nmeth.2019][PMID: 22743772]

[131] Jumper J, Evans R, Pritzel A*, et al.* Highly accurate protein structure prediction with AlphaFold. Nature 2021; 596(7873): 583–9
[https://doi.org/10.1038/s41586-021-03819-2][PMID: 34265844]

[132] van Kempen M, Kim SS, Tumescheit C*, et al.* Fast and accurate protein structure search with Foldseek. Nat Biotechnol 2023
[https://doi.org/10.1038/s41587-023-01773-0][PMID: 37156916]

[133] Taboada B, Estrada K, Ciria R, Merino E. Operon-mapper: a web server for precise operon identification in bacterial and archaeal genomes. Bioinformatics 2018; 34(23): 4118–20
[https://doi.org/10.1093/bioinformatics/bty496][PMID: 29931111]

[134] Zhang J, Zhang Y, Inouye M. Characterization of the interactions within the mazEF addiction module of Escherichia coli. J Biol Chem 2003; 278(34): 32300–6
[https://doi.org/10.1074/jbc.M304767200][PMID: 12810711]

[135] Yamaguchi Y, Inouye M. Regulation of growth and death in Escherichia coli by toxin-antitoxin systems. Nat Rev Microbiol 2011; 9(11): 779–90
[https://doi.org/10.1038/nrmicro2651][PMID: 21927020]

[136] Tripathi A, Dewan PC, Siddique SA, Varadarajan R. MazF-induced growth inhibition and persister generation in Escherichia coli. J Biol Chem 2014; 289(7): 4191–205
[https://doi.org/10.1074/jbc.M113.510511][PMID: 24375411]

[137] Park J-H, Yamaguchi Y, Inouye M. Bacillus subtilis MazF-bs (EndoA) is a UACAU-specific mRNA interferase. FEBS Lett 2011; 585(15): 2526–32
[https://doi.org/10.1016/j.febslet.2011.07.008][PMID: 21763692]

[138] Amitai S, Yassin Y, Engelberg-Kulka H. MazF-mediated cell death in Escherichia coli: a point of no return. J Bacteriol 2004; 186(24): 8295–300
[https://doi.org/10.1128/JB.186.24.8295-8300.2004][PMID: 15576778]

[139] Jose D, Weitzel SE, Baase WA, Hippel PH von. Mapping the interactions of the single-stranded DNA binding protein of bacteriophage T4 (gp32) with DNA lattices at single nucleotide resolution: gp32 monomer binding. Nucleic Acids Res 2015; 43(19): 9276–90
[https://doi.org/10.1093/nar/gkv817][PMID: 26275775]

[140] UniProt: the universal protein knowledgebase. Nucleic Acids Res 2017; 45(D1): D158-D169
[https://doi.org/10.1093/nar/gkw1099][PMID: 27899622]

[141] Kelly A, Arrowsmith TJ, Went SC, Blower TR. Toxin-antitoxin systems as mediators of phage defence and the implications for abortive infection. Curr Opin Microbiol 2023; 73: 102293
[https://doi.org/10.1016/j.mib.2023.102293][PMID: 36958122]

[142] Cui Y, Su X, Wang C*, et al.* Bacterial MazF/MazE toxin-antitoxin suppresses lytic propagation of arbitrium-containing phages. Cell Rep 2022; 41(10): 111752
[https://doi.org/10.1016/j.celrep.2022.111752][PMID: 36476854]

[143] Fineran PC, Blower TR, Foulds IJ, Humphreys DP, Lilley KS, Salmond GPC. The phage abortive infection system, ToxIN, functions as a protein-RNA toxin-antitoxin pair. Proc Natl Acad Sci U S A 2009; 106(3): 894–9
[https://doi.org/10.1073/pnas.0808832106][PMID: 19124776]

[144] Ghisotti D, Finkel S, Halling C, Dehò G, Sironi G, Calendar R. Nonessential region of bacteriophage P4: DNA sequence, transcription, gene products, and functions. J Virol 1990; 64(1): 24–36
[https://doi.org/10.1128/JVI.64.1.24-36.1990][PMID: 2403440]

[145] Cooper TF, Paixão T, Heinemann JA. Within-host competition selects for plasmid-encoded toxin-antitoxin systems. Proc Biol Sci 2010; 277(1697): 3149–55
[https://doi.org/10.1098/rspb.2010.0831][PMID: 20504809]

[146] Cooper TF, Heinemann JA. Postsegregational killing does not increase plasmid stability but acts to mediate the exclusion of competing plasmids. Proc Natl Acad Sci U S A 2000; 97(23): 12643–8
[https://doi.org/10.1073/pnas.220077897][PMID: 11058151]

[147] Yarmolinsky MB. Programmed cell death in bacterial populations. Science 1995; 267(5199): 836–7
[https://doi.org/10.1126/science.7846528][PMID: 7846528]

[148] Tiemann B, Depping R, Gineikiene E, Kaliniene L, Nivinskas R, Rüger W. ModA and ModB, two ADP-ribosyltransferases encoded by bacteriophage T4: catalytic properties and mutation analysis. J Bacteriol 2004; 186(21): 7262–72
[https://doi.org/10.1128/JB.186.21.7262-7272.2004][PMID: 15489438]

[149] Rohrer H, Zillig W, Mailhammer R. ADP-ribosylation of DNA-dependent RNA polymerase of Escherichia coli by an NAD+: protein ADP-ribosyltransferase from bacteriophage T4. Eur J Biochem 1975; 60(1): 227–38
[https://doi.org/10.1111/j.1432-1033.1975.tb20995.x][PMID: 173540]

[150] Skórko R, Zillig W, Rohrer H, Fujiki H, Mailhammer R. Purification and properties of the NAD+: protein ADP-ribosyltransferase responsible for the T4-phage-induced modification of the alpha subunit of DNA-dependent RNA polymerase of Escherichia coli. Eur J Biochem 1977; 79(1): 55–66
[https://doi.org/10.1111/j.1432-1033.1977.tb11783.x][PMID: 199442]

[151] Tiemann B, Depping R, Rüger W. Overexpression, purification, and partial characterization of ADP-ribosyltransferases modA and modB of bacteriophage T4. Gene Expr 1999; 8(3): 187–96
[PMID: 10634320]

[152] Wolfram-Schauerte M, Pozhydaieva N, Grawenhoff J*, et al.* A viral ADP-ribosyltransferase attaches RNA chains to host proteins. Nature 2023; 620(7976): 1054–62
[https://doi.org/10.1038/s41586-023-06429-2][PMID: 37587340]

[153] Tal N, Millman A, Stokar-Avihail A*, et al.* Bacteria deplete deoxynucleotides to defend against bacteriophage infection. Nat Microbiol 2022; 7(8): 1200–9
[https://doi.org/10.1038/s41564-022-01158-0][PMID: 35817891]

[154] Mahler M, Costa AR, van Beljouw SPB, Fineran PC, Brouns SJJ. Approaches for bacteriophage genome engineering. Trends Biotechnol 2023; 41(5): 669–85
[https://doi.org/10.1016/j.tibtech.2022.08.008][PMID: 36117025]

[155] Shitrit D, Hackl T, Laurenceau R*, et al.* Genetic engineering of marine cyanophages reveals integration but not lysogeny in T7-like cyanophages. ISME J 2022; 16(2): 488–99
[https://doi.org/10.1038/s41396-021-01085-8][PMID: 34429521]

[156] Russel M, Model P. Genetic analysis of the filamentous bacteriophage packaging signal and of the proteins that interact with it. J Virol 1989; 63(8): 3284–95
[https://doi.org/10.1128/JVI.63.8.3284-3295.1989][PMID: 2746731]

[157] Davis BM, Lawson EH, Sandkvist M, Ali A, Sozhamannan S, Waldor MK. Convergence of the secretory pathways for cholera toxin and the filamentous phage, CTXphi. Science 2000; 288(5464): 333–5
[https://doi.org/10.1126/science.288.5464.333][PMID: 10764646]

[158] Webster RE. FILAMENTOUS PHAGES (INOVIRIDAE). In: Encyclopedia of Virology. Elsevier 1999; 547–52.

[159] Haigh NG, Webster RE. The pI and pXI assembly proteins serve separate and essential roles in filamentous phage assembly. J Mol Biol 1999; 293(5): 1017–27
[https://doi.org/10.1006/jmbi.1999.3227][PMID: 10547282]

[160] Bennett NJ, Gagic D, Sutherland-Smith AJ, Rakonjac J. Characterization of a dual-function domain that mediates membrane insertion and excision of Ff filamentous bacteriophage. J Mol Biol 2011; 411(5): 972–85
[https://doi.org/10.1016/j.jmb.2011.07.002][PMID: 21763316]

[161] Løset GÅ, Roos N, Bogen B, Sandlie I. Expanding the versatility of phage display II: improved affinity selection of folded domains on protein VII and IX of the filamentous phage. PLoS One 2011; 6(2): e17433
[https://doi.org/10.1371/journal.pone.0017433][PMID: 21390283]

[162] Dogic Z, Fraden S. Development of model colloidal liquid crystals and the kinetics of the isotropic–smectic transition. Philosophical Transactions of the Royal Society of London. Series A: Mathematical, Physical and Engineering Sciences 2001; 359(1782): 997–1015
[https://doi.org/10.1098/rsta.2000.0814]

[163] Kever L, Hardy A, Luthe T*, et al.* Aminoglycoside Antibiotics Inhibit Phage Infection by Blocking an Early Step of the Infection Cycle. mBio 2022; 13(3): e0078322
[https://doi.org/10.1128/mbio.00783-22][PMID: 35506667]

[164] Krebber C, Spada S, Desplancq D, Plückthun A. Co-selection of cognate antibody-antigen pairs by selectively-infective phages. FEBS Lett 1995; 377(2): 227–31
[https://doi.org/10.1016/0014-5793(95)01348-2][PMID: 8543056]

[165] O'Callaghan R, Bradley R, Paranchych W. The effect of M13 phage infection upon the F pili of E. coli. Virology 1973; 54(1): 220–9
[https://doi.org/10.1016/0042-6822(73)90131-1][PMID: 4123460]

[166] Campos J, Martínez E, Suzarte E*, et al.* VGJ phi, a novel filamentous phage of Vibrio cholerae, integrates into the same chromosomal site as CTX phi. J Bacteriol 2003; 185(19): 5685–96
[https://doi.org/10.1128/JB.185.19.5685-5696.2003][PMID: 13129939]

[167] TZAGOLOFF H, PRATT D. THE INITIAL STEPS IN INFECTION WITH COLIPHAGE M13. Virology 1964; 24: 372–80
[https://doi.org/10.1016/0042-6822(64)90174-6][PMID: 14227038]

[168] Abedon ST, editor. Bacteriophage ecology: Population growth, evolution, and impact of bacterial viruses. 1. publ. Cambridge: Cambridge Univ. Press; 2008.

[169] Horne T, Orr VT, Hall JP. How do interactions between mobile genetic elements affect horizontal gene transfer? Curr Opin Microbiol 2023; 73: 102282
[https://doi.org/10.1016/j.mib.2023.102282][PMID: 36863168]

[170] Jia K, Peng Y, Chen X*, et al.* A Novel Inovirus Reprograms Metabolism and Motility of Marine Alteromonas. Microbiol Spectr 2022; 10(6): e0338822
[https://doi.org/10.1128/spectrum.03388-22][PMID: 36301121]

[171] Bertozzi Silva J, Storms Z, Sauvageau D. Host receptors for bacteriophage adsorption. FEMS Microbiol Lett 2016; 363(4)
[https://doi.org/10.1093/femsle/fnw002][PMID: 26755501]

[172] Saville RM, Dieckmann N, Spormann AM. Spatiotemporal activity of the mshA gene system in Shewanella oneidensis MR-1 biofilms. FEMS Microbiol Lett 2010; 308(1): 76–83
[https://doi.org/10.1111/j.1574-6968.2010.01995.x][PMID: 20487019]

[173] Römling U, Galperin MY, Gomelsky M. Cyclic di-GMP: the first 25 years of a universal bacterial second messenger. Microbiol Mol Biol Rev 2013; 77(1): 1–52
[https://doi.org/10.1128/MMBR.00043-12][PMID: 23471616]

[174] Scholl D, Adhya S, Merril C. Escherichia coli K1's capsule is a barrier to bacteriophage T7. Appl Environ Microbiol 2005; 71(8): 4872–4
[https://doi.org/10.1128/AEM.71.8.4872-4874.2005][PMID: 16085886]

[175] Vassallo CN, Doering CR, Littlehale ML, Teodoro GIC, Laub MT. A functional selection reveals previously undetected anti-phage defence systems in the E. coli pangenome. Nat Microbiol 2022; 7(10): 1568–79
[https://doi.org/10.1038/s41564-022-01219-4][PMID: 36123438]

[176] Santos-López A, Rodríguez-Beltrán J, San Millán Á. The bacterial capsule is a gatekeeper for mobile DNA. PLoS Biol 2021; 19(7): e3001308
[https://doi.org/10.1371/journal.pbio.3001308][PMID: 34228713]

[177] Secor PR, Sweere JM, Michaels LA*, et al.* Filamentous Bacteriophage Promote Biofilm Assembly and Function. Cell Host Microbe 2015; 18(5): 549–59
[https://doi.org/10.1016/j.chom.2015.10.013][PMID: 26567508]

[178] Smirnova NI, Agafonov DA, Kul'shan' TA*, et al.* Effect of CTXφ prophage deletion in cholera agent on expression of regulatory genes controlling virulence and biofilm formation. Russ J Genet 2017; 53(3): 302–13
[https://doi.org/10.1134/S1022795417020119]

[179] Addy HS, Askora A, Kawasaki T, Fujie M, Yamada T. The filamentous phage ϕRSS1 enhances virulence of phytopathogenic Ralstonia solanacearum on tomato. Phytopathology 2012; 102(3): 244–51
[https://doi.org/10.1094/PHYTO-10-11-0277][PMID: 22085298]

[180] Hickman AB, Ronning DR, Kotin RM, Dyda F. Structural unity among viral origin binding proteins: crystal structure of the nuclease domain of adeno-associated virus Rep. Mol Cell 2002; 10(2): 327–37
[https://doi.org/10.1016/s1097-2765(02)00592-0][PMID: 12191478]

[181] Vega-Rocha S, Byeon I-JL, Gronenborn B, Gronenborn AM, Campos-Olivas R. Solution structure, divalent metal and DNA binding of the endonuclease domain from the replication initiation protein from porcine circovirus 2. J Mol Biol 2007; 367(2): 473–87
[https://doi.org/10.1016/j.jmb.2007.01.002][PMID: 17275023]

[182] Devine KM, Hogan ST, Higgins DG, McConnell DJ. Replication and segregational stability of Bacillus plasmid pBAA1. J Bacteriol 1989; 171(2): 1166–72
[https://doi.org/10.1128/jb.171.2.1166-1172.1989][PMID: 2492507]

[183] Noirot-Gros MF, Bidnenko V, Ehrlich SD. Active site of the replication protein of the rolling circle plasmid pC194. EMBO J 1994; 13(18): 4412–20
[https://doi.org/10.1002/j.1460-2075.1994.tb06761.x][PMID: 7925284]

[184] Novick RP. Contrasting lifestyles of rolling-circle phages and plasmids. Trends Biochem Sci 1998; 23(11): 434–8
[https://doi.org/10.1016/s0968-0004(98)01302-4][PMID: 9852762]

[185] Dotto GP, Enea V, Zinder ND. Functional analysis of bacteriophage f1 intergenic region. Virology 1981; 114(2): 463–73
[https://doi.org/10.1016/0042-6822(81)90226-9][PMID: 7292986]

[186] Brockhurst MA, Harrison E. Ecological and evolutionary solutions to the plasmid paradox. Trends Microbiol 2022; 30(6): 534–43
[https://doi.org/10.1016/j.tim.2021.11.001][PMID: 34848115]

[187] Iranzo J, Puigbò P, Lobkovsky AE, Wolf YI, Koonin EV. Inevitability of Genetic Parasites. Genome Biol Evol 2016; 8(9): 2856–69
[https://doi.org/10.1093/gbe/evw193][PMID: 27503291]

[188] Koonin EV, Dolja VV. A virocentric perspective on the evolution of life. Curr Opin Virol 2013; 3(5): 546–57
[https://doi.org/10.1016/j.coviro.2013.06.008][PMID: 23850169]

[189] Newbury A, Dawson B, Klümper U*, et al.* Fitness effects of plasmids shape the structure of bacteria-plasmid interaction networks. Proc Natl Acad Sci U S A 2022; 119(22): e2118361119
[https://doi.org/10.1073/pnas.2118361119][PMID: 35613058]

[190] van Melderen L. Toxin-antitoxin systems: why so many, what for? Curr Opin Microbiol 2010; 13(6): 781–5
[https://doi.org/10.1016/j.mib.2010.10.006][PMID: 21041110]

[191] Gerdes K, Rasmussen PB, Molin S. Unique type of plasmid maintenance function: postsegregational killing of plasmid-free cells. Proc Natl Acad Sci U S A 1986; 83(10): 3116–20
[https://doi.org/10.1073/pnas.83.10.3116][PMID: 3517851]

[192] Fraikin N, Goormaghtigh F, van Melderen L. Type II Toxin-Antitoxin Systems: Evolution and Revolutions. J Bacteriol 2020; 202(7)
[https://doi.org/10.1128/jb.00763-19][PMID: 31932311]

[193] Chan WT, Espinosa M, Yeo CC. Keeping the Wolves at Bay: Antitoxins of Prokaryotic Type II Toxin-Antitoxin Systems. Front Mol Biosci 2016; 3: 9
[https://doi.org/10.3389/fmolb.2016.00009][PMID: 27047942]

[194] Reygaert WC. An overview of the antimicrobial resistance mechanisms of bacteria. AIMS Microbiol 2018; 4(3): 482–501
[https://doi.org/10.3934/microbiol.2018.3.482][PMID: 31294229]

[195] Kamada K, Hanaoka F, Burley SK. Crystal structure of the MazE/MazF complex: molecular bases of antidote-toxin recognition. Mol Cell 2003; 11(4): 875–84
[https://doi.org/10.1016/S1097-2765(03)00097-2][PMID: 12718874]

[196] Harrison E, Brockhurst MA. Plasmid-mediated horizontal gene transfer is a coevolutionary process. Trends Microbiol 2012; 20(6): 262–7
[https://doi.org/10.1016/j.tim.2012.04.003][PMID: 22564249]

[197] Bergstrom CT, Lipsitch M, Levin BR. Natural selection, infectious transfer and the existence conditions for bacterial plasmids. Genetics 2000; 155(4): 1505–19
[https://doi.org/10.1093/genetics/155.4.1505][PMID: 10924453]

[198] Stewart FM, Levin BR. The Population Biology of Bacterial Plasmids: A PRIORI Conditions for the Existence of Conjugationally Transmitted Factors. Genetics 1977; 87(2): 209–28 [https://doi.org/10.1093/genetics/87.2.209][PMID: 17248761]

[199] Probing the plasmid paradox. Nat Ecol Evol 2021; 5(12): 1559 [https://doi.org/10.1038/s41559-021-01613-x][PMID: 34857893]

[200] Bennett PM. Plasmids: freelance drivers of bacterial evolution. Trends in Genetics 2001; 17(3): 165 [https://doi.org/10.1016/S0168-9525(00)02200-9]

[201] Summers DK. The biology of plasmids. Oxford: Blackwell Science 1996.

[202] LEDERBERG J. Cell genetics and hereditary symbiosis. Physiol Rev 1952; 32(4): 403–30 [https://doi.org/10.1152/physrev.1952.32.4.403][PMID: 13003535]

[203] Chiang YN, Penadés JR, Chen J. Genetic transduction by phages and chromosomal islands: The new and noncanonical. PLoS Pathog 2019; 15(8): e1007878 [https://doi.org/10.1371/journal.ppat.1007878][PMID: 31393945]

[204] Du Toit A. A small coat for satellites. Nat Rev Microbiol 2023; 21(9): 553 [https://doi.org/10.1038/s41579-023-00948-5][PMID: 37433960]

[205] Krupovic M, Kuhn JH, Fischer MG. A classification system for virophages and satellite viruses. Arch Virol 2016; 161(1): 233–47 [https://doi.org/10.1007/s00705-015-2622-9][PMID: 26446887]

[206] Subirana JA, Messeguer X. Satellites in the prokaryote world. BMC Evol Biol 2019; 19(1): 181 [https://doi.org/10.1186/s12862-019-1504-2][PMID: 31533616]

[207] Netter Z, Boyd CM, Silvas TV, Seed KD. A phage satellite tunes inducing phage gene expression using a domesticated endonuclease to balance inhibition and virion hijacking. Nucleic Acids Res 2021; 49(8): 4386–401 [https://doi.org/10.1093/nar/gkab207][PMID: 33823541]

[208] O'Hara BJ, Barth ZK, McKitterick AC, Seed KD. A highly specific phage defense system is a conserved feature of the Vibrio cholerae mobilome. PLoS Genet 2017; 13(6): e1006838 [https://doi.org/10.1371/journal.pgen.1006838][PMID: 28594826]

[209] Nilssen O, Fossdal CG, Johansen BV, Lindqvist BH. Bacteriophage P4 capsid-size determination and its relationship to P2 helper interference. Virology 1996; 219(2): 443–52 [https://doi.org/10.1006/viro.1996.0270][PMID: 8638410]

[210] deCarvalho T, Mascolo E, Caruso SM*, et al.* Simultaneous entry as an adaptation to virulence in a novel satellite-helper system infecting Streptomyces species. ISME J 2023; 17(12): 2381–8 [https://doi.org/10.1038/s41396-023-01548-0][PMID: 37907733]

[211] Dokland T. Molecular Piracy: Redirection of Bacteriophage Capsid Assembly by Mobile Genetic Elements. Viruses 2019; 11(11) [https://doi.org/10.3390/v11111003][PMID: 31683607]

[212] Eppley JM, Biller SJ, Luo E, Burger A, DeLong EF. Marine viral particles reveal an expansive repertoire of phage-parasitizing mobile elements. Proc Natl Acad Sci U S A 2022; 119(43): e2212722119 [https://doi.org/10.1073/pnas.2212722119][PMID: 36256808]

[213] Das B. Mechanistic insights into filamentous phage integration in Vibrio cholerae. Front Microbiol 2014; 5: 650 [https://doi.org/10.3389/fmicb.2014.00650][PMID: 25506341]

[214] Das B, Bischerour J, Barre F-X. VGJphi integration and excision mechanisms contribute to the genetic diversity of Vibrio cholerae epidemic strains. Proc Natl Acad Sci U S A 2011; 108(6): 2516–21
[https://doi.org/10.1073/pnas.1017061108][PMID: 21262799]

[215] Clokie MR, Kropinski AM, editors. Bacteriophages: Methods and Protocols, Volume 1: Isolation, Characterization, and Interactions. Totowa, NJ: Humana Press; 2009.

[216] Krupovic M, Dolja VV, Koonin EV. Origin of viruses: primordial replicators recruiting capsids from hosts. Nat Rev Microbiol 2019; 17(7): 449–58
[https://doi.org/10.1038/s41579-019-0205-6][PMID: 31142823]

[217] Koonin EV, Senkevich TG, Dolja VV. The ancient Virus World and evolution of cells. Biol Direct 2006; 1: 29
[https://doi.org/10.1186/1745-6150-1-29][PMID: 16984643]

[218] Erdmann S, Tschitschko B, Zhong L, Raftery MJ, Cavicchioli R. A plasmid from an Antarctic haloarchaeon uses specialized membrane vesicles to disseminate and infect plasmid-free cells. Nat Microbiol 2017; 2(10): 1446–55
[https://doi.org/10.1038/s41564-017-0009-2][PMID: 28827601]

[219] Pfeifer E, Moura de Sousa JA, Touchon M, Rocha EPC. Bacteria have numerous distinctive groups of phage-plasmids with conserved phage and variable plasmid gene repertoires. Nucleic Acids Res 2021; 49(5): 2655–73
[https://doi.org/10.1093/nar/gkab064][PMID: 33590101]

[220] Ravin NV, Svarchevsky AN, Dehò G. The anti-immunity system of phage-plasmid N15: identification of the antirepressor gene and its control by a small processed RNA. Mol Microbiol 1999; 34(5): 980–94
[https://doi.org/10.1046/j.1365-2958.1999.01658.x][PMID: 10594823]

[221] Humphrey S, San Millán Á, Toll-Riera M*, et al.* Staphylococcal phages and pathogenicity islands drive plasmid evolution. Nat Commun 2021; 12(1): 5845
[https://doi.org/10.1038/s41467-021-26101-5][PMID: 34615859]

[222] Konthur Z, Glökler J, Skriner K. Protein Interaction Analysis: Phage Display. In: Ganten D, Ruckpaul K, editors. Encyclopedic reference of genomics and proteomics in molecular medicine. Berlin u.a: Springer 2006; 1509–14.

[223] Lerner TJ, Model P. The "steady state" of coliphage f1: DNA synthesis late in infection. Virology 1981; 115(2): 282–94
[https://doi.org/10.1016/0042-6822(81)90111-2][PMID: 7032054]

[224] Michel B, Zinder ND. Translational repression in bacteriophage f1: characterization of the gene V protein target on the gene II mRNA. Proc Natl Acad Sci U S A 1989; 86(11): 4002–6
[https://doi.org/10.1073/pnas.86.11.4002][PMID: 2657734]

[225] Fulford W, Model P. Bacteriophage f1 DNA replication genes. II. The roles of gene V protein and gene II protein in complementary strand synthesis. J Mol Biol 1988; 203(1): 39–48
[https://doi.org/10.1016/0022-2836(88)90089-7][PMID: 3054122]

[226] Brandão A, Pires DP, Coppens L, Voet M, Lavigne R, Azeredo J. Differential transcription profiling of the phage LUZ19 infection process in different growth media. RNA Biol 2021; 18(11): 1778–90
[https://doi.org/10.1080/15476286.2020.1870844][PMID: 33448239]

[227] Mojardín L, Salas M. Global Transcriptional Analysis of Virus-Host Interactions between Phage ϕ29 and Bacillus subtilis. J Virol 2016; 90(20): 9293–304
[https://doi.org/10.1128/JVI.01245-16][PMID: 27489274]

[228] Miller ES, Kutter E, Mosig G, Arisaka F, Kunisawa T, Rüger W. Bacteriophage T4 genome. Microbiol Mol Biol Rev 2003; 67(1): 86-156, table of contents
[https://doi.org/10.1128/MMBR.67.1.86-156.2003][PMID: 12626685]

[229] Liu C, Yu X. ADP-ribosyltransferases and poly ADP-ribosylation. Curr Protein Pept Sci 2015; 16(6): 491–501
[https://doi.org/10.2174/1389203716666150504122435][PMID: 25938242]

[230] Palazzo L, Mikoč A, Ahel I. ADP-ribosylation: new facets of an ancient modification. FEBS J 2017; 284(18): 2932–46
[https://doi.org/10.1111/febs.14078][PMID: 28383827]

[231] Lüscher B, Bütepage M, Eckei L, Krieg S, Verheugd P, Shilton BH. ADP-Ribosylation, a Multifaceted Posttranslational Modification Involved in the Control of Cell Physiology in Health and Disease. Chem Rev 2018; 118(3): 1092–136
[https://doi.org/10.1021/acs.chemrev.7b00122][PMID: 29172462]

[232] Simon NC, Aktories K, Barbieri JT. Novel bacterial ADP-ribosylating toxins: structure and function. Nat Rev Microbiol 2014; 12(9): 599–611
[https://doi.org/10.1038/nrmicro3310][PMID: 25023120]

[233] Aravind L, Zhang D, Souza RF de, Anand S, Iyer LM. The natural history of ADP-ribosyltransferases and the ADP-ribosylation system. Curr Top Microbiol Immunol 2015; 384: 3–32
[https://doi.org/10.1007/82_2014_414][PMID: 25027823]

[234] Fehr AR, Singh SA, Kerr CM, Mukai S, Higashi H, Aikawa M. The impact of PARPs and ADP-ribosylation on inflammation and host-pathogen interactions. Genes Dev 2020; 34(5-6): 341–59
[https://doi.org/10.1101/gad.334425.119][PMID: 32029454]

[235] Parker CE, Mocanu V, Mocanu M, Dicheva N, Warren MR. Neuroproteomics: Mass Spectrometry for Post-Translational Modifications. Boca Raton (FL) 2010.

[236] Griffin MA, Davis JH, Strobel SA. Bacterial toxin RelE: a highly efficient ribonuclease with exquisite substrate specificity using atypical catalytic residues. Biochemistry 2013; 52(48): 8633–42
[https://doi.org/10.1021/bi401325c][PMID: 24251350]

[237] Schumacher MA, Piro KM, Xu W, Hansen S, Lewis K, Brennan RG. Molecular mechanisms of HipA-mediated multidrug tolerance and its neutralization by HipB. Science 2009; 323(5912): 396–401
[https://doi.org/10.1126/science.1163806][PMID: 19150849]

[238] Maisonneuve E, Shakespeare LJ, Jørgensen MG, Gerdes K. Bacterial persistence by RNA endonucleases. Proc Natl Acad Sci U S A 2011; 108(32): 13206–11
[https://doi.org/10.1073/pnas.1100186108][PMID: 21788497]

[239] Ren D, Bedzyk LA, Thomas SM, Ye RW, Wood TK. Gene expression in Escherichia coli biofilms. Appl Microbiol Biotechnol 2004; 64(4): 515–24
[https://doi.org/10.1007/s00253-003-1517-y][PMID: 14727089]

[240] Wang X, Wood TK. Toxin-antitoxin systems influence biofilm and persister cell formation and the general stress response. Appl Environ Microbiol 2011; 77(16): 5577–83
[https://doi.org/10.1128/AEM.05068-11][PMID: 21685157]

[241] Dy RL, Przybilski R, Semeijn K, Salmond GPC, Fineran PC. A widespread bacteriophage abortive infection system functions through a Type IV toxin-antitoxin mechanism. Nucleic Acids Res 2014; 42(7): 4590–605
[https://doi.org/10.1093/nar/gkt1419][PMID: 24465005]

[242] Koga M, Otsuka Y, Lemire S, Yonesaki T. Escherichia coli rnlA and rnlB compose a novel toxin-antitoxin system. Genetics 2011; 187(1): 123–30
[https://doi.org/10.1534/genetics.110.121798][PMID: 20980243]

[243] Otsuka Y, Yonesaki T. Dmd of bacteriophage T4 functions as an antitoxin against Escherichia coli LsoA and RnlA toxins. Mol Microbiol 2012; 83(4): 669–81
[https://doi.org/10.1111/j.1365-2958.2012.07975.x][PMID: 22403819]

[244] Alawneh AM, Qi D, Yonesaki T, Otsuka Y. An ADP-ribosyltransferase Alt of bacteriophage T4 negatively regulates the Escherichia coli MazF toxin of a toxin-antitoxin module. Mol Microbiol 2016; 99(1): 188–98
[https://doi.org/10.1111/mmi.13225][PMID: 26395283]

[245] Barnes CO, Wu Y, Song J*, et al.* The crystal structure of dGTPase reveals the molecular basis of dGTP selectivity. Proc Natl Acad Sci U S A 2019; 116(19): 9333–9
[https://doi.org/10.1073/pnas.1814999116][PMID: 31019074]

[246] Goldstone DC, Ennis-Adeniran V, Hedden JJ*, et al.* HIV-1 restriction factor SAMHD1 is a deoxynucleoside triphosphate triphosphohydrolase. Nature 2011; 480(7377): 379–82
[https://doi.org/10.1038/nature10623][PMID: 22056990]

[247] Ka D, Oh H, Park E, Kim J-H, Bae E. Structural and functional evidence of bacterial antiphage protection by Thoeris defense system via NAD+ degradation. Nat Commun 2020; 11(1): 2816
[https://doi.org/10.1038/s41467-020-16703-w][PMID: 32499527]

[248] Islam R, Brown S, Taheri A, Dumenyo CK. The Gene Encoding NAD-Dependent Epimerase/Dehydratase, wcaG, Affects Cell Surface Properties, Virulence, and Extracellular Enzyme Production in the Soft Rot Phytopathogen, Pectobacteriumcarotovorum. Microorganisms 2019; 7(6)
[https://doi.org/10.3390/microorganisms7060172][PMID: 31200539]

[249] Somers WS, Stahl ML, Sullivan FX. GDP-fucose synthetase from Escherichia coli: structure of a unique member of the short-chain dehydrogenase/reductase family that catalyzes two distinct reactions at the same active site. Structure 1998; 6(12): 1601–12
[https://doi.org/10.1016/s0969-2126(98)00157-9][PMID: 9862812]

[250] Tamayo R. The characterization of a cyclic-di-GMP (c-Di-GMP) pathway leads to a new tool for studying c-Di-GMP metabolic genes. J Bacteriol 2013; 195(21): 4779–81
[https://doi.org/10.1128/JB.00925-13][PMID: 23955008]

[251] Smet J de, Wagemans J, Hendrix H*, et al.* Bacteriophage-mediated interference of the c-di-GMP signalling pathway in Pseudomonas aeruginosa. Microb Biotechnol 2021; 14(3): 967–78
[https://doi.org/10.1111/1751-7915.13728][PMID: 33314648]

[252] Huertas-Rosales Ó, Ramos-González MI, Espinosa-Urgel M. Self-Regulation and Interplay of Rsm Family Proteins Modulate the Lifestyle of Pseudomonas putida. Appl Environ Microbiol 2016; 82(18): 5673–86
[https://doi.org/10.1128/AEM.01724-16][PMID: 27422830]

[253] Pletnev P, Guseva E, Zanina A*, et al.* Comprehensive Functional Analysis of Escherichia coli Ribosomal RNA Methyltransferases. Front Genet 2020; 11: 97
[https://doi.org/10.3389/fgene.2020.00097][PMID: 32174967]

[254] Saito K, Kratzat H, Campbell A*, et al.* Ribosome collisions induce mRNA cleavage and ribosome rescue in bacteria. Nature 2022; 603(7901): 503–8
[https://doi.org/10.1038/s41586-022-04416-7][PMID: 35264790]

[255] Onodera H, Niwa T, Taguchi H, Chadani Y. Prophage excision switches the primary ribosome rescue pathway and rescue-associated gene regulations in Escherichia coli. Mol Microbiol 2023; 119(1): 44–58
[https://doi.org/10.1111/mmi.15003][PMID: 36471624]

[256] Moller AG, Winston K, Ji S*, et al.* Genes Influencing Phage Host Range in Staphylococcus aureus on a Species-Wide Scale. mSphere 2021; 6(1)
[https://doi.org/10.1128/mSphere.01263-20][PMID: 33441407]

[257] Razew A, Schwarz J-N, Mitkowski P, Sabala I, Kaus-Drobek M. One fold, many functions-M23 family of peptidoglycan hydrolases. Front Microbiol 2022; 13: 1036964
[https://doi.org/10.3389/fmicb.2022.1036964][PMID: 36386627]

[258] Gescher JS, Cordova CD, Spormann AM. Dissimilatory iron reduction in Escherichia coli: identification of CymA of Shewanella oneidensis and NapC of E. coli as ferric reductases. Mol Microbiol 2008; 68(3): 706–19
[https://doi.org/10.1111/j.1365-2958.2008.06183.x][PMID: 18394146]

[259] BERTANI G. Studies on lysogenesis. I. The mode of phage liberation by lysogenic Escherichia coli. J Bacteriol 1951; 62(3): 293–300
[https://doi.org/10.1128/jb.62.3.293-300.1951][PMID: 14888646]

[260] Paulick A, Koerdt A, Lassak J*, et al.* Two different stator systems drive a single polar flagellum in Shewanella oneidensis MR-1. Mol Microbiol 2009; 71(4): 836–50
[https://doi.org/10.1111/j.1365-2958.2008.06570.x][PMID: 19170881]

[261] Venkateswaran K, Moser DP, Dollhopf ME*, et al.* Polyphasic taxonomy of the genus Shewanella and description of Shewanella oneidensis sp. nov. Int J Syst Bacteriol 1999; 49 Pt 2: 705–24
[https://doi.org/10.1099/00207713-49-2-705][PMID: 10319494]

[262] Bubendorfer S, Ishihara M, Dohlich K*, et al.* Analyzing the modification of the Shewanella oneidensis MR-1 flagellar filament. PLoS One 2013; 8(9): e73444
[https://doi.org/10.1371/journal.pone.0073444][PMID: 24039942]

[263] Claudia Julia Walasek. Untersuchungen zu Shewanella-Phagen. Master-ThesisJustus-Liebig-Universität Gießen 2020 Mar 26.

[264] Jung-Schroers V, Jung A, Ryll M, Bauer J, Teitge F, Steinhagen D. Methods for identification and differentiation of different Shewanella spp. isolates for diagnostic use. J Fish Dis 2018; 41(4): 689–714
[https://doi.org/10.1111/jfd.12772][PMID: 29280153]

[265] Venkateswaran K, Dollhopf ME, Aller R, Stackebrandt E, Nealson KH. Shewanella amazonensis sp. nov., a novel metal-reducing facultative anaerobe from Amazonian shelf muds. Int J Syst Bacteriol 1998; 48 Pt 3: 965–72
[https://doi.org/10.1099/00207713-48-3-965][PMID: 9734053]

[266] Fredrickson JK, Zachara JM, Kennedy DW*, et al.* Biogenic iron mineralization accompanying the dissimilatory reduction of hydrous ferric oxide by a groundwater bacterium. Geochimica et Cosmochimica Acta 1998; 62(19-20): 3239–57
[https://doi.org/10.1016/s0016-7037(98)00243-9]

[267] Dwarakanath S, Brenzinger S, Gleditzsch D*, et al.* Interference activity of a minimal Type I CRISPR-Cas system from Shewanella putrefaciens. Nucleic Acids Res 2015; 43(18): 8913–23 [https://doi.org/10.1093/nar/gkv882][PMID: 26350210]

[268] Murray AE, Lies D, Li G, Nealson K, Zhou J, Tiedje JM. DNA/DNA hybridization to microarrays reveals gene-specific differences between closely related microbial genomes. Proc Natl Acad Sci U S A 2001; 98(17): 9853–8 [https://doi.org/10.1073/pnas.171178898][PMID: 11493693]

[269] Saltikov CW, Cifuentes A, Venkateswaran K, Newman DK. The ars detoxification system is advantageous but not required for As(V) respiration by the genetically tractable Shewanella species strain ANA-3. Appl Environ Microbiol 2003; 69(5): 2800–9 [https://doi.org/10.1128/AEM.69.5.2800-2809.2003][PMID: 12732551]

[270] Nealson KH, Myers CR, Wimpee BB. Isolation and identification of manganese-reducing bacteria and estimates of microbial Mn(IV)-reducing potential in the Black Sea. Deep Sea Research Part A. Oceanographic Research Papers 1991; 38: S907-S920 [https://doi.org/10.1016/s0198-0149(10)80016-0]

[271] Jensen KF. The Escherichia coli K-12 "wild types" W3110 and MG1655 have an rph frameshift mutation that leads to pyrimidine starvation due to low pyrE expression levels. J Bacteriol 1993; 175(11): 3401–7 [https://doi.org/10.1128/jb.175.11.3401-3407.1993][PMID: 8501045]

[272] Miller VL, Mekalanos JJ. A novel suicide vector and its use in construction of insertion mutations: osmoregulation of outer membrane proteins and virulence determinants in Vibrio cholerae requires toxR. J Bacteriol 1988; 170(6): 2575–83 [https://doi.org/10.1128/jb.170.6.2575-2583.1988][PMID: 2836362]

[273] Nelson KE, Weinel C, Paulsen IT*, et al.* Complete genome sequence and comparative analysis of the metabolically versatile Pseudomonas putida KT2440. Environmental Microbiology 2002; 4(12): 799–808 [https://doi.org/10.1046/j.1462-2920.2002.00366.x][PMID: 12534463]

[274] Heidelberg JF, Eisen JA, Nelson WC*, et al.* DNA sequence of both chromosomes of the cholera pathogen Vibrio cholerae. Nature 2000; 406(6795): 477–83 [https://doi.org/10.1038/35020000][PMID: 10952301]

[275] Lassak J, Henche A-L, Binnenkade L, Thormann KM. ArcS, the cognate sensor kinase in an atypical Arc system of Shewanella oneidensis MR-1. Appl Environ Microbiol 2010; 76(10): 3263–74 [https://doi.org/10.1128/AEM.00512-10][PMID: 20348304]

[276] Guzman LM, Belin D, Carson MJ, Beckwith J. Tight regulation, modulation, and high-level expression by vectors containing the arabinose PBAD promoter. J Bacteriol 1995; 177(14): 4121–30 [https://doi.org/10.1128/jb.177.14.4121-4130.1995][PMID: 7608087]

[277] Karimova G, Pidoux J, Ullmann A, Ladant D. A bacterial two-hybrid system based on a reconstituted signal transduction pathway. Proc Natl Acad Sci U S A 1998; 95(10): 5752–6 [https://doi.org/10.1073/pnas.95.10.5752][PMID: 9576956]

[278] Zhang Y, Li X, Spremulli LL. Role of the conserved aspartate and phenylalanine residues in prokaryotic and mitochondrial elongation factor Ts in guanine nucleotide exchange. FEBS Lett 1996; 391(3): 330–2 [https://doi.org/10.1016/0014-5793(96)00789-2][PMID: 8765000]

[279] Alina Kemmler. Charakterisierung des lytischen Shewanella Phagen Phonos. Master-ThesisJustus-Liebig-Universität Gießen 2023 Jul 24.

[280] Gibson DG, Young L, Chuang R-Y, Venter JC, Hutchison CA, Smith HO. Enzymatic assembly of DNA molecules up to several hundred kilobases. Nat Methods 2009; 6(5): 343–5 [https://doi.org/10.1038/nmeth.1318][PMID: 19363495]

[281] Dreiseikelmann B, Bunk B, Spröer C, Rohde M, Nimtz M, Wittmann J. Characterization and genome comparisons of three Achromobacter phages of the family Siphoviridae. Arch Virol 2017; 162(8): 2191–201 [https://doi.org/10.1007/s00705-017-3347-8][PMID: 28357512]

[282] Wick RR, Judd LM, Gorrie CL, Holt KE. Unicycler: Resolving bacterial genome assemblies from short and long sequencing reads. PLoS Comput Biol 2017; 13(6): e1005595 [https://doi.org/10.1371/journal.pcbi.1005595][PMID: 28594827]

[283] Jumper J, Evans R, Pritzel A*, et al.* Applying and improving AlphaFold at CASP14. Proteins 2021; 89(12): 1711–21 [https://doi.org/10.1002/prot.26257][PMID: 34599769]

[284] Terzian P, Olo Ndela E, Galiez C*, et al.* PHROG: families of prokaryotic virus proteins clustered using remote homology. NAR Genom Bioinform 2021; 3(3): lqab067 [https://doi.org/10.1093/nargab/lqab067][PMID: 34377978]

[285] Laemmli UK. Cleavage of structural proteins during the assembly of the head of bacteriophage T4. Nature 1970; 227(5259): 680–5 [https://doi.org/10.1038/227680a0][PMID: 5432063]

[286] Wiśniewski JR. Filter-Aided Sample Preparation for Proteome Analysis. Methods Mol Biol 2018; 1841: 3–10 [https://doi.org/10.1007/978-1-4939-8695-8_1][PMID: 30259475]

[287] Turriziani B, Garcia-Munoz A, Pilkington R, Raso C, Kolch W, Kriegsheim A von. On-Beads Digestion in Conjunction with Data-Dependent Mass Spectrometry: A Shortcut to Quantitative and Dynamic Interaction Proteomics. Biology (Basel) 2014; 3(2): 320–32 [https://doi.org/10.3390/biology3020320][PMID: 24833512]